1981

An investigation of engine and test cell operating conditions on the effectiveness of smoke suppressant fuel additives.

Thornburg, Donald Wendell

Monterey, California. Naval Postgraduate School

NAVAL POSTGRADUATE SCHOOL
Monterey, California

THESIS

AN INVESTIGATION OF ENGINE AND TEST CELL OPERATING CONDITIONS ON THE EFFECTIVENESS OF SMOKE SUPPRESSANT FUEL ADDITIVES

by

Donald Wendell Thornburg

December 1981

Thesis Advisor: D. W. Netzer

Approved for public release; distribution unlimited

REPORT DOCUMENTATION PAGE

READ INSTRUCTIONS BEFORE COMPLETING FORM

1. REPORT NUMBER	2. GOVT ACCESSION NO. / 3. RECIPIENT'S CATALOG NUMBER
4. TITLE (and Subtitle): An Investigation of Engine and Test Cell Operating Conditions on the Effectiveness of Smoke Suppressant Fuel Additives	5. TYPE OF REPORT & PERIOD COVERED: Master's Thesis; December 1981
	6. PERFORMING ORG. REPORT NUMBER
7. AUTHOR(s): Donald Wendell Thornburg	8. CONTRACT OR GRANT NUMBER(s): N6237681WR00014
9. PERFORMING ORGANIZATION NAME AND ADDRESS: Naval Postgraduate School, Monterey, California 93940	10. PROGRAM ELEMENT, PROJECT, TASK AREA & WORK UNIT NUMBERS
11. CONTROLLING OFFICE NAME AND ADDRESS: Naval Air Propulsion Center, Trenton, New Jersey 08628	12. REPORT DATE: December 1981
	13. NUMBER OF PAGES: 102
14. MONITORING AGENCY NAME & ADDRESS (if different from Controlling Office): Naval Postgraduate School, Monterey, California 93940	15. SECURITY CLASS. (of this report): Unclassified
	15a. DECLASSIFICATION/DOWNGRADING SCHEDULE

16. DISTRIBUTION STATEMENT (of this Report)

Approved for public release; distribution unlimited

17. DISTRIBUTION STATEMENT (of the abstract entered in Block 20, if different from Report)

18. SUPPLEMENTARY NOTES

19. KEY WORDS (Continue on reverse side if necessary and identify by block number)

Turbojet
Test Cell
Pollution
Fuel Additives

20. ABSTRACT (Continue on reverse side if necessary and identify by block number)

Tests were conducted in a one-eighth scale turbojet test cell with a ramjet type combustor to investigate the effects of fuel additives on smoke reduction. Particle size and mass concentrations were determined at the engine and stack exhausts using three wavelength optical detector systems. Particulate samples were also collected at the engine exhaust and analyzed with a scanning electron microscope.

Combustor temperature and fuel additives were found to significantly affect particulate mass concentrations emitted from the engine while particle size appeared to be unaffected. No significant changes in the particulate size or mass occurred from the engine exhaust to the stack exhaust.

The optical determination of exhaust mean particulate size/mass concentration with three wavelength optical detector systems appears to be a good and reasonably accurate technique for evaluating the effects of engine and test cell operating conditions and fuel composition changes on the emitted particulates.

An Investigation of Engine and Test Cell Operating Conditions on the Effectiveness of Smoke Suppressant Fuel Additives

by

Donald Wendell Thornburg
Lieutenant, United States Navy
B.S., University of Tennessee, 1974

Submitted in partial fulfillment of the requirements for the degree of

MASTER OF SCIENCE IN AERONAUTICAL ENGINEERING

from the

NAVAL POSTGRADUATE SCHOOL
December 1981

ABSTRACT

Tests were conducted in a one-eighth scale turbojet test cell with a ramjet type combustor to investigate the effects of fuel additives on smoke reduction. Particle size and mass concentrations were determined at the engine and stack exhausts using three wavelength optical detector systems. Particulate samples were also collected at the engine exhaust and analyzed with a scanning electron microscope.

Combustor temperature and fuel additives were found to significantly affect particulate mass concentrations emitted from the engine while particle size appeared to be unaffected. No significant changes in the particulate size or mass occurred from the engine exhaust to the stack exhaust.

The optical determination of exhaust mean particulate size/mass concentration with three wavelength optical detector systems appears to be a good and reasonably accurate technique for evaluating the effects of engine and test cell operating conditions and fuel composition changes on the emitted particulates.

TABLE OF CONTENTS

LIST OF TABLES

LIST OF FIGURES

TABLE OF SYMBOLS AND ABBREVIATIONS

AUG. RATIO	Augmentation ratio
C_{m_e}	Engine exhaust particulate mass concentration ($\times 10^{-6}$ gm./liter gas)
C_{m_s}	Stack exhaust particulate mass concentration ($\times 10^{-6}$ gm./liter gas)
D_{32}	Volume-to-surface mean particle diameter (microns)
$\left(\frac{f}{a}\right)_p$	Fuel to air ratio (primary air); $\dot{m}_f/\dot{m}_p$
$\left(\frac{f}{a}\right)_{p+s}$	Fuel to air ratio (primary + secondary air); $\dot{m}_f/\dot{m}_e$
m	Complex refractive index
$\dot{m}_{aug.\ T.}$	Augmentor Tube mass flow rate (lbm/sec.)
$\dot{m}_{BP}$	Bypass air mass flow rate (lbm/sec.)
$\dot{m}_{c_e}$	Particulate mass flow rate at the engine exhaust (gm./sec.)
$\dot{m}_{c_s}$	Particulate mass flow rate at the stack exhaust (gm./sec.)
$\dot{m}_e$	Engine air mass flow rate ($\dot{m}_p + \dot{m}_s$) (lbm/sec.)
$\dot{m}_{e_T}$	Total engine air mass flow rate ($\dot{m}_{BP} + \dot{m}_e$) (lbm/sec.)
$\dot{m}_f$	Fuel mass flow rate (lbm/sec.)
$\dot{m}_p$	Combustor primary air mass flow rate (lbm/sec.)
$\dot{m}_s$	Combustor secondary air mass flow rate (lbm/sec.)

NO_x	Nitrogen Oxide concentration; parts per million (PPM), non-calibrated
T_λ	Percent transmittance at wavelength λ
T_2	Combustor gas temperature at the tail pipe (°R)
T_{BP}	Bypass air temperature (°R)
T_c	Combustor exhaust temperature at combustor exit (°R)
T_{MIX}	Bulk temperature of the fuel/air mixture at the engine exhaust (°R)
T_R	Gas stagnation temperature at the stack end of the augmentor tube (°R)
Q_e	Volume flow rate of gas at the engine exhaust ($\times 10^4$ in^3/sec.)
Q_s	Volume flow rate of gas at the stack exhaust ($\times 10^4$ in^3/sec.)
σ	Geometric standard deviation

ACKNOWLEDGMENTS

I am very grateful to Dr. David W. Netzer, Professor of Aeronautics, for his support, guidance, and technical expertise. As a thesis advisor, Dr. Netzer spent many after-hour periods with me in order to ensure the successful completion of this research project.

I would also like to thank Supervisory Aerospace Engineering Technicians Robert Besel and Ted Dunton and Electronics Technician Ray Garcia for their technical aid throughout my tour at the Naval Postgraduate School. Special thanks goes to Ronald Ramaker, Glen Middleton and Patrick Hickey for their technical support and aid in helping with the design and configuration of equipment used during this thesis.

Finally, I would like to thank my wife, Eileen, for her expert typing, eager help, and her unfaltering support in helping me through another trying time.

I. INTRODUCTION

The Navy utilizes jet engine test cells as a means of statically testing and evaluating the operating characteristics of high performance, turbojet engines. The test cells are large, permanent structures located at facilities where jet engine overhaul is performed. The primary advantage of using test cells is that the engine can be removed from the aircraft, overhauled, and then tested in a controlled environment prior to reinstallation aboard the aircraft. This technique of engine maintenance insures a high degree of engine reliability following major overhauls.

The Navy's use of jet engine test cells has come under close scrutiny by the Environmental Protection Agency (EPA) and some local pollution control boards in recent years. The chief concern involves the large amount of pollutants being produced by the engines while installed and operating in a test cell environment.

The EPA requirements initiate national guidelines for pollution control which may be augmented with further, more stringent requirements by local pollution control boards. Although military jet engines are exempt from pollution control requirements while installed and operating in an aircraft, they are subject to locally imposed requirements while operating in a test cell. Local standards of pollution

control imposed by the San Diego and Bay Area Pollution Control Districts have resulted in lawsuits against the Navy for its inability to meet these standards [Ref. 1]. Of primary concern is the large amount of smoke emitted from the engines while operating in the test cells. Future concerns will probably include emissions of the oxides of nitrogen. As technology has not yet advanced to the point of being able to produce pollution-free, high-performance engines for use in military aircraft, another means of reducing pollutant levels is necessary. Modifications to existing test cells are possible but are extremely expensive. As an easy, cost-effective solution, smoke suppressant fuel additives are being investigated to determine their overall effect on engine performance.

The research documented in the following pages describes an investigation into the effects of engine operating conditions (flow rates, fuel/air ratio, temperature) and the use of fuel additives as a means of controlling particulate emissions from jet engines operating in a test cell environment. Darnell [Ref. 2] initiated the program at the Naval Postgraduate School using a one-eighth scale turbojet test cell together with a dump combustor operated at a pressure of ten atmospheres. This investigation was a follow-on effort incorporating recommended changes to test procedures and apparatus.

Darnell [Ref. 2] attempted to measure exhaust particle size and concentration using a two frequency light transmission technique. A helium-neon laser and an argon-ion laser were used for light sources. The lasers were mounted in a building next to the test cell and the light beams were directed to the detector boxes using beam splitters and mirrors. Alignment of the source/detector units using this procedure was awkward and vibrations caused by running the engine made accurate measurements difficult.

In order to compensate for the above problems, the light sources were changed from lasers to collimated white light sources; and they were installed directly across from the detector boxes. This change greatly simplified alignment and insured measurement of the exhaust streams only. The detectors and collimated white light sources were mounted on freestanding platforms, separate from the test cell, to reduce vibrational problems. Since a white light source contains many frequencies of light, three narrow pass filters were installed in each detector unit to isolate specific frequencies. Only two frequencies are necessary for measurement purposes; the third frequency served as a redundant check on accuracy. It was felt that this technique would improve the reliability of the measurements significantly.

In order to verify measurements of particle size using the three frequency light transmission technique, it was

necessary to physically collect exhaust particulate matter and measure the particle sizes with a Scanning Electron Microscope (SEM). Darnell [Ref. 2] used impact particle collectors which were inserted directly into the exhaust streams. This technique proved unsatisfactory and made particle size measurement difficult since the particulate matter was distorted upon impacting the collector. In order to eliminate this problem, an improved dry impinger particle collection technique was implemented.

A large number of fuel additives have been developed and many have been tested by the Naval Air Propulsion Center to determine their effects on smoke production in turbojet engines. Those which proved to be most effective in reducing smoke output during tests were further evaluated by Darnell [Ref. 2] and during this investigation. Tests during this investigation were conducted using Ferrocene, 12% Rare Earth Hex-Chem, and 12% Cerium Hex-Chem.

During previous investigations at the Naval Postgraduate School the fuel additives were mixed directly with JP-4 and then pressure fed to the combustion chamber of the engine. This procedure was time-consuming as fuel tanks had to be drained and refilled each time fuel additives or concentrations were changed. In order to overcome this problem, precision metering pumps were added to the fuel system. The pumps allowed accurate fuel additive injection and provided

ease in changing fuel additive concentrations while the engine was operating.

The effects of smoke suppressant fuel additives upon the production of nitrogen oxides was also considered during this investigation. In particular, NO_x was monitored at the test cell stack exhaust to determine if the fuel additives produced any notable changes in the production of this gas.

II. EXPERIMENTAL APPARATUS

A. SUB-SCALE TURBOJET TEST CELL AND ENGINE

The test cell used during this investigation was a one-eighth scale model of an actual test cell located at the Naval Air Station in Alameda, California. It is fully documented in Refs. 3 and 4, and is also addressed by Darnell in Ref. 2. The test cell, shown in figure 1, has a ramjet type combustor which simulated the combustion chamber of a turbojet engine. The combustor is illustrated in figure 2 and fully documented in Ref. 5.

High pressure air supplied by a compressor was directed through the combustor where ignition and burning of the fuel/air mixture occurred. The hot, high pressure gases produced in the combustor were then directed through an exhaust pipe in the test cell where they were mixed with bypass air and exhausted through a converging nozzle. The nozzle directed the mixture of combustor exhaust gases and bypass air into an augmentor tube which was connected directly to an exhaust stack. The test cell augmentation ratio could be changed by varying the diameter of the augmentor tube, the engine-augmentor tube spacing, and/or the flow restrictions in the stack.

The engine inlet was simulated by using a six inch suction line which effectively pulled air in through the test

cell inlet. All air feed lines and the six-inch suction line were fitted with pneumatically controlled valves which provided precise metering of the flow rates through the test cell during engine operation. The pneumatically controlled valves were connected to a control panel to provide for remote operation of the valves and flow rates. By judiciously controlling the high pressure air, fuel flow, and the suction air, actual test cell conditions could be simulated for a variety of engine operating conditions.

B. FUEL SYSTEM

The fuel system consisted of a portable fuel supply, a remote control panel, and two precision metering pumps for fuel additive injection.

The portable fuel supply, shown in figure 3, consisted of two interconnected fuel tanks, a cavitating venturi for flow-rate control, and remotely controlled, electrically actuated solenoid valves. The fuel tanks were pressurized using gaseous nitrogen and a hand operated regulator located on the control panel (figure 4). Each tank was equipped with an electrically activated vent valve. A single fuel line connected both tanks to the combustor through an electrically operated shut-off valve. Fuel flow rate to the combustor was controlled by means of a cavitating venturi installed in the fuel line. The cavitating venturi allowed fuel flow adjustments by simply regulating the upstream

pressure in the fuel tanks. A calibration curve for fuel flow rate versus venturi pressure is shown in figure 5.

Two Eldex, Model E, precision metering pumps, shown in figure 6, were utilized for fuel additive injection into the fuel line just prior to the combustor. A swirl type mixer was incorporated to ensure that mixing of the fuel and additive occurred prior to the combustor. Each pump was capable of delivering between 0.2 and 5.0 ml./min. of fuel additive. The flow rate versus pump micrometer setting was pre-calibrated and the results are shown in figure 7.

C. TEST CELL INSTRUMENTATION AND DATA COLLECTION

The subscale test cell at the Naval Postgraduate School provides the opportunity for easy measurement of pressures and temperatures anywhere within the system during engine operation. Using standard ASME flow calculations [Ref. 6], mass flow rates anywhere within the test cell could be calculated. The pressure tap and temperature sensor locations used during this investigation are shown on a schematic of the test cell in figure 8.

All pressure lines were connected to an automatic-stepping Scanivalve with a 500-psi pressure transducer. Thermocouple leads from the temperature sensors and electrical leads from the Scanivalve were connected to HP-3495A scanners.

Automatic data acquisition and data processing were provided on demand by an HP-21 MX computer system. Data was acquired by systematically addressing the scanners and an HP-3455A digital voltmeter. The analog data were passed through an A/D converter and then processed by a computer program which provided flow rates and other pertinent system computations. Temperatures, pressures, flow rates, and other pertinent test cell data were then printed out.

During previous investigations of fuel additive effects on the production of smoke in turbojet engines, it was noted that the combustor exhaust temperature played a significant role. For this reason, it was desirable to have a permanent record of the combustor exhaust temperature for each fuel additive analyzed. To provide this record, a high temperature thermocouple was installed at the combustor exhaust and its output was connected to a strip chart recorder.

D. TRANSMISSOMETER

The transmissometer utilized during this study was a Leads and Northrop model 6597. The transmissometer consisted of a white light source, a detector unit and a signal conditioner/display unit. The white light source and the detector unit were mounted at the top of the test cell on opposite sides of the stack to provide readouts of exhaust

stream opacity. Figure 9 shows the source and detector and figure 4 shows the signal conditioner/display unit.

During this investigation, the transmissometer output was connected directly to a strip chart recorder, thus providing recorded values of exhaust opacity as the fuel additives were evaluated.

E. OPTICAL DETECTOR SYSTEM

The transmission of light through a cloud of uniform particles is derived from Bouguer's Law [Ref. 7]:

$$T = \exp(-QAnL) = \exp\left[-(3QC_m L/2\rho d)\right] \qquad (1)$$

where (T) is the fraction of light transmitted, (Q) is the dimensionless extinction coefficient, (A) is the cross sectional area of a particle, (n) is the number concentration of particles, (ρ) is the density of an individual particle, (L) is the path length the beam of light traverses, (C_m) is the mass concentration of particles, and (d) is the particle diameter.

From Bouguer's Law it is seen that the transmissivity of a beam of light decreases exponentially as the path length, particle concentration, and Q/d ratio increase.

Mie light scattering theory allows the extinction coefficient (Q) to be calculated as a function of particle size, wavelength of light and the complex refractive index of the particles.

In a paper presented by Dobbins [Ref. 8], Bouguer's Law was revised to allow for a distribution of particle sizes:

$$T = \exp[-(3\bar{Q}C_m L/2\rho d_{32})] \tag{2}$$

where $\bar{Q}$ represents an average extinction coefficient and d_{32} represents the volume-to-surface mean particle diameter. The average extinction coefficient can be calculated as a function of the particle size distribution, the wavelength of light, and the complex refractive index of the particles. Taking the natural logarithm of equation (2):

$$\ln[T] = \bar{Q}[-3C_m L/2\rho d_{32}] \tag{3}$$

Since the transmittance of a beam of light passing through an aerosol of polydisperse particles is directly related to the wavelength of the light, equation (3) can be written for a specific wavelength of light:

$$\ln[T_\lambda] = \bar{Q}_\lambda[-3C_m L/2\rho d_{32}] \tag{4}$$

For two wavelengths of light, the ratio of the natural logs of the transmittances is then given by:

$$\frac{\ln[T_{\lambda_1}]}{\ln[T_{\lambda_2}]} = \frac{\bar{Q}_{\lambda_1}}{\bar{Q}_{\lambda_2}} \tag{5}$$

where C_m, L, ρ, and d_{32} remain constant for both wavelengths. A Mie scattering computer program provided by K. L. Cashdollar of the Pittsburgh Mining and Safety Research Center,

Bureau of Mines allowed calculation of $\bar{Q}_\lambda$ and the $\bar{Q}_\lambda$ ratios as a function of d_{32} based on inputs of the complex refractive index of the particles, the refractive index of the surrounding medium, the standard deviation of the distribution and the wavelengths of light. During this investigation, the surrounding medium was assumed to be air with a refractive index of one. The complex refractive index and the standard deviation of the particle size distribution for the exhaust particulate were unknown. Most of the exhaust particulate can be reasonably assumed to be carbon. Therefore, a number of reasonable values for carbon [Ref. 7] were supplied as inputs to the computer program. Once $\bar{Q}_\lambda$, d_{32}, and T_λ are known, mass concentration can be calculated according to the following rearrangement of equation (3).

$$C_m = -\frac{2}{3}\left[\frac{\rho d_{32}}{\bar{Q}_\lambda L}\right] \ln T_\lambda \qquad (6)$$

In order to measure transmissivity, a collimated beam of white light was directed through the exhaust stream to a detector which split the light into three wavelengths. Light intensity was measured using linear photodiodes. Transmissivity was determined by comparing the percentage of photodiode output without particles present to the percentage of photodiode output with particles present. Only two values (two wavelengths) of transmittance are required to calculate d_{32} and C_m if the index of refraction and

standard deviation are known. The third wavelength provides for three ratios which can be used to determine three values of d_{32}. Various refractive indices and standard deviation combinations are tried until all three ratios provide the same d_{32}. This redundant calculation of d_{32} provides reasonable assurance that the correct index of refraction and standard deviation have been used [Ref. 7].

The light detectors, shown in figure 10, have a single entry point for the beam of collimated light, two beam splitters, three narrow pass filters, and three photodiodes. The entry point for the collimated light was a 0.25 inch I.D. tube fashioned to minimize forward scattered light effects [Ref. 7]. After the light entered the detector box, it was passed through two beam splitters which resulted in three separate beams of light. Each of the three beams of light was directed through a narrow pass filter and onto a photodiode. Neutral density filters were used to decrease the light intensity in order to prevent the photodiodes from being overdriven. Figure 11 is a schematic of the detector box and shows the paths followed by the light inside the detector.

The white light source was provided by a projector with a 750 watt incandescent bulb. By adjusting the lens on the projector, a nearly parallel beam of light was realized. In order to provide light of uniform intensity, a piece of

diffuser glass was placed between the projector lamp and the focusing lens. The nearly parallel source was then directed onto a 0.040 inch pinhole to develop a point source of light. The divergent beam of light exiting the pinhole was routed through a 31.5mm diameter achromatic lens with an 80mm focal length to provide collimated light. The collimated beam of light was then reduced to 0.50 inch diameter by passing it through a reducer tube. The collimated white light source is shown in figure 12.

Two source/detector systems were utilized during this investigation. One source/detector pair was mounted at the test cell stack exhaust and the other pair was mounted at the motor nozzle exhaust.

Alignment of the source/detector pairs was critical, and they were extremely sensitive to vibration during engine operation. To eliminate vibrational problems and the need for continuous realignment, the source/detector pairs were permanently mounted on free-standing platforms separate from the test cell.

Aluminum covers were fabricated to prevent dust and moisture from entering the circuitry and affecting the optics. To further preclude moisture from the systems, heaters in the form of 15 watt light bulbs were utilized to keep the inside of the covers dry.

The detector unit mounted at the stack exhaust incorporated narrow pass filters of 10140, 6500, and 4500

angstroms while the combustor exhaust unit incorporated filters of 10000, 6943, and 4000 angstroms. It was necessary to use filters separated by at least 2000 angstroms to insure accurate transmittance ratios.

The output of each detector unit was connected to a strip chart recorder to provide real time visual indications and records of fuel additive effects during engine operation.

F. EXHAUST PARTICLE COLLECTION

In order to provide a means of physically collecting exhaust particulate matter, a dry impinger collection train was implemented [Ref. 9]. The sampling train, shown in figure 13, was composed of a sampling tube located at the combustor exhaust, a collection box with six sample holders, and a vacuum pump with in-line filters and control valves. The sampling tube, shown in figure 14, was made of 0.25 inch inner diameter stainless steel and was located in the center of the augmentor tube, aft of the combustor exhaust. In order to minimize flow distortion about the sampling tube, it was necessary to remove samples of exhaust gas and particulate matter iso-kinetically. A sonic choke was used to regulate the flow rate through the sampling train. A vacuum pump supplied the pressure differential necessary for proper operation of the sonic choke.

The sample box was designed so that up to six samples of exhaust particulate could be taken during engine operation. Collection times were manually controlled by opening and closing the sliding doors covering each sample holder at ten to twenty second time intervals. An in-line filter prevented clogging of the sonic choke and ingestion of exhaust particulate by the vacuum pump.

G. NITROGEN OXIDES ANALYZER

A Monitor Labs, Model 8440 E, Nitrogen Oxides Analyzer shown in figure 15 was used to determine fuel additive effects on NO_x production during engine operations. The analyzer is fully described in Ref. 10.

Test cell exhaust gas was sampled using a stainless steel probe mounted on the stack cover. The gas sample was routed through a twelve inch Mott Inertial Filter which removed particulate matter greater than 0.5 microns in diameter. From the filter, teflon tubing was utilized to route the gas to the analyzer.

III. EXPERIMENTAL PROCEDURE

Initially, all test equipment was turned on and allowed to warm up. This was done to insure that the measurement and recording devices were functioning properly and also to eliminate condensation which might have formed on the optics of the transmissometer and the optical detector system.

After the initial warm-up period, the optical detector systems and the transmissometer were checked to insure that the alignment between sources and detectors had not been disturbed. The transmissometer was checked by insuring that a zero and a one hundred percent opacity reading were realizable. The optical detector system was checked by measuring the maximum detector outputs and comparing them to output data taken when the system was first installed and aligned.

Once it was evident that the measurement equipment outputs were reliable and correct, air pressures within the test cell were adjusted. Using the remote control cart (figure 16) located near the computer console, pneumatically actuated valves in the six-inch suction line and the three high-pressure lines were opened. The computer then analyzed test cell conditions and a printout of test cell pressures, temperatures, and flow rates was provided. The pneumatically

actuated valves were manipulated until desired test cell conditions and flow rates were set.

The air flowing through the test cell caused the optical detector system outputs to decrease and the opacity reading from the transmissometer to increase slightly. In order to obtain test results due to exhaust particulate only, the transmissometer was rezeroed and the new one hundred percent transmittance point for each output of the optical detector systems was marked on the strip chart recorders.

With final adjustments made, the fuel tank/cavitating venturi pressure was adjusted to provide the desired fuel flow rate (figure 5). An oxygen/ethylene ignition torch was used to ignite the JP-air mixture within the combustor.

Once the desired combustor exhaust temperature was achieved through manipulation of the fuel flow rate, and steady state outputs were obtained, a particulate sample and data were taken. In all tests conducted during this investigation values for fuel tank pressure, venturi pressure, NO_x concentration, opacity, and combustor exhaust temperature were manually recorded. The latter two were also recorded by a strip-chart recorder. Once JP-4 data were obtained, the fuel additive pumps were activated. Additive flow rates were adjusted until minimum opacity readings occurred. Data were recorded at each pump setting and a particulate sample was collected when the minimum opacity readings occurred. After data collection was

completed, and the engine had been shut down, post-run zeros and one hundred percent points were marked on the strip chart recordings to insure that alignment of the optical measuring equipment had not changed.

In order to standardize the experimental investigation of fuel additive effects on smoke production, the fuel flow rates and air mass flow rates were set to the same values each time a test was conducted. Nominal values for test cell air mass flow rates were:

6 inch suction line ------ 1.031 (lbm/sec)
3 inch bypass line ------- .939 (lbm/sec)
Combustor primary air ---- .281 (lbm/sec)
Combustor secondary air -- .198 (lbm/sec)

These settings provided a test cell augmentation ratio of 3.95 and an augmentor tube mass flow rate of 7.025 (lbm/sec) with the nominal flow resistance grid installed in the exhaust stack. The cavitating venturi pressure was normally set at 560 psig to insure a fuel flow rate of .0169 (lbm/sec) and a combustor exhaust temperature of 2010°R.

The particulate samples collected during each test were analyzed for particle size using a scanning electron microscope and the results were used to verify data obtained from the outputs of the optical detector systems.

IV. RESULTS AND DISCUSSION

A. INTRODUCTION

Four series of tests were conducted during this investigation. Two series of tests were completed using Ferrocene; one on 10 November 1981 and the other on 19 November 1981. The tests using 12% Cerium Hex-Chem and 12% Rare Earth Hex-Chem were both conducted on 19 November 1981.

The data collected during this investigation are summarized in tables I and II. Recorded data and data reduced from strip chart recordings are summarized in tables III, IV, and V. A typical set of strip chart recordings is shown in figures 39-42. To supplement the information presented in tables I-V, pertinent data from these tables are presented graphically in figures 17-22. SEM photographs of exhaust particulate collected during the fuel additive tests are shown in figures 43-52.

All data presented should be analyzed for trends and averages vice specific point data since the sampling technique did not average the momentary changes in test cell air flow rates caused by compressor fluctuations. As an example, figure 17 shows the discrete data for combustor fuel/air ratio connected by a series of straight lines. A least-squares polynomial fit of the discrete points results

in an average combustor fuel/air ratio shown by the dashed line.

Figure 17 implies that significant changes in stack gas opacity and engine exhaust particulate mass concentration (C_{m_e}) result from small changes in combustor fuel/air ratio $(f/a)_c$. Combustor exhaust temperature (T_c) and combustor fuel/air ratio are directly related and both serve as good indicators of overall engine operating conditions.

In an effort to determine the effects of fuel additives and test cell operating conditions on opacity, and average particle size (D_{32}) and mass concentration; run-to-run variations in combustor exhaust temperature were considered in analysis of the data presented in figures 17-22. If T_c remained constant, changes in opacity, etc. should be due primarily to varying fuel additive concentrations.

B. ADDITIVE EFFECTS ON STACK GAS OPACITY

Figure 18 summarizes the effects of additive concentration on stack gas opacity for each fuel additive tested. For additive concentrations of zero, the points plotted actually represent the average value of opacity taken before and after the fuel additive test. Ferrocene and 12% Cerium Hex-Chem produced significant decreases in test cell stack opacity for additive concentrations between twenty and thirty milliliters per gallon of JP-4. The additive 12% Rare Earth Hex-Chem did not work well as the stack opacity

actually increased as the additive concentration was increased.

Ferrocene was tested on two separate days with slightly different test cell operating parameters. The tests on 10 November were conducted at a slightly higher combustor exhaust temperature than the tests on 19 November. Increasing combustor exhaust temperature tends to decrease the opacity and this is why one curve appears lower than the other on figure 18. However, the effects of ferrocene were about the same on both days with a twenty-five to thirty percent maximum decrease in opacity.

The 12% Cerium Hex-Chem additive was also tested on 19 November with essentially the same results as Ferrocene. The curve in figure 18 is lower than for Ferrocene, partly due to the higher combustor exhaust temperatures during the test.

To summarize, 12% Rare Earth Hex-Chem increased stack gas opacity rather than decreasing it. Considering variations in test cell operating conditions, Ferrocene and 12% Cerium Hex-Chem additives both decreased opacity about twenty-five to thirty percent for additive concentrations between twenty and thirty milliliters per gallon of JP-4.

C. ADDITIVE EFFECTS ON D_{32}

Using the three transmittance values derived from the strip chart recordings (Table III), three extinction

coefficient ratios were determined for each fuel additive concentration tested. With the use of the Mie Scattering computer program outputs and equation 5, three D_{32} values were determined for each additive concentration for a specific complex refractive index and standard deviation. Sample outputs of the computer program are included as figures 23-38. The refractive indices and standard deviations used in these figures were the only ones which provided consistent D_{32} values (from the three transmittance ratios) throughout this investigation. An average value of $D_{32} \pm .03$ microns was used as the basis for accepting data derived in the above manner. The derived values for engine and stack exhaust mean particle diameter (D_{32}) are shown in Table IV. Stack values are also presented graphically in figures 19-22.

Throughout this investigation D_{32} varied between .18 and .24 microns with an average value of about .21 microns. Considering the inaccuracies in measurements of the transmittance values, .18 to .24 microns was not considered a significant change in average particle diameter. For this reason, it is felt that the particle diameters remained essentially the same throughout all the tests and that varying additive concentrations had no significant effect on D_{32}. The data presented in table IV also indicated that no variations in particle diameter occurred between the engine exhaust and the stack exhaust.

D. ADDITIVE EFFECTS ON MASS CONCENTRATION

Using the derived D_{32} values from table IV, figures 23-38 were entered to determine a value for the extinction coefficient ($\overline{Q}_\lambda$) at each wavelength of light analyzed. The curve used in determining $\overline{Q}_\lambda$ had the same complex refractive index and standard deviation as the curves used to obtain D_{32}. Equation 6 was then used to calculate a mass concentration value at each wavelength. The value for particle density was assumed to be 1.5 gm/cm^3. The value for L was .762 meters at the stack exhaust and .0498 meters at the engine exhaust. Calculated values of concentration are less accurate than D_{32} values due to the uncertainty in both ρ and $\overline{Q}$. Table IV lists the results for wavelengths of 10000 Angstroms (engine exhaust) and 10140 Angstroms (stack exhaust). The mass concentrations obtained using the other wavelengths were essentially the same and are not included. Engine and stack mass concentration values are also plotted in figures 19-22.

The mass concentrations at the engine and stack exhausts were significantly affected by the fuel additive concentrations and also by variations in the combustor operating conditions. As the combustor exhaust temperature increased, the mass concentration decreased and vice versa (Figure 17). For approximately constant combustor conditions, Ferrocene and 12% Cerium Hex-Chem tended to decrease the mass concentrations for additive concentrations between twenty and

thirty milliliters per gallon of JP-4 while 12% Rare Earth Hex-Chem tended to increase the mass concentration as additive concentration was increased.

Since there was a significant decrease in particulate mass concentration between the engine exhaust and the stack exhaust, mass flow rates of particulate at the engine and stack were calculated to determine if the decrease was due in part to chemical reactions within the test cell or due strictly to the dilution by augmentation air. The particulate mass flow rates can be written as:

$$\dot{m}_{c_e} = C_{m_e} Q_e \tag{7}$$

$$\dot{m}_{c_s} = C_{m_s} Q_s \tag{8}$$

Q is the volume flowrate which can be calculated assuming perfect gases from

$$Q = AV = \frac{\dot{m}RT}{P} \tag{9}$$

at the engine and stack exhausts. The following assumptions were made in these calculations.

$$R = R_{AIR} = 53.3 \text{ ft-lbf/lbm-}^\circ\text{R}$$

$$P = P_{engine} = P_{stack} = 14.7 \text{ PSI}$$

$$\dot{m}_{engine} = \dot{m}_P + \dot{m}_s + \dot{m}_{BP}$$

$$\dot{m}_{st} = \dot{m}_{stack} = \dot{m}_{augmentor\ tube}$$

$$T_{stack} = T_R$$

$$T_{engine} = T_{MIX} = \frac{\dot{m}_{BP} T_{BP} + \dot{m}_e T_2}{\dot{m}_{e_T}}$$

The particulate mass flow rates were then ratioed:

$$\frac{\dot{m}_{c_e}}{\dot{m}_{c_s}} = \frac{C_{m_e} Q_e}{C_{m_s} Q_s} = \frac{C_{m_e} \dot{m}_e T_{MIX}}{C_{m_s} \dot{m}_{ST} T_R} \qquad (10)$$

Within the limitations of the above approximations, a ratio of 1.0 would indicate that there was no change in the mass flow rates of particulate between the engine and stack exhaust; therefore, any decrease in mass concentration at the stack would be due strictly to dilution of the exhaust particulate with augmentation air. Table V presents these ratios and the general results indicate (within the limited accuracy of the calculations) that no significant chemical reactions involving the particulates occured within the augmentor tube or exhaust stack.

In summary, fuel additives and increased engine operating temperature decreased the mass concentration of exhaust particulates, and the decrease in mass concentration between the engine exhaust and stack exhaust was due primarily to dilution of the engine exhaust gases within the augmentor tube.

E. ADDITIVE EFFECTS ON NO_x CONCENTRATION

Values for NO_x concentration measured at the stack exhaust are included in table III. None of the additives

produced any significant change in NO_x concentrations at the stack exhaust.

F. SEM ANALYSIS OF ENGINE EXHAUST PARTICULATE SAMPLES

Scanning electron microscope photographs of engine exhaust particulate collected during tests with JP-4 only are shown in figures 43 and 44. The variation in particle diameters exhibited in these photographs is of particular interest. Figures 43 and 44 show individual particle sizes varying from about .05 microns up to about .40 microns. D_{32} values determined using the light transmission technique represent the volume-to-surface mean particle diameter based on a specific log-normal distribution. As an example, a D_{32} value of .21 microns, derived using a complex refractive index of 1.8-.60i and a geometric standard deviation of 2.0, is the mean of the distribution. The tails of the distribution for this case were .031 microns and 1.20 microns. Therefore, particle sizes inside the tails of the distribution are to be expected in varying amounts. The predominant particle size should occur around the mean and this appears to be the case for both figures 43 and 44. The optical detector system provided values of .20 and .21 microns for tests conducted using JP-4 only.

Figure 43 also shows large agglomerations of particles but it is not known whether they formed within the combustor/tailpipe or whether they formed during the sampling process.

Figures 45 and 46 are SEM photographs of particles collected during fuel additive tests with Ferrocene on 10 November 1981. The fuel additive concentration was 32.30 ml./gal. JP-4. A D_{32} value was not calculated from the photographs but the particle sizes in the photographs appear to be very similar to those in figures 43 and 44.

Figures 47 and 48 are photographs of particles collected during tests on 19 November 1981 with a Ferrocene concentration of 19.20 ml./gal. JP-4 and figures 49 and 50 are photographs of particles collected during the same tests with a Ferrocene concentration of 28.80 ml./gal. JP-4. The photographs again indicate no significant change in particle diameters when compared with the photographs with no additives (Figures 43-44).

Figures 51 and 52 are photographs of particles collected during tests with 12% Cerium Hex-Chem. The additive concentration was 19.60 ml./gal. JP-4. Although there were fewer particles in these particular photographs, there did not seem to be a significant change in mean particle diameter when compared with the photographs of the other samples.

Particle samples were not taken during the tests using 12% Rare Earth Hex-Chem. This additive did not reduce opacity, and it was felt a sample would provide no useful data.

Overall, the SEM photographs indicate that the values of D_{32} determined using light transmission measurement were

reasonably accurate representations of the actual average particle sizes. No attempt was made to determine D_{32} from the photographs because of the probable effects of the collection method on the sizes collected and on the agglomeration processes.

V. SUMMARY OF RESULTS

From the data collected during this investigation, it appears that variations in test cell exhaust opacity were due primarily to changes in exhaust particle mass concentration rather than to changes in exhaust particulate size. Increased combustor temperature and the effective fuel additives both reduced the amount of particulate matter. The effects of increasing augmentation ratio were to simply dilute the exhaust stream, reducing opacity but not changing particulate mass or size.

The optical determination of mean particulate size at the engine and stack exhausts appears to be a good and reasonably accurate technique for evaluating the effects of engine and test cell operating conditions and fuel composition changes on the emitted particulates.

TABLE I

TEST CELL FLOW RATES DURING ADDITIVE TESTS

ADDITIVE/ CONCENTRATION (ml./gal. JP-4)	$\dot{m}_{BP}$	$\dot{m}_P$	$\dot{m}_s$	$\dot{m}_e$	$\dot{m}_{e_T}$	$\dot{m}_f$	$\left(\frac{f}{a}\right)_P$	$\left(\frac{f}{a}\right)_{p+s}$
*FERROCENE/ 0.0	.830	.268	.186	.454	1.284	.0168	.0627	.0370
*FERROCENE/22.70	.830	.268	.186	.454	1.284	.0168	.0627	.0370
*FERROCENE/25.90	.830	.268	.186	.454	1.284	.0168	.0627	.0370
*FERROCENE/29.10	.830	.268	.186	.454	1.284	.0168	.0627	.0370
*FERROCENE/32.30	.830	.268	.186	.454	1.284	.0168	.0627	.0370
FERROCENE/ 0.0	.810	.254	.154	.408	1.218	.0170	.0671	.0418
FERROCENE/19.20	.850	.255	.190	.445	1.294	.0170	.0668	.0383
FERROCENE/28.80	.829	.248	.169	.417	1.246	.0170	.0687	.0409
FERROCENE/ 0.0	.842	.247	.178	.425	1.267	.0170	.0690	.0401
12% CERIUM HEX-CHEM/ 0.0	.834	.249	.175	.424	1.258	.0168	.0673	.0395
12% CERIUM HEX-CHEM/19.60	.822	.250	.183	.433	1.254	.0168	.0670	.0387
12% CERIUM HEX-CHEM/29.30	.831	.255	.185	.444	1.275	.0168	.0657	.0377
12% CERIUM HEX-CHEM/48.90	.831	.255	.189	.444	1.275	.0168	.0657	.0377
12% RARE EARTH HEX-CHEM/ 0.0	.886	.244	.194	.438	1.324	.0172	.0705	.0393
12% RARE EARTH HEX-CHEM/19.10	.871	.270	.185	.455	1.326	.0172	.0637	.0378
12% RARE EARTH HEX-CHEM/47.60	.899	.252	.155	.407	1.306	.0172	.0682	.0422
12% RARE EARTH HEX-CHEM/ 0.0	.899	.252	.155	.407	1.306	.0172	.0682	.0422

*Data taken on 10 November 1981; all other data collected on 19 November 1981. See table of symbols and abbreviations for explanation of column headings/units.

TABLE II

TEST CELL FLOW RATES/TEMPERATURES DURING ADDITIVE TESTS

ADDITIVE CONCENTRATION (ml./gal. JP-4)	$\dot{m}_{aug.\ T.}$	AUG. RATIO	T_{BP}	T_2	T_R	T_{MIX}	T_C
*FERROCENE/ 0.0	7.406	4.77	608	1910	642	1068	2048
*FERROCENE/22.70	7.406	4.77	608	1910	642	1068	2058
*FERROCENE/25.90	7.406	4.77	608	1910	642	1068	2013
*FERROCENE/29.10	7.406	4.77	608	1910	642	1068	2067
*FERROCENE/32.30	7.406	4.77	608	1910	642	1068	2008
FERROCENE/ 0.0	7.453	5.12	610	1900	649	1042	2017
FERROCENE/19.20	7.416	4.73	609	1890	639	1049	1997
FERROCENE/28.80	7.484	5.01	608	1890	641	1037	2012
FERROCENE/ 0.0	7.274	4.74	571	1855	616	1002	1972
12% CERIUM HEX-CHEM/ 0.0	7.239	4.76	609	1900	643	1044	2026
12% CERIUM HEX-CHEM/19.60	7.266	4.79	609	1920	644	1061	2035
12% CERIUM HEX-CHEM/29.30	7.252	4.69	610	1920	643	1066	2035
12% CERIUM HEX-CHEM/48.90	7.252	4.69	610	1920	643	1066	2040
12% RARE EARTH HEX-CHEM/ 0.0	7.464	4.64	607	1885	642	1030	2022
12% RARE EARTH HEX-CHEM/19.10	7.469	4.63	607	1880	640	1044	2022
12% RARE EARTH HEX-CHEM/47.60	7.521	4.76	607	1885	640	1005	2022
12% RARE EARTH HEX-CHEM/ 0.0	7.521	4.76	607	1880	640	1004	2022

*Data collected on 10 November 1981; all other data collected on 19 November 1981. See table of symbols and abbreviations for explanation of column headings/units.

TABLE III

STACK GAS OPACITY, NO_x CONCENTRATIONS, AND TRANSMITTANCE VALUES

ADDITIVE/ CONCENTRATION (ml./gal. JP-4)	PERCENT OPACITY	NO_x	T_λ 10140	T_λ 6500	T_λ 4500	T_λ 10000	T_λ 6943	T_λ 4000
*FERROCENE/ 0.0	39.00	-	86.20	79.00	73.80	95.00	93.10	88.50
*FERROCENE/22.70	28.80	-	90.70	85.40	81.20	96.10	96.90	92.30
*FERROCENE/25.90	28.80	-	93.80	89.10	85.40	97.50	96.40	94.60
*FERROCENE/29.10	23.70	-	93.80	89.50	86.40	99.10	98.10	96.40
*FERROCENE/32.30	42.00	-	89.20	83.50	78.60	97.80	97.70	94.80
FERROCENE/ 0.0	41.20	2.0	84.10	76.40	69.40	94.90	93.60	90.40
FERROCENE/19.20	34.90	2.0	86.30	80.10	74.20	95.70	94.20	91.70
FERROCENE/28.80	33.00	2.0	83.10	75.70	68.50	95.40	93.60	90.40
FERROCENE/ 0.0	50.30	2.0	78.40	69.90	61.80	93.90	91.70	88.40
12% CERIUM HEX-CHEM/ 0.0	44.70	1.7	84.20	76.40	64.90	96.40	94.70	92.40
12% CERIUM HEX-CHEM/19.60	28.10	1.9	88.00	81.60	76.10	96.70	95.00	92.40
12% CERIUM HEX-CHEM/29.30	33.60	1.9	88.30	82.30	77.00	97.20	95.60	93.10
12% CERIUM HEX-CHEM/48.90	33.90	2.0	87.20	80.90	75.80	97.20	95.40	92.30
12% RARE EARTH HEX-CHEM/ 0.0	48.10	2.0	80.30	71.20	63.30	94.70	92.40	88.20
12% RARE EARTH HEX-CHEM/19.10	56.90	1.6	76.40	66.30	58.00	93.40	90.90	86.50
12% RARE EARTH HEX-CHEM/47.60	53.60	1.7	78.20	68.80	61.30	93.40	91.50	87.20
12% RARE EARTH HEX-CHEM/ 0.0	49.50	1.9	79.70	71.50	65.00	94.40	92.40	88.70

*Data collected on 10 November 1981; all other data collected on 19 November 1981.
-Data not available
See table of symbols and abbreviations for explanation of column headings/units.

TABLE IV

MEAN PARTICLE DIAMETERS (D_{32}) AND MASS CONCENTRATIONS (C_m) FOR EACH TEST

ADDITIVE/ CONCENTRATION (ml./gal. JP-4)	D_{32} STACK EXHAUST (10140/6500/4500)	D_{32} ENGINE EXHAUST (10000/6943/4000)	C_{ms} STACK (10140)	C_{me} ENGINE (10000)
*FERROCENE/ 0.0	.21 ± .01 ; b,d	----------	40.30	-----
*FERROCENE/22.70	.20 ± .005; d	----------	26.90	-----
*FERROCENE/25.90	.20 ± .004; c	.21 ± .01; b,d	17.50	103.3
*FERROCENE/29.10	.22 ± .003; a,c	----------	16.60	-----
*FERROCENE/32.30	.20 ± .003; b	----------	33.50	-----
FERROCENE/ 0.0	.20 ± .02 ; b	----------	51.10	-----
FERROCENE/19.20	.22 ± .03 ; b,d	.24 ± .02; d	40.00	178.0
FERROCENE/28.80	.21 ± .03 ; b,d	.21 ± .02; b,d	54.20	205.0
FERROCENE/ 0.0	.23 ± .03 ; b	.24 ± .01; d	70.40	254.1
12% CERIUM HEX-CHEM/ 0.0	----------	.21 ± .01; d	-----	149.8
12% CERIUM HEX-CHEM/19.60	.19 ± .001; b	.18 ± .01; b,d	37.80	152.7
12% CERIUM HEX-CHEM/29.30	.20 ± .01 ; b,d	.21 ± .01; a,c	34.10	122.6
12% CERIUM HEX-CHEM/48.90	.22 ± .003; b	.19 ± .01; a,c	39.90	128.2
12% RARE EARTH HEX-CHEM/ 0.0	.20 ± .01 ; b	.20 ± .02; b,d	64.40	242.9
12% RARE EARTH HEX-CHEM/19.10	.22 ± .01 ; b	.22 ± .03; b,d	78.10	299.9
12% RARE EARTH HEX-CHEM/47.60	.22 ± .01 ; b,d	----------	66.70	-----
12% RARE EARTH HEX-CHEM/ 0.0	.24 ± .02 ; b,d	.23 ± .03; b,d	65.40	251.6

Key to complex refractive index/standard deviation:
a) m = 1.80-.60i/1.5 b) m = 1.80-.60i/2.0
c) m = 1.95-.66i/1.5 c) m = 1.95-.66i/2.0

*Data collected on 10 November 1981; all other data collected on 19 November 1981.
-Data not available.
See table of symbols and abbreviations for explanation of column headings/units.

TABLE V

TEST CELL VOLUME FLOW RATES AND PARTICULATE MASS FLOW RATES/RATIOS FOR EACH ADDITIVE TEST

ADDITIVE/ CONCENTRATION (ml./gal. JP-4)	Q_e	Q_s	$\dot{m}_{ce}$	$\dot{m}_{cs}$	$\left[\frac{\dot{m}_{ce}}{\dot{m}_{cs}}\right]$
*FERROCENE/ 0.0	5.97	20.69	-----	8.35	----
*FERROCENE/22.70	5.97	20.69	-----	5.56	----
*FERROCENE/25.90	5.97	20.69	6.16	3.61	1.70
*FERROCENE/29.10	5.97	20.69	-----	3.43	----
*FERROCENE/32.30	5.97	20.69	-----	6.94	----
FERROCENE/ 0.0	5.52	21.04	-----	10.75	----
FERROCENE/19.20	5.91	20.63	10.51	8.25	1.27
FERROCENE/28.80	5.62	20.88	11.53	11.31	1.02
FERROCENE/ 0.0	5.52	19.51	14.04	13.73	1.02
12% CERIUM HEX-CHEM/ 0.0	----	-----	-----	-----	----
12% CERIUM HEX-CHEM/19.60	5.79	20.35	8.84	7.70	1.15
12% CERIUM HEX-CHEM/29.30	5.91	20.28	7.25	6.90	1.05
12% CERIUM HEX-CHEM/48.90	5.91	20.28	7.58	8.09	0.94
12% RARE EARTH HEX-CHEM/ 0.0	5.93	20.86	14.41	13.44	1.07
12% RARE EARTH HEX-CHEM/19.10	6.02	20.81	18.06	16.24	1.11
12% RARE EARTH HEX-CHEM/47.60	----	-----	-----	-----	----
12% RARE EARTH HEX-CHEM/ 0.0	5.71	20.95	14.35	13.70	1.05

*Data collected on 10 November 1981; all other data collected on 19 November 1981.
-Data not available.
See table of symbols and abbreviations for explanation of column headings/units.

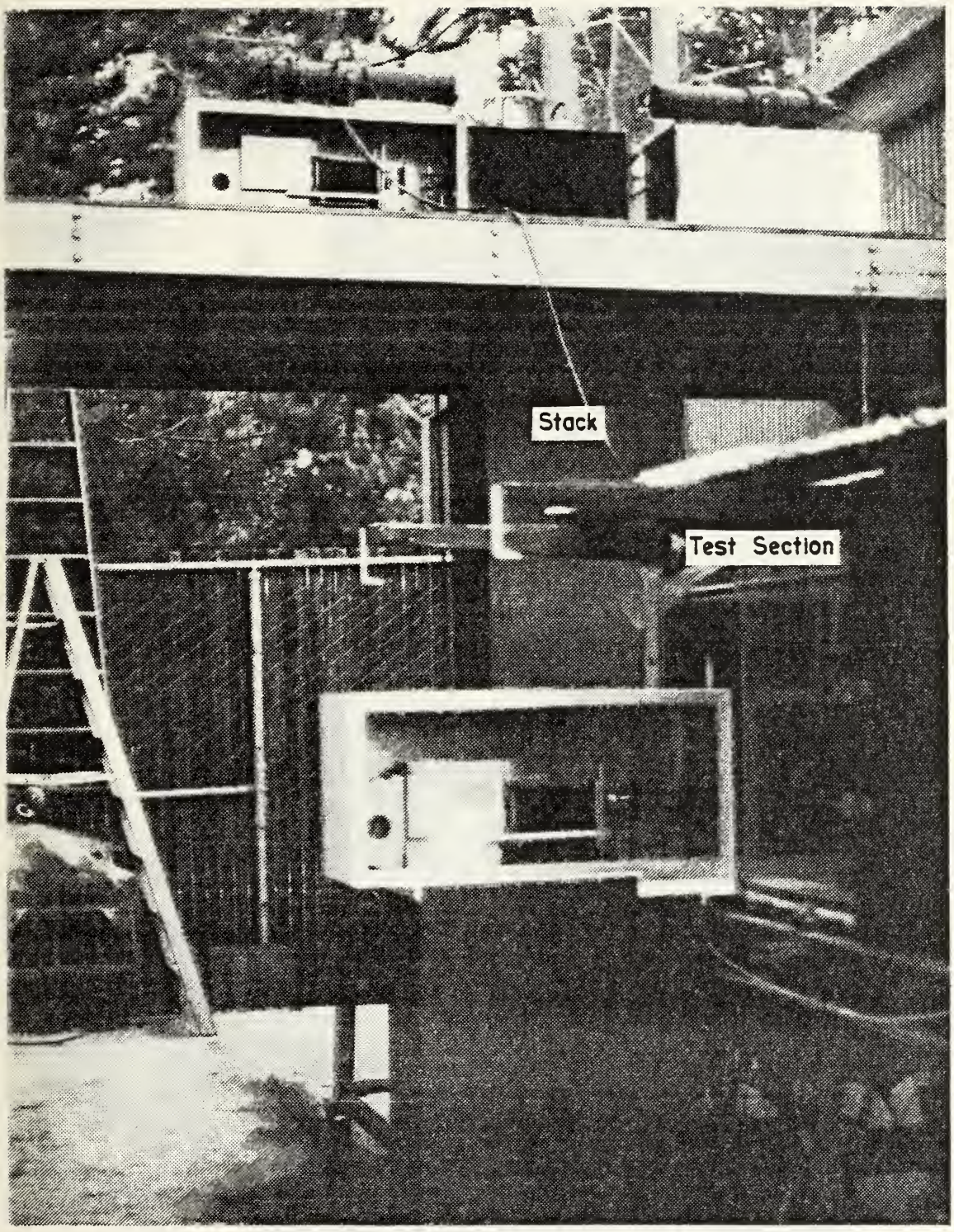

Figure 1. Sub-Scale Turbojet Test Cell

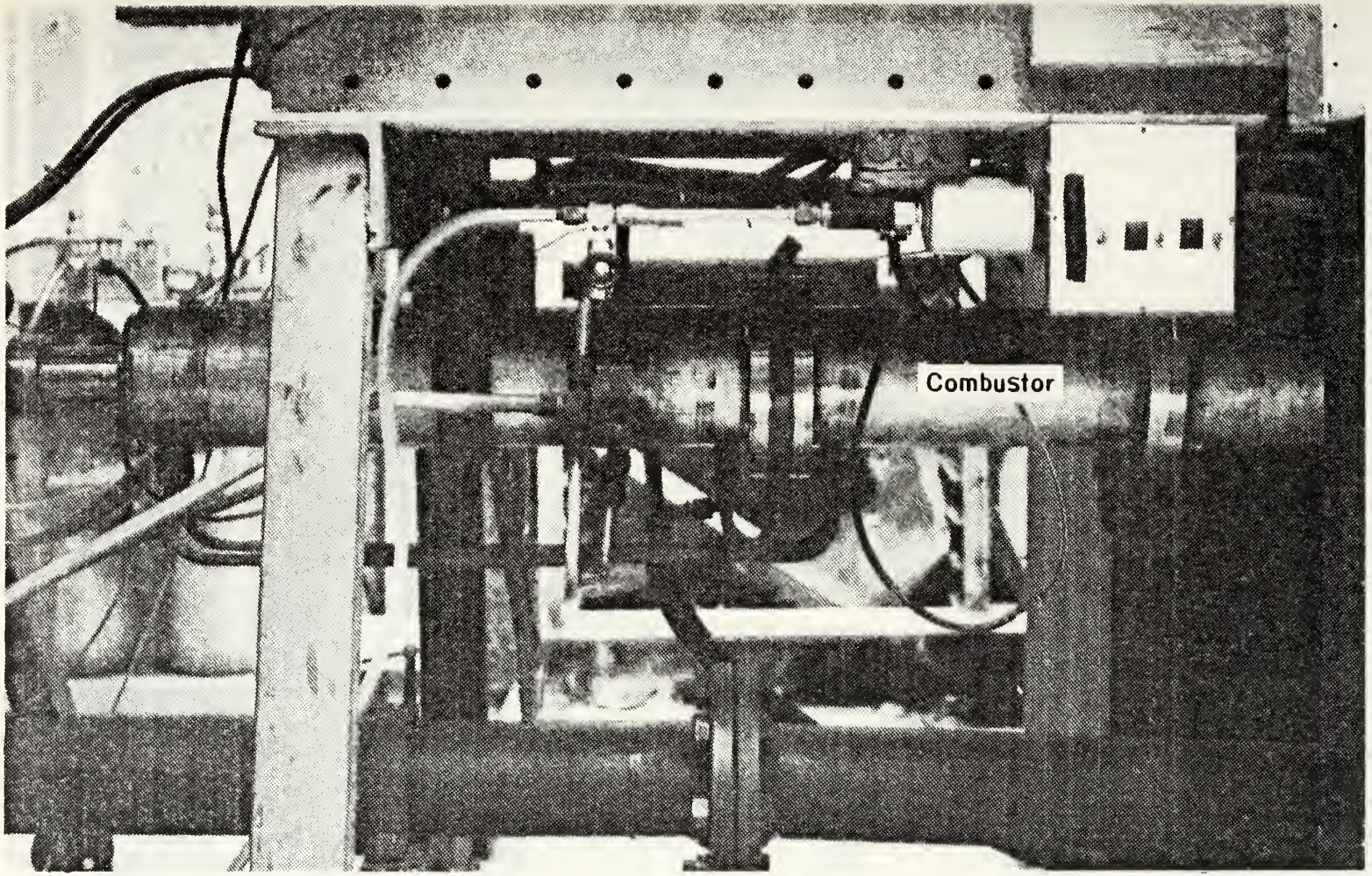

Figure 2. Sub-Scale Turbojet Test Cell Combustor

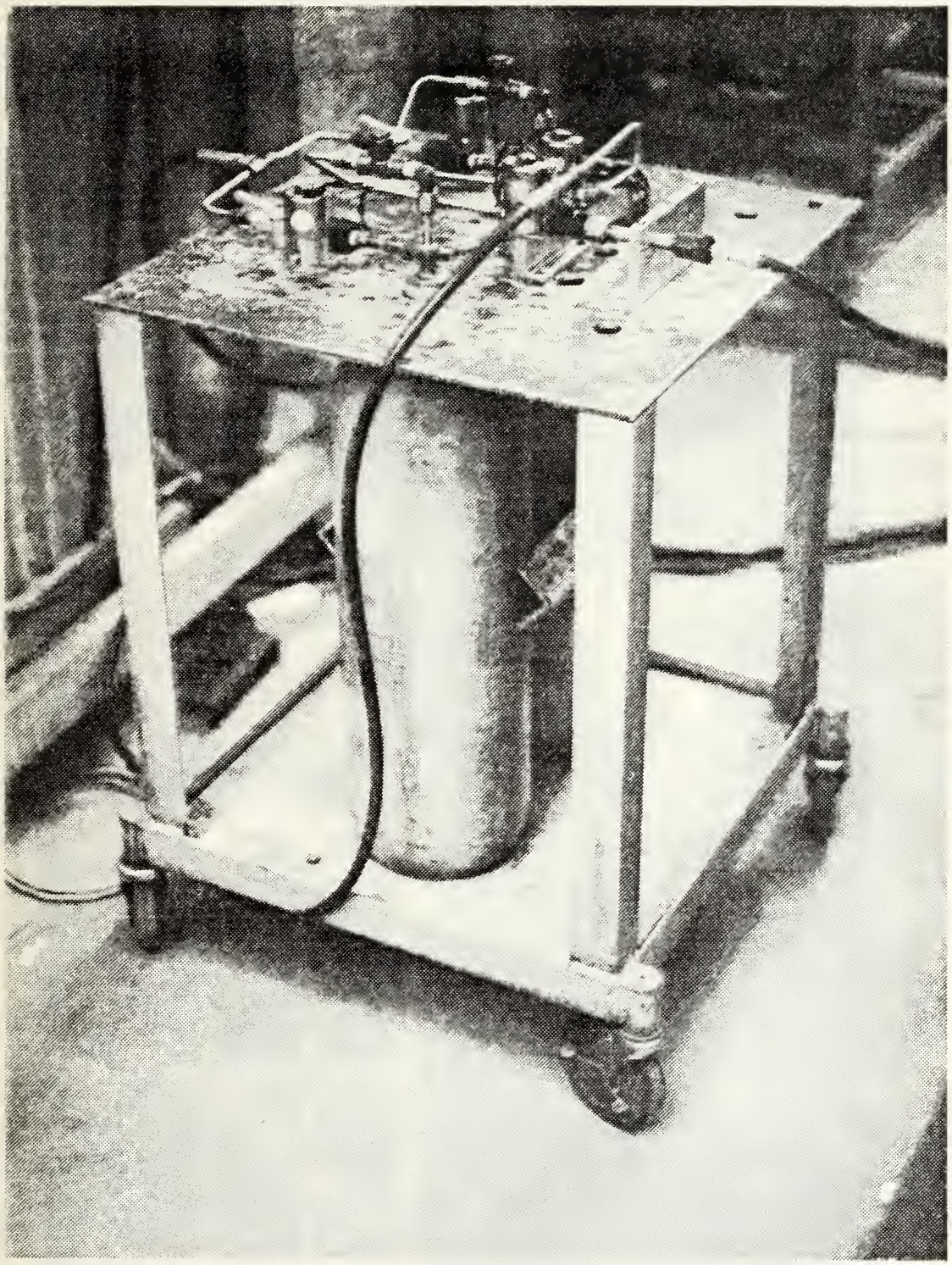

Figure 3. Portable Fuel Supply System

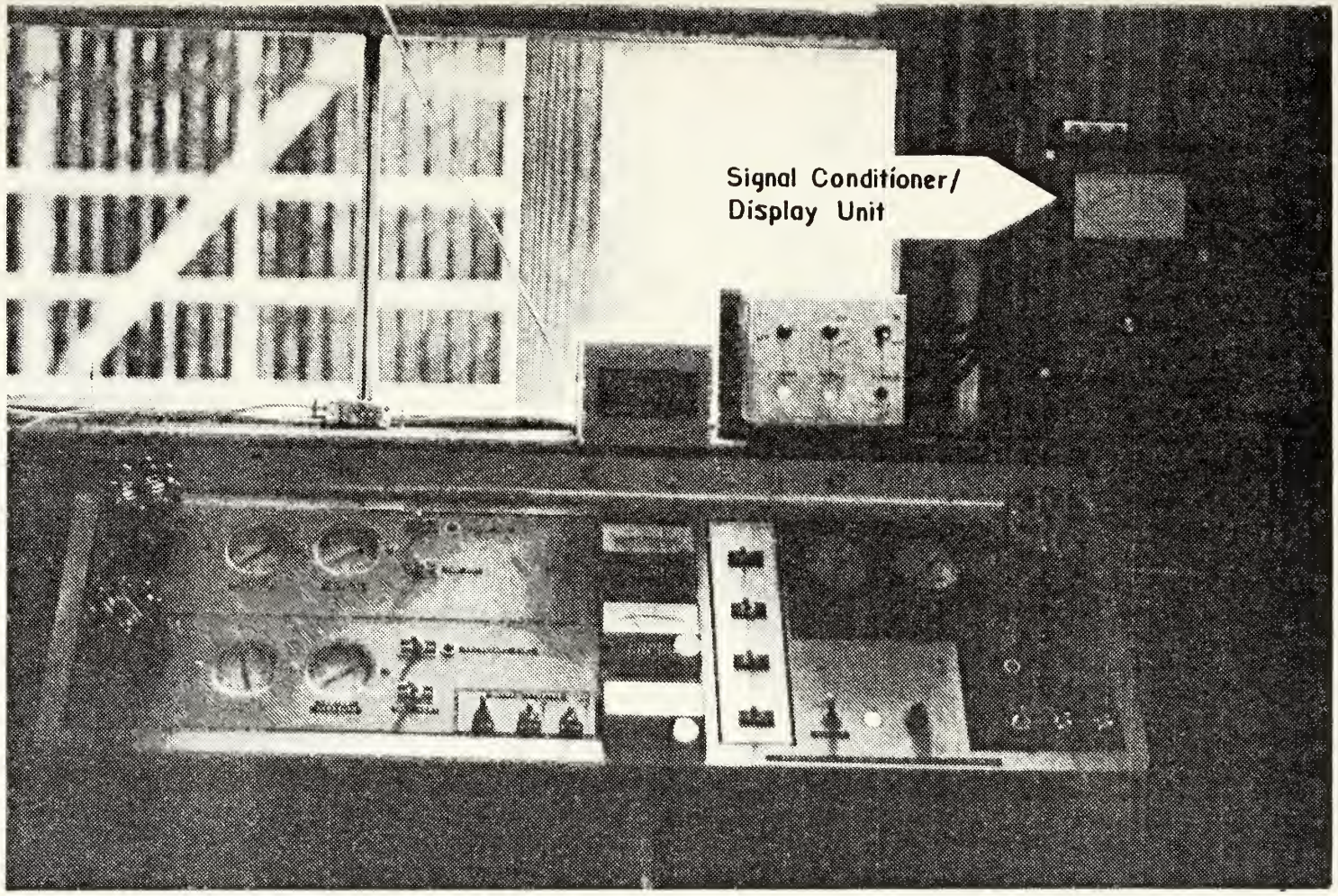

Figure 4. Remote Control Panel and Signal Conditioner/Display Unit

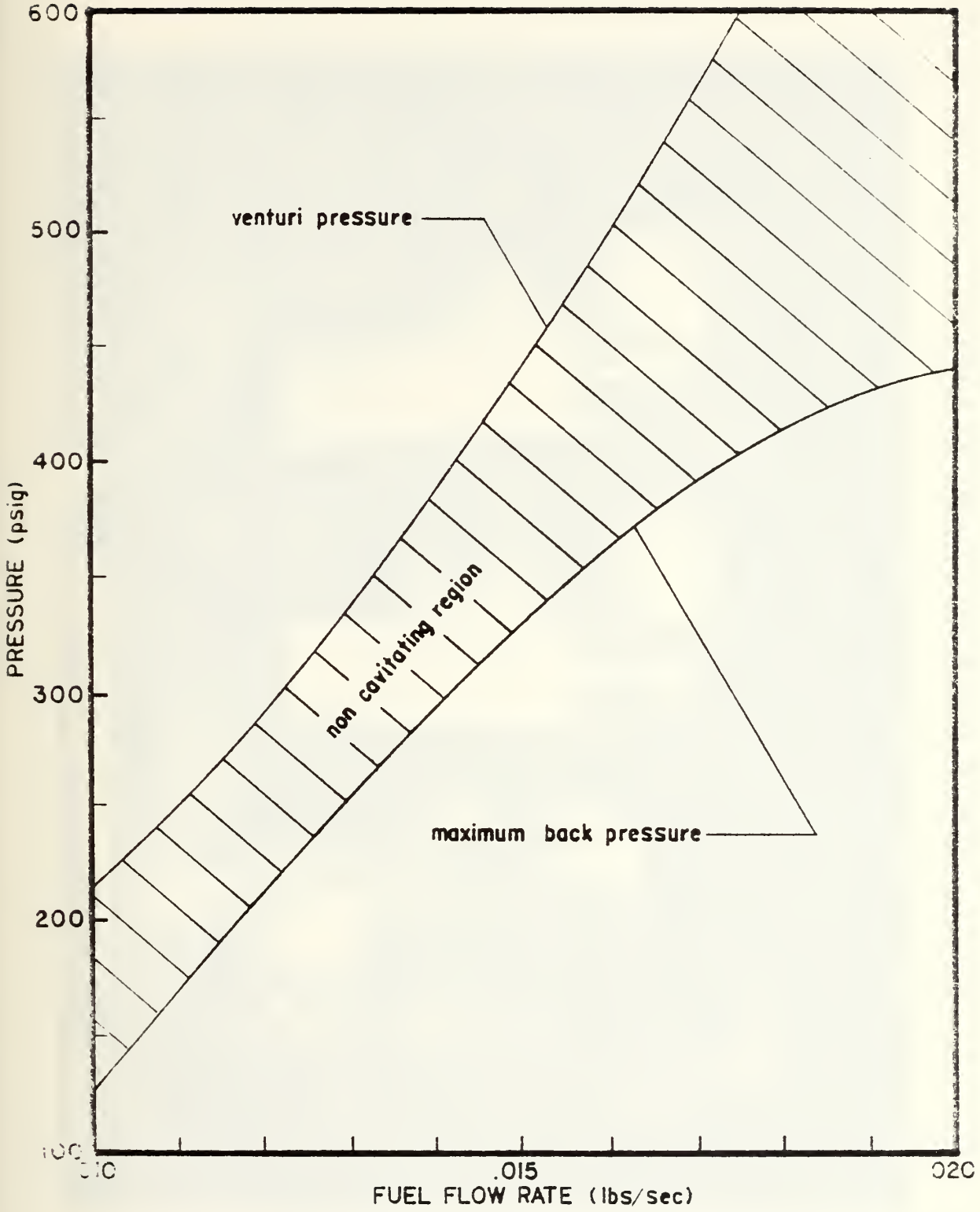

Figure 5. 0.016 Inch Diameter Cavitating Venturi; Calibration Curve

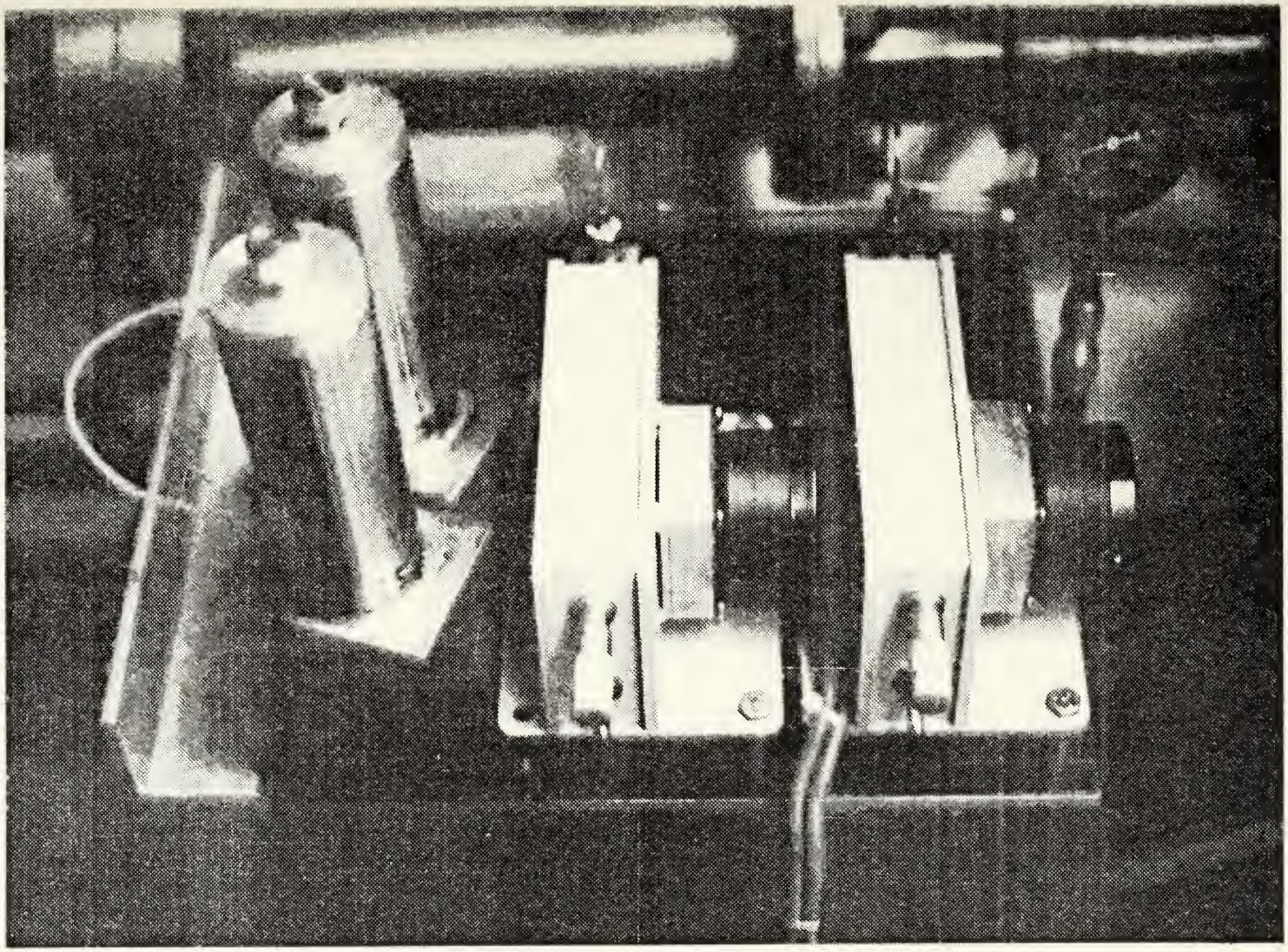

Figure 6. Precision Metering Pumps

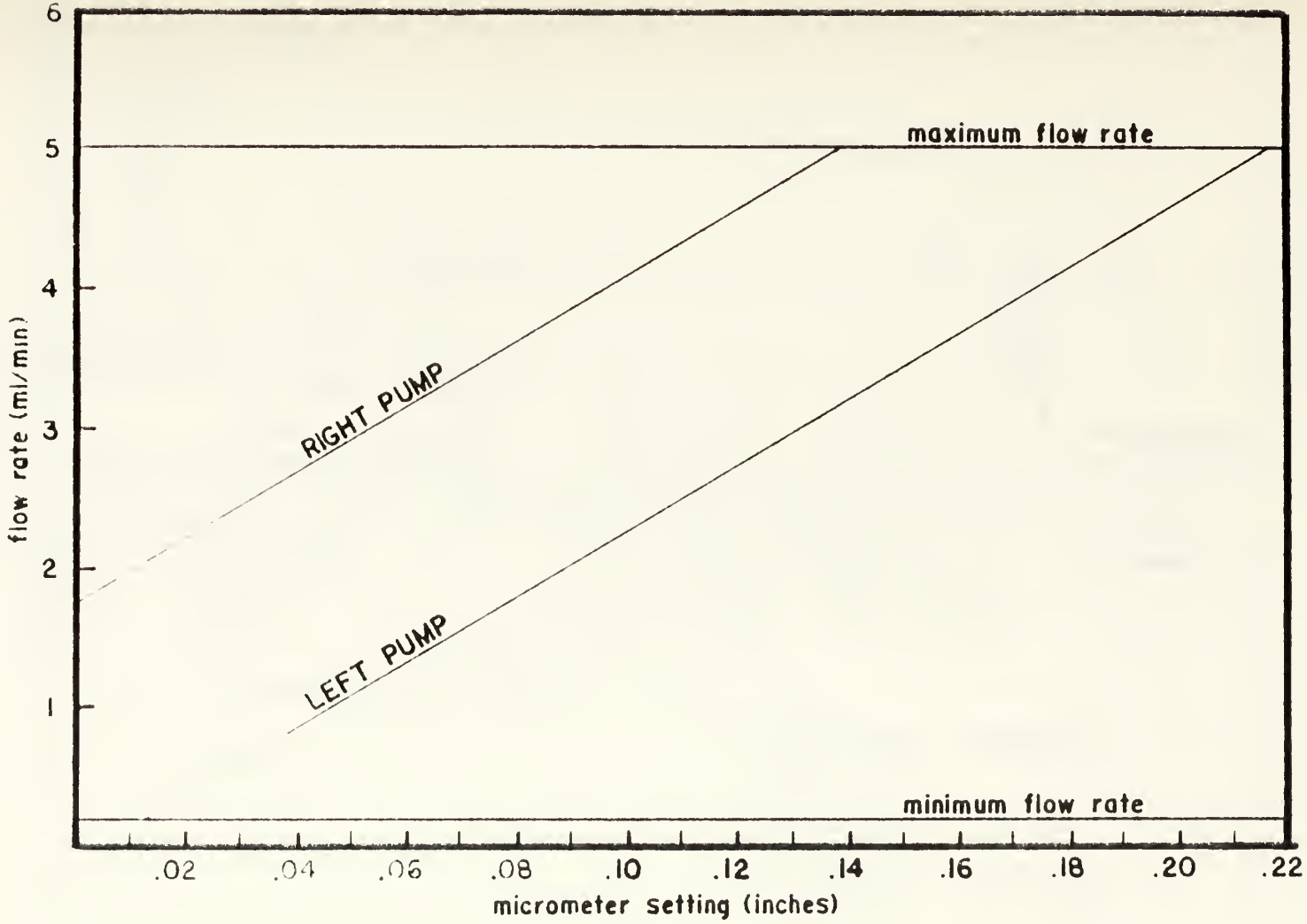

Figure 7. Precision Metering Pump Calibration Curves

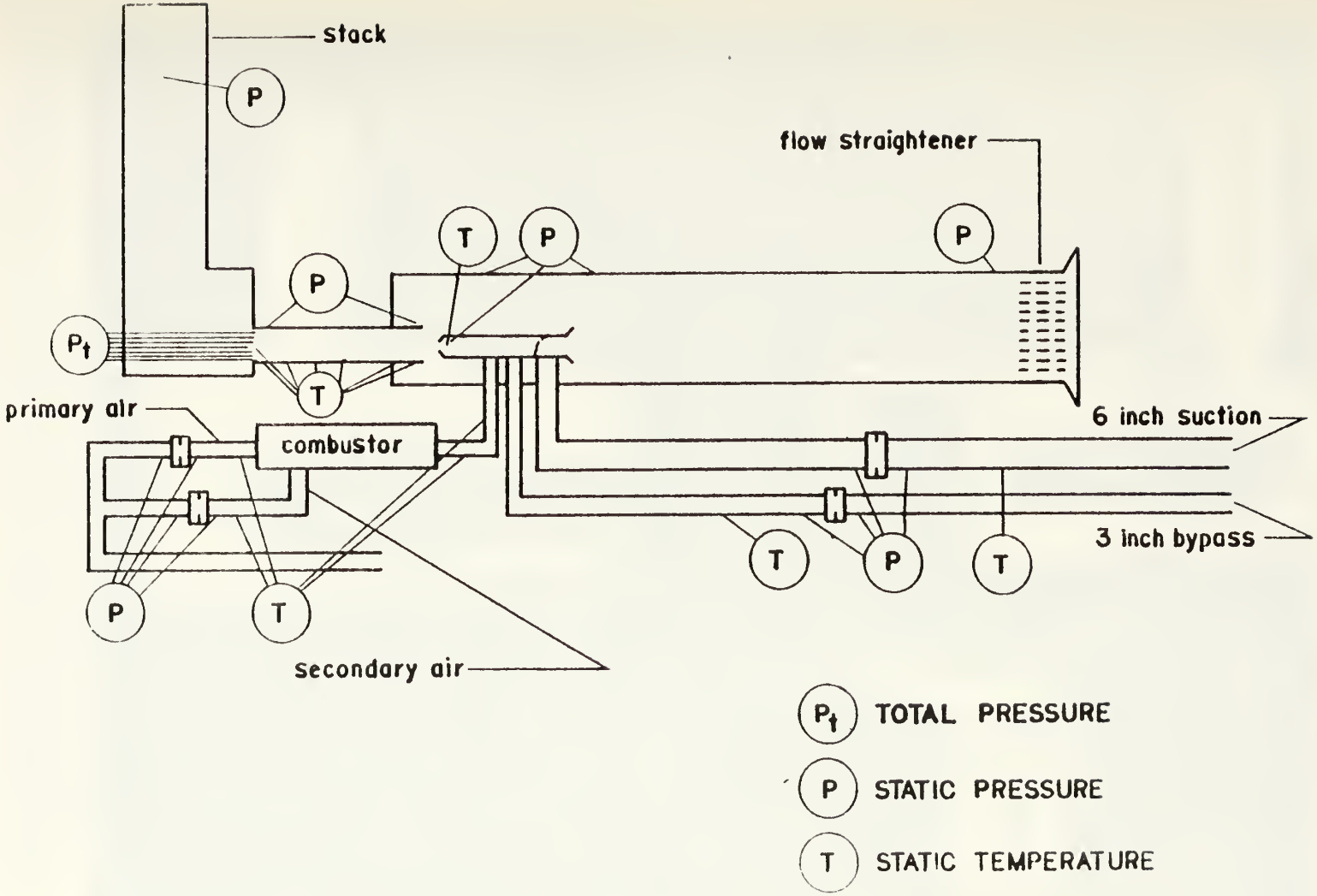

Figure 8. Pressure Tap and Temperature Sensor Locations

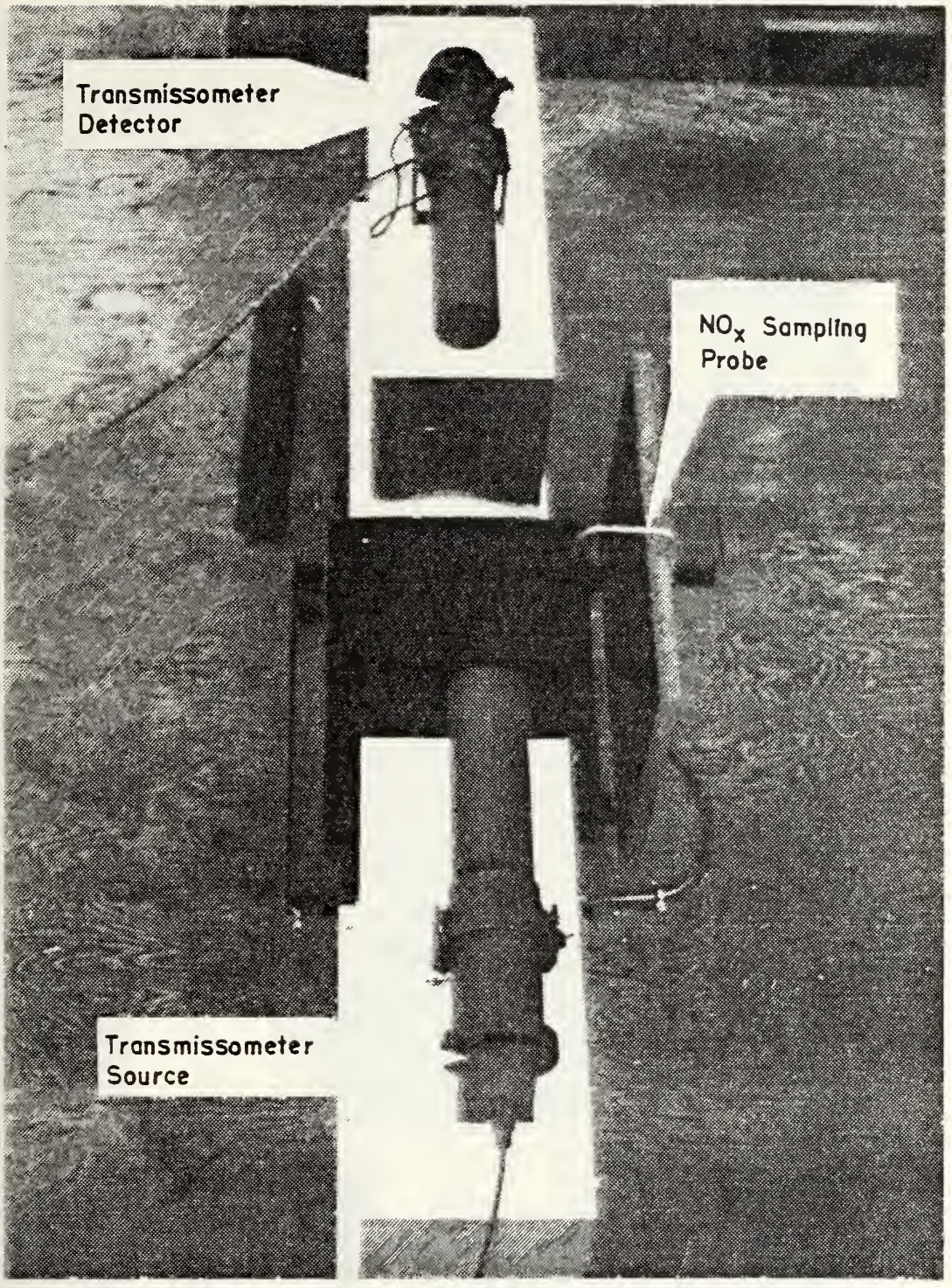

Figure 9. Transmissometer Source/Detector Unit

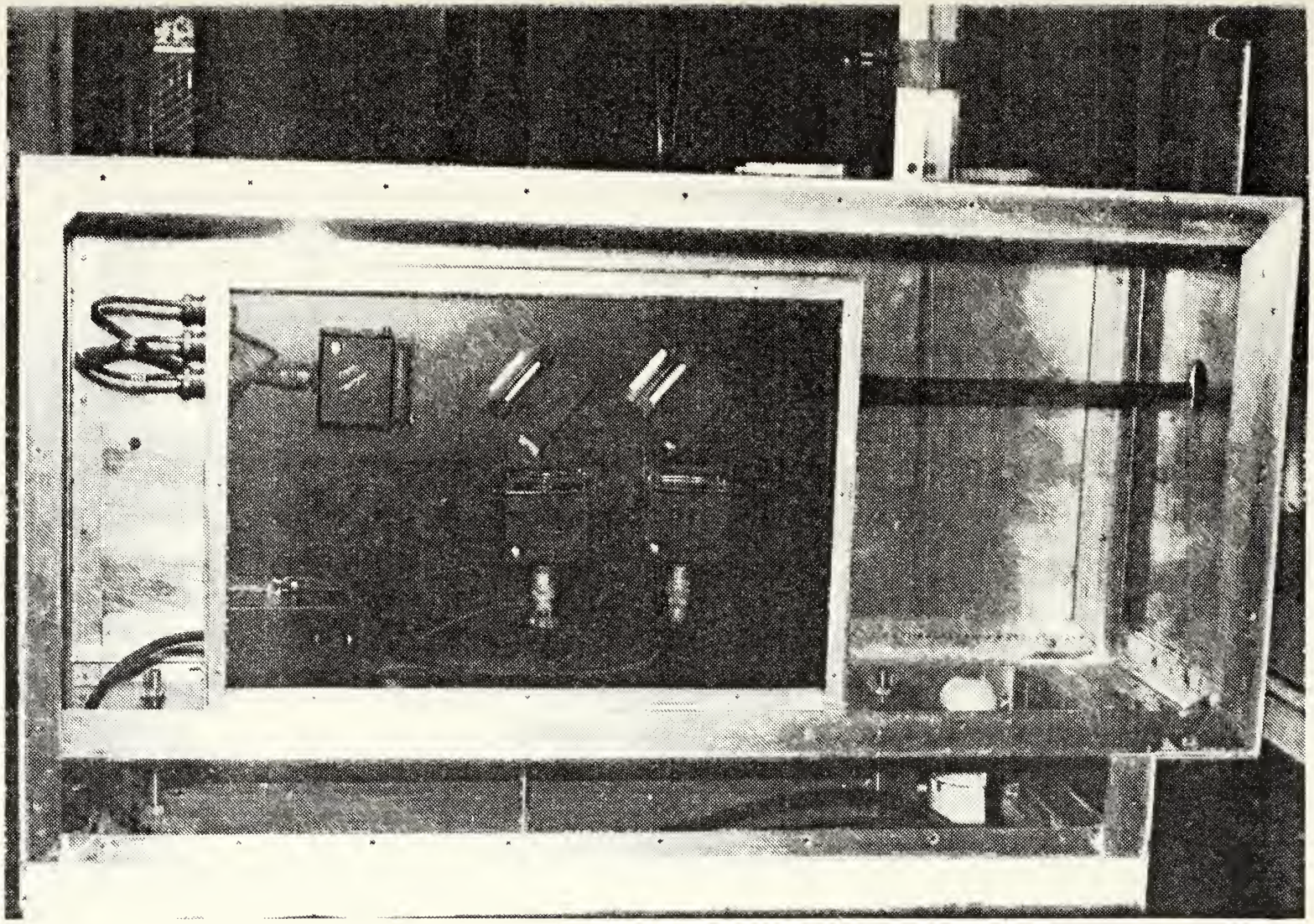

Figure 10. Light Detector

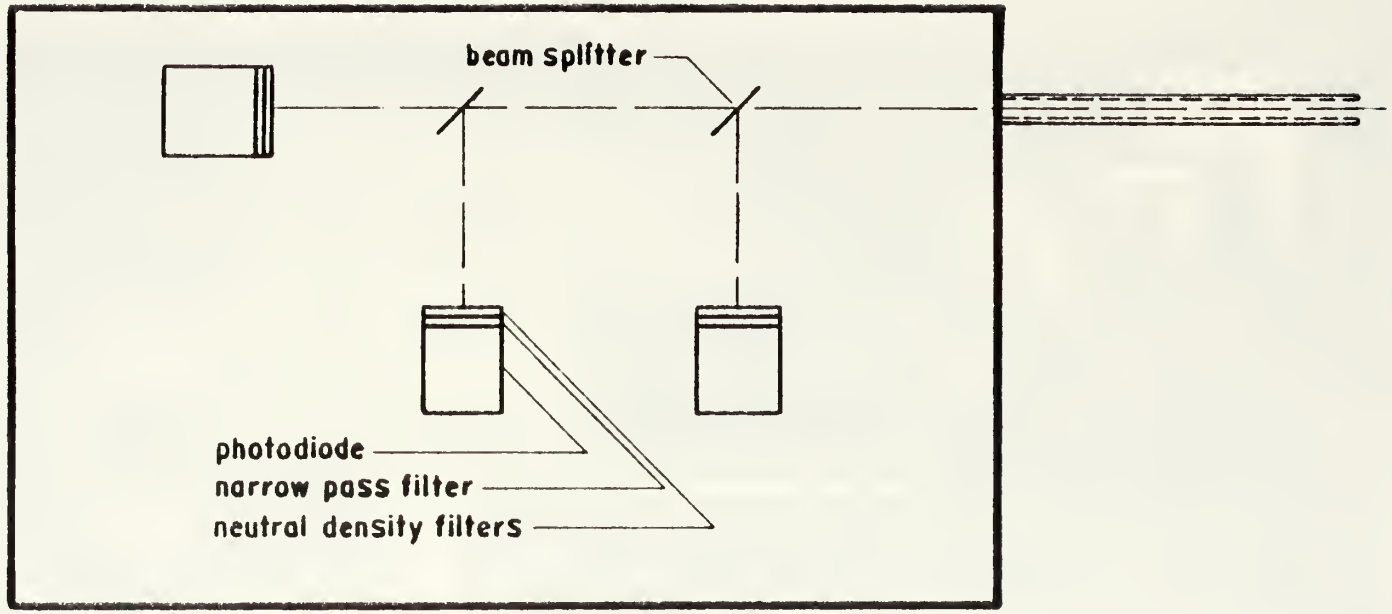

Figure 11. Schematic of Light Path Through the Optical Detector

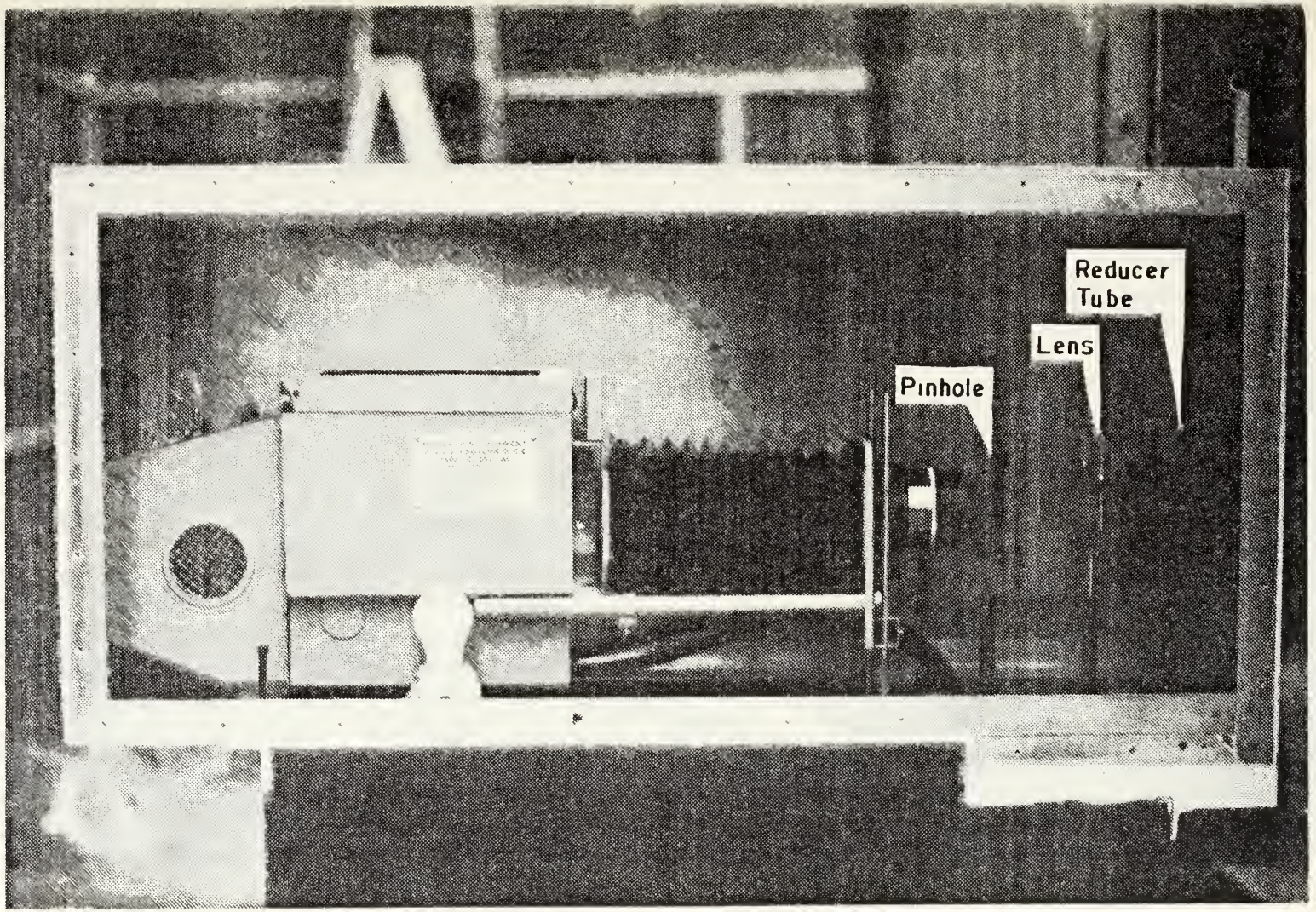

Figure 12. Collimated White Light Source

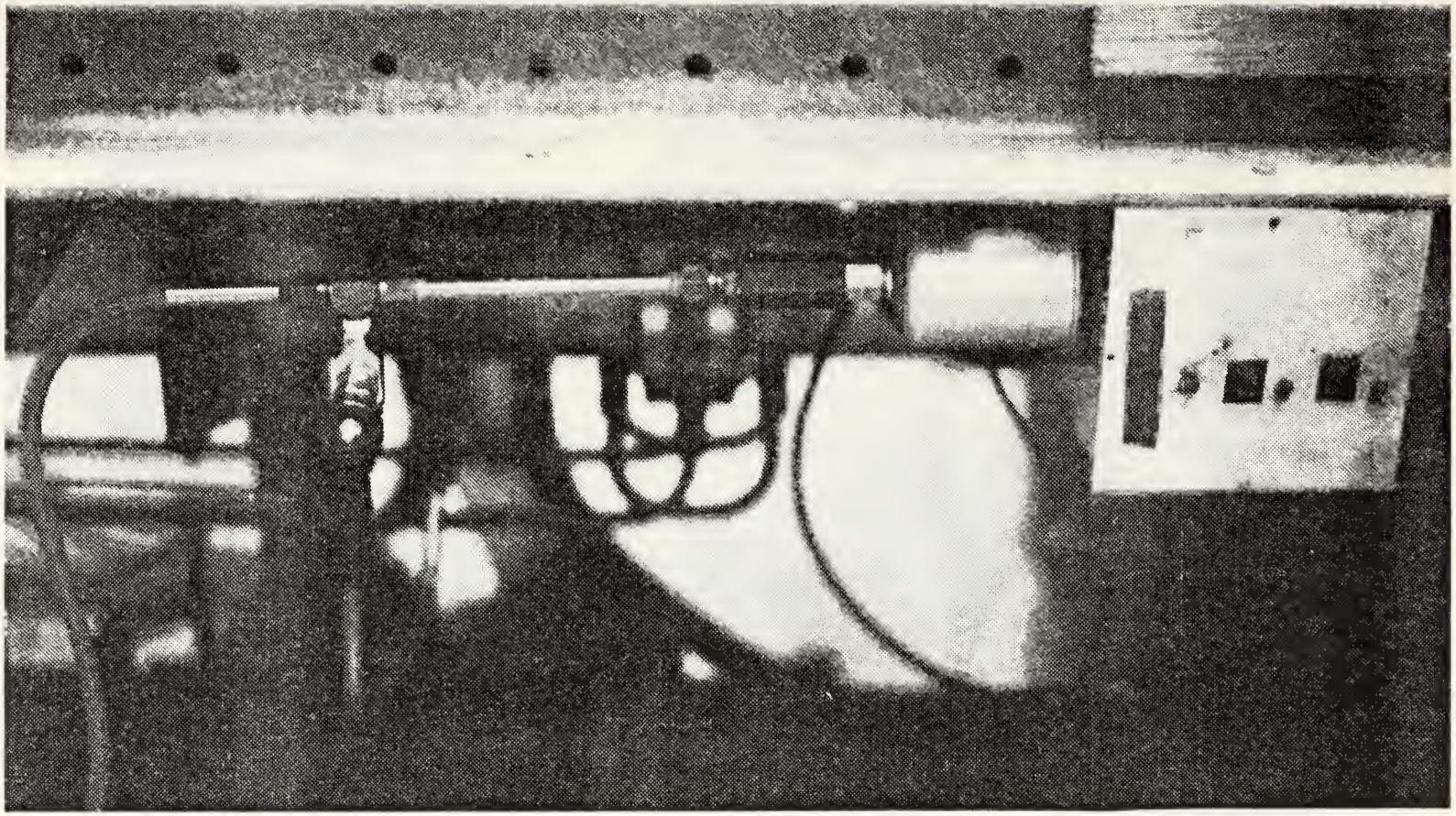

Figure 13. Sampling Train

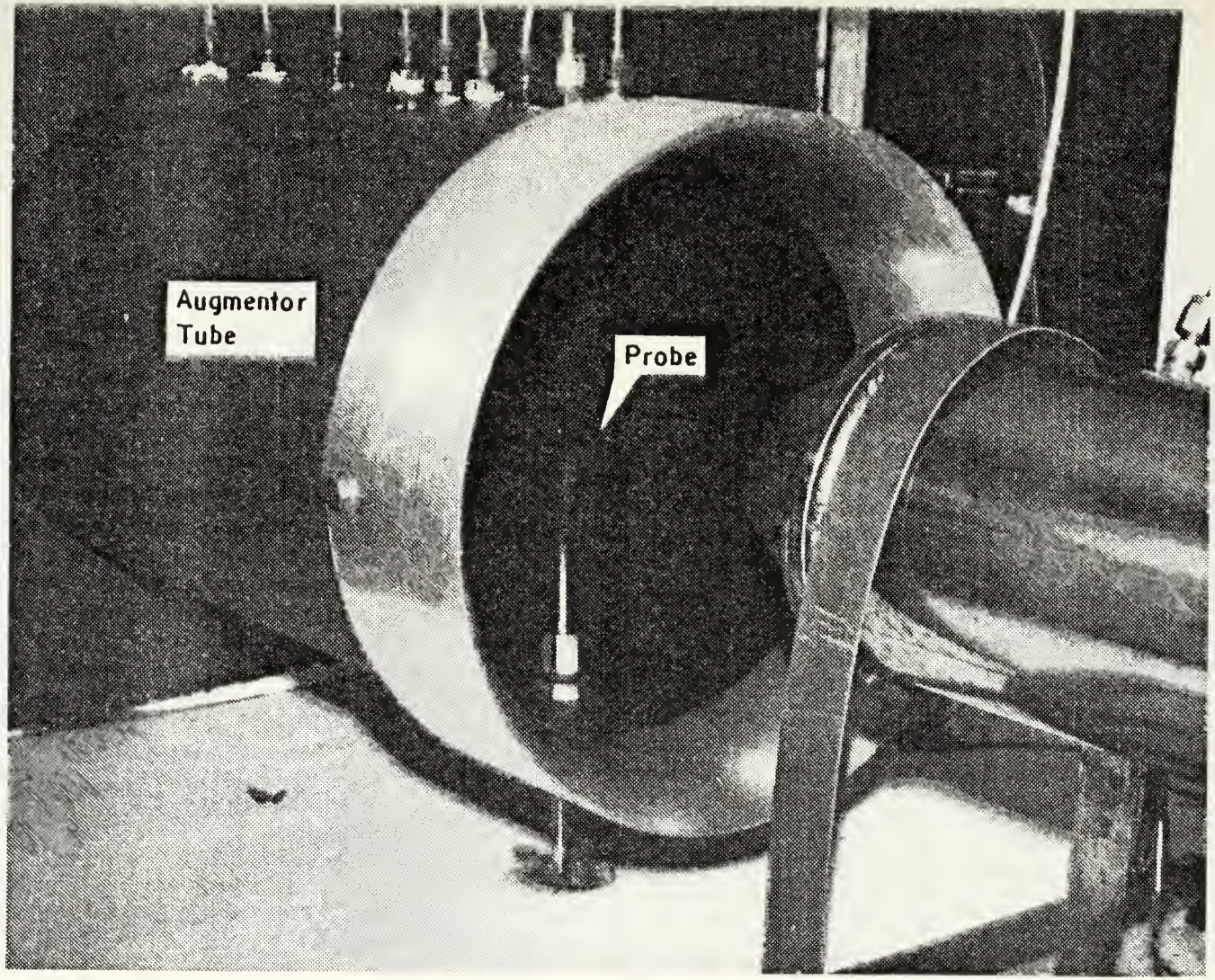

Figure 14. Sampling Probe

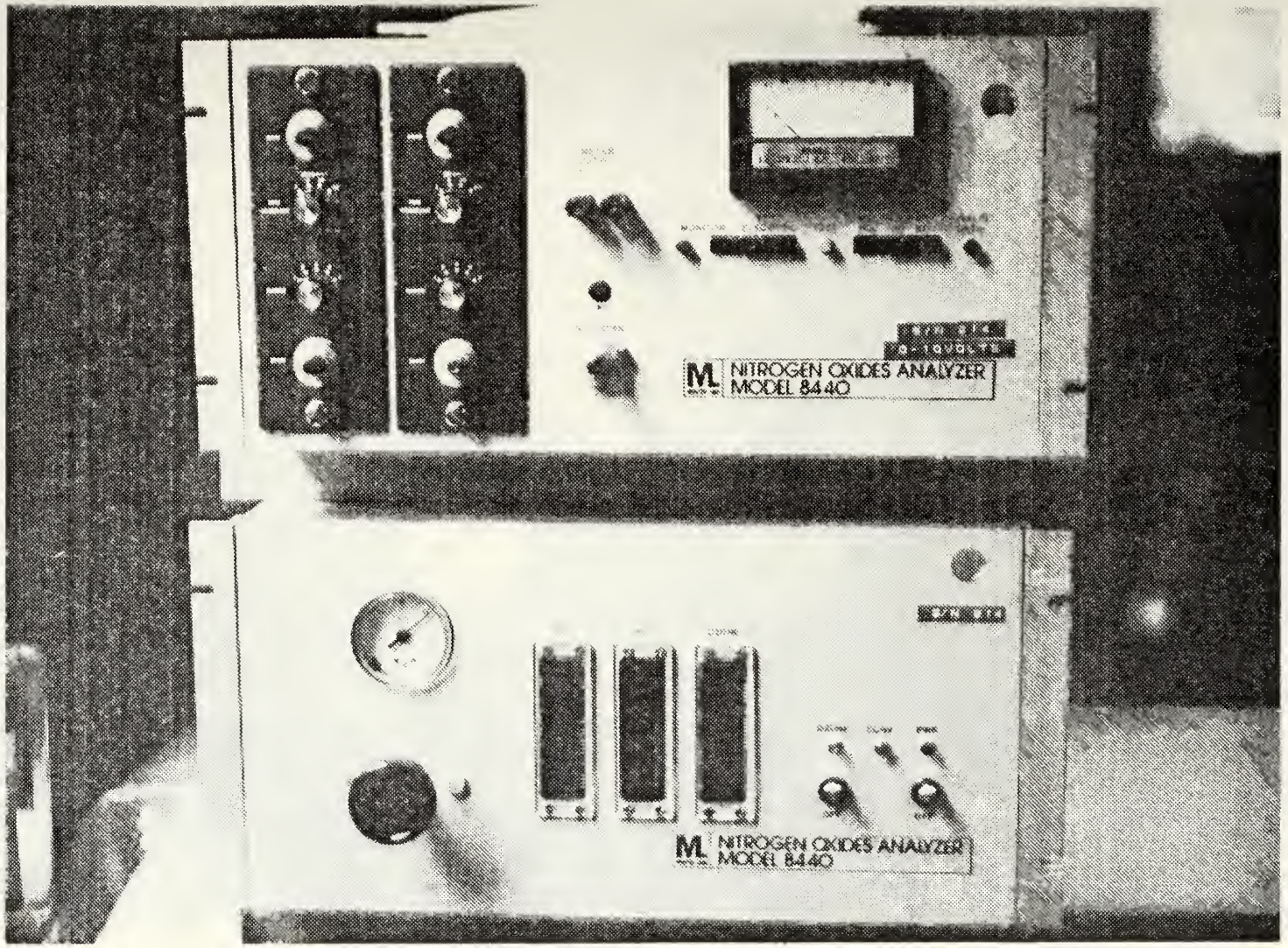

Figure 15. Nitrogen Oxides Analyzer

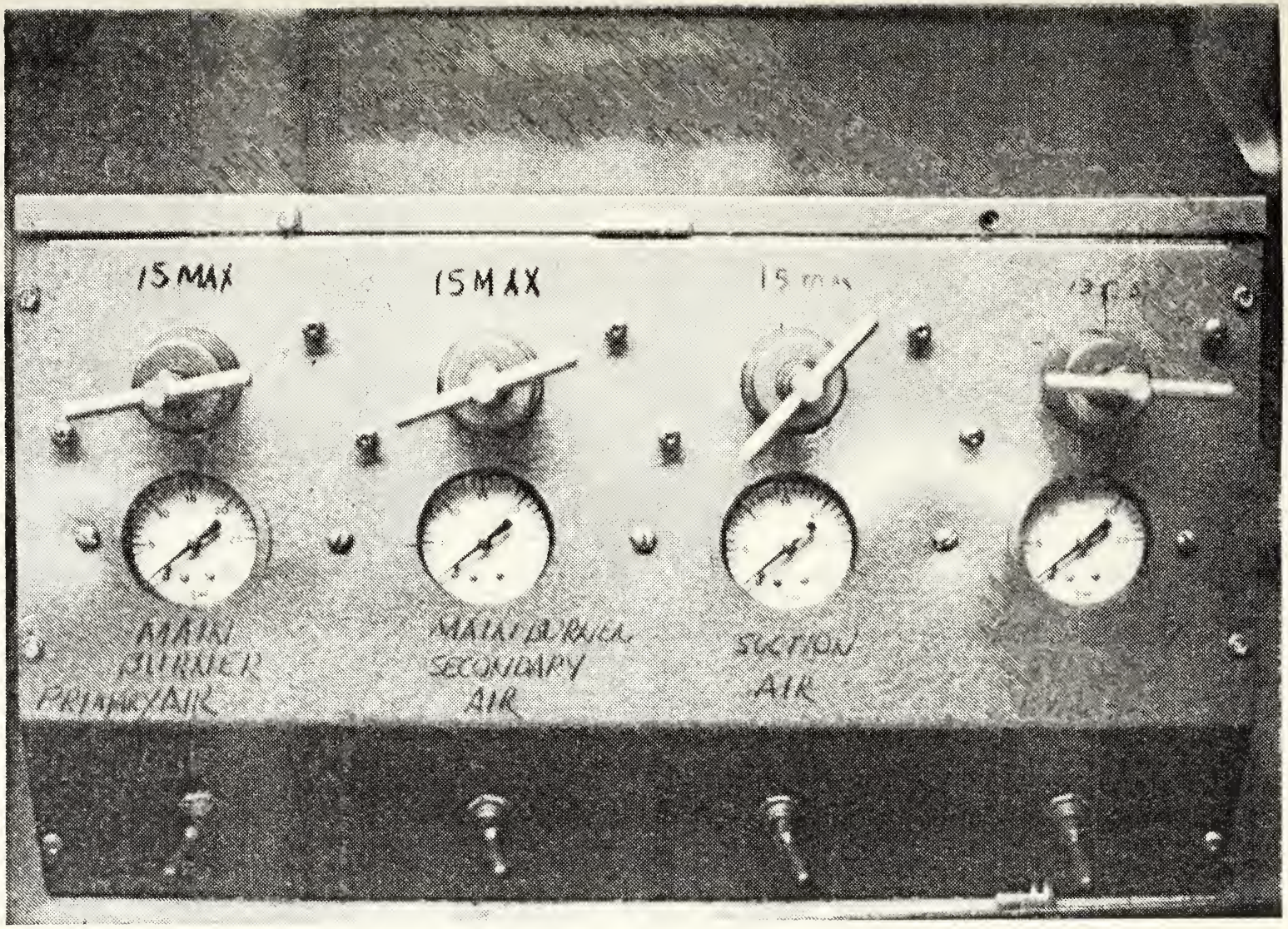

Figure 16. Remote Control Cart

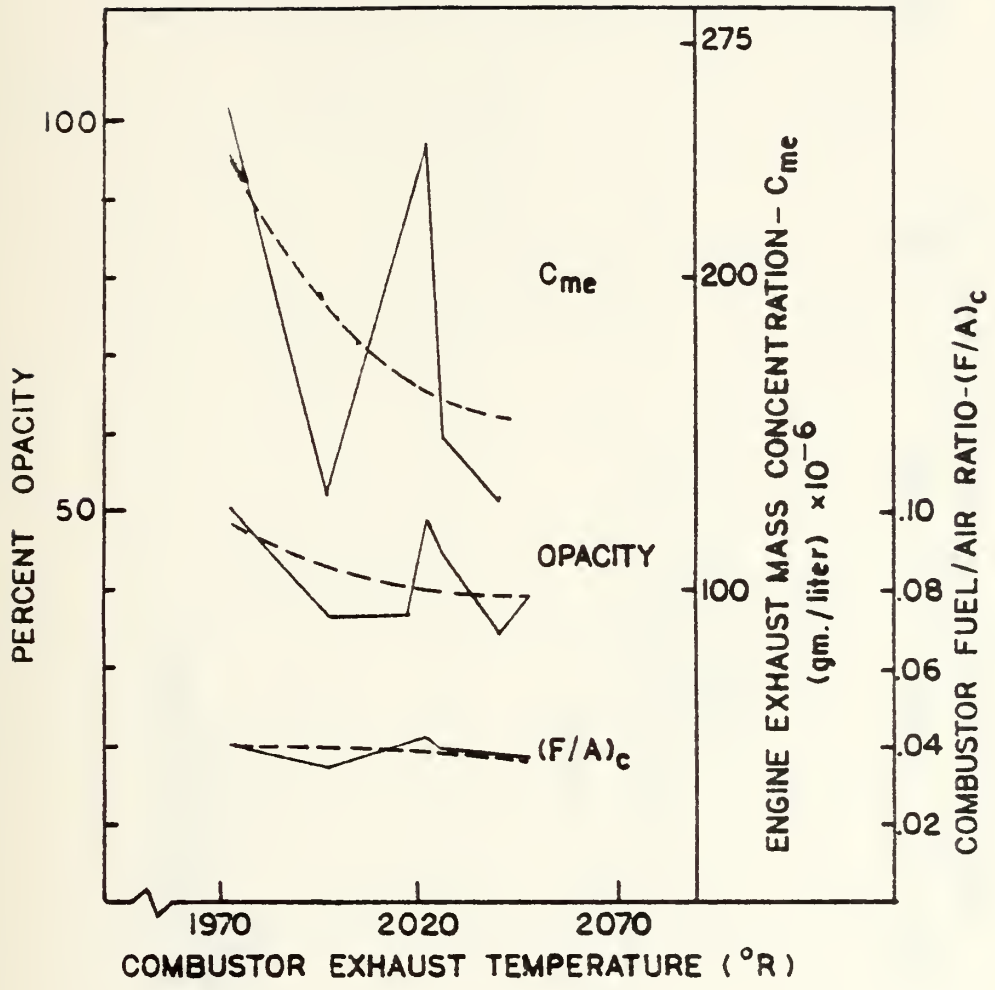

Figure 17. Graph of Engine Mass Concentration, Stack Gas Opacity, and Combustor Fuel/Air Ratio vs. Combustor Exhaust Temperature for JP-4

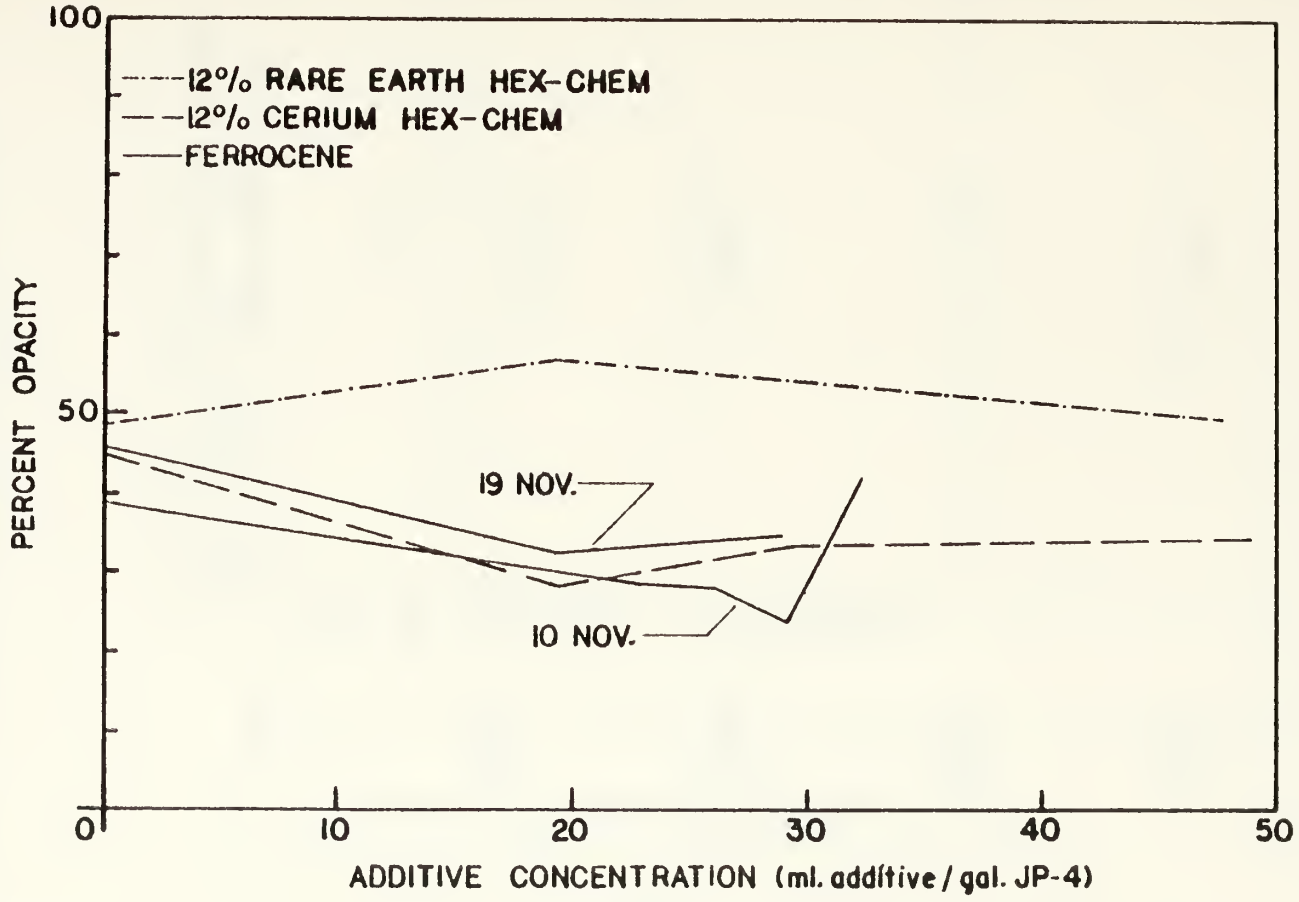

Figure 18. Effects of Additive Concentration on Stack Gas Opacity

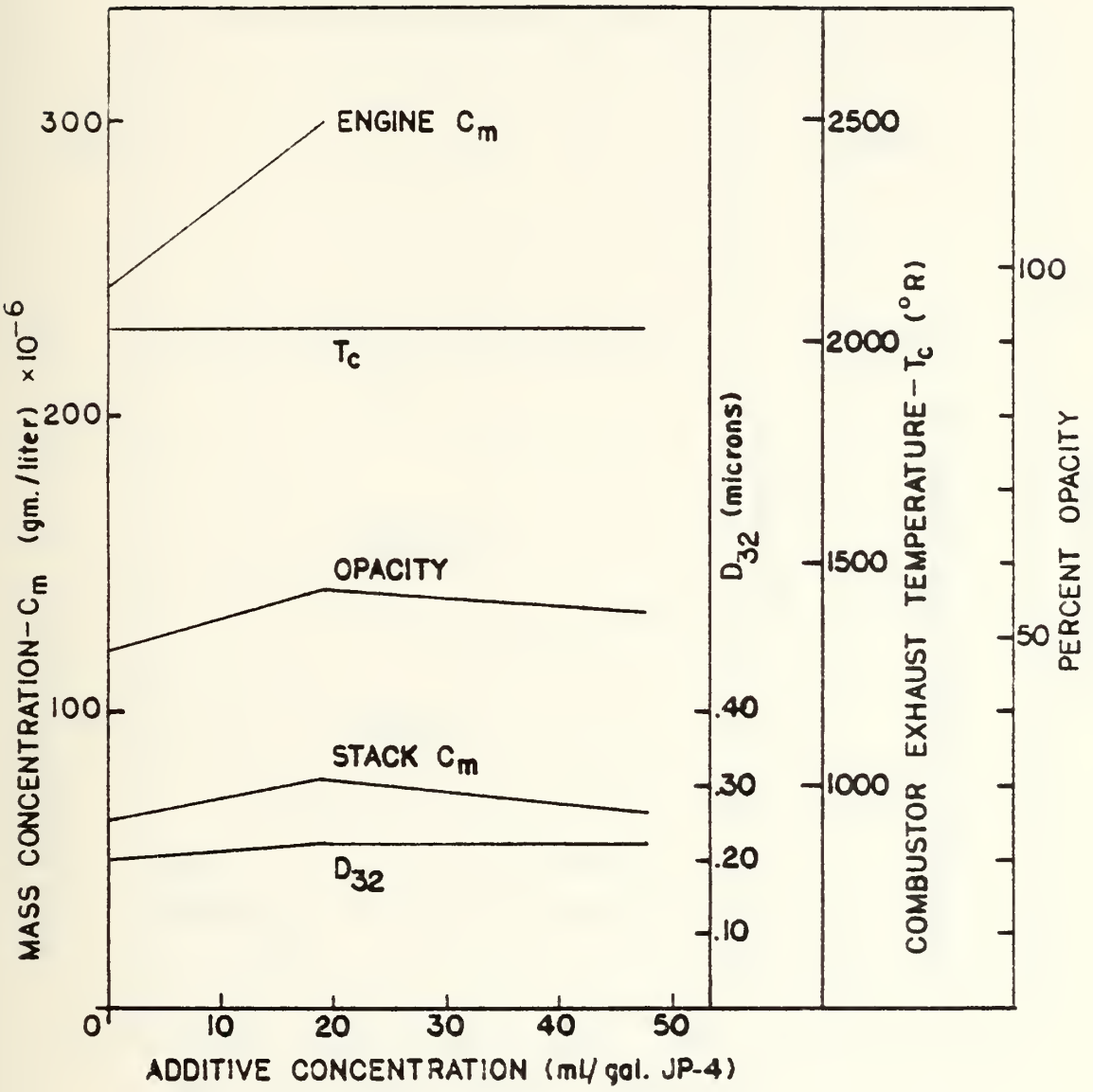

Figure 19. 12% Rare Earth Hex-Chem Concentration vs. Engine/Stack C_m, Stack Gas Opacity, D_{32}, and Combustor Exhaust Temperature

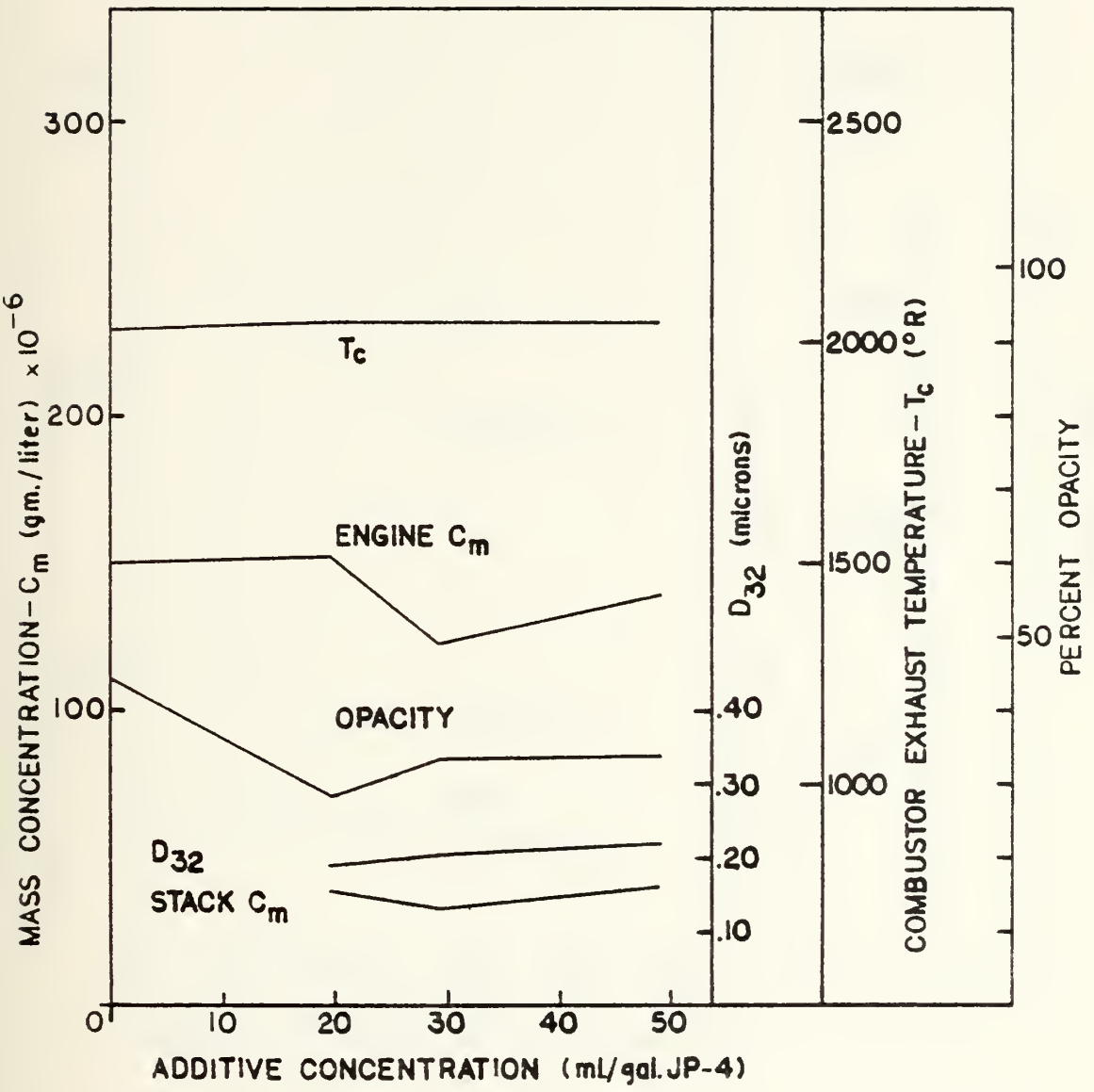

Figure 20. 12% Cerium Hex-Chem Concentration vs. Combustor Exhaust Temperature, Engine/Stack C_m, Stack Gas Opacity, and D_{32}

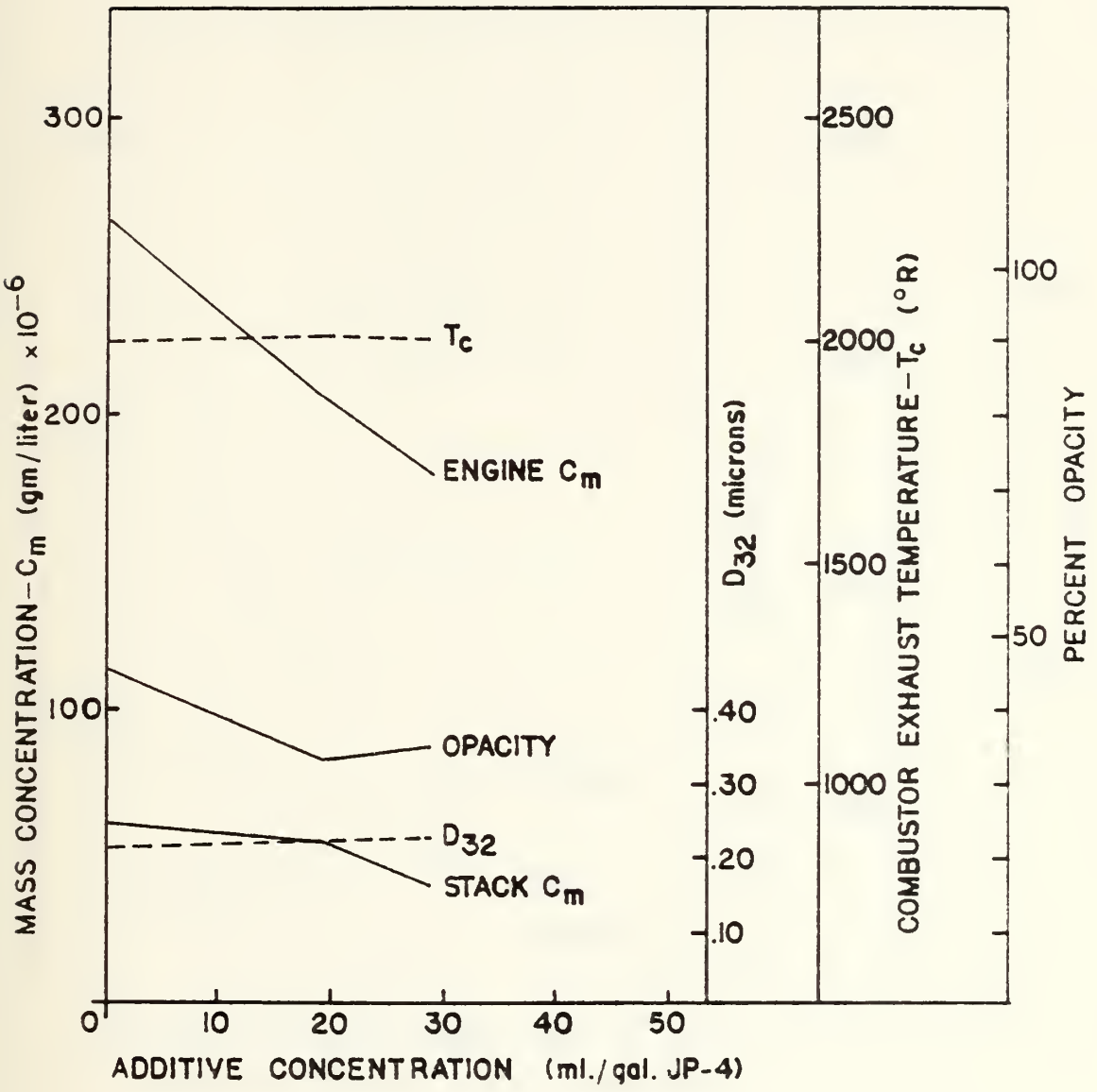

Figure 21. Ferrocene Concentration vs. Combustor Exhaust Temperature, Engine/Stack C_m, Stack Gas Opacity, and D_{32}. 19 November 1981

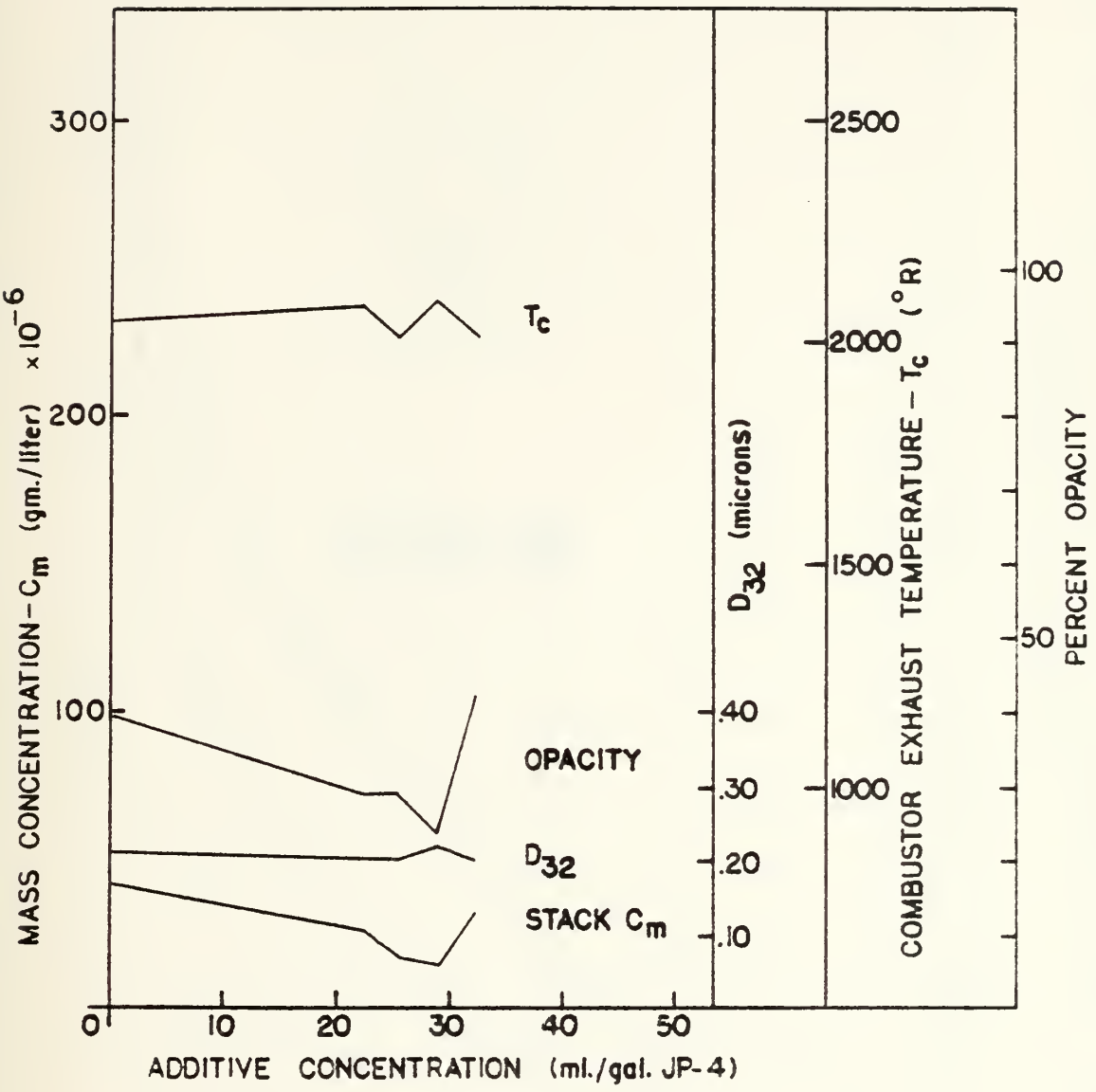

Figure 22. Ferrocene Concentration vs. Combustor Exhaust Temperature, Stack C_m, Stack Gas Opacity, and D_{32}. 10 November 1981

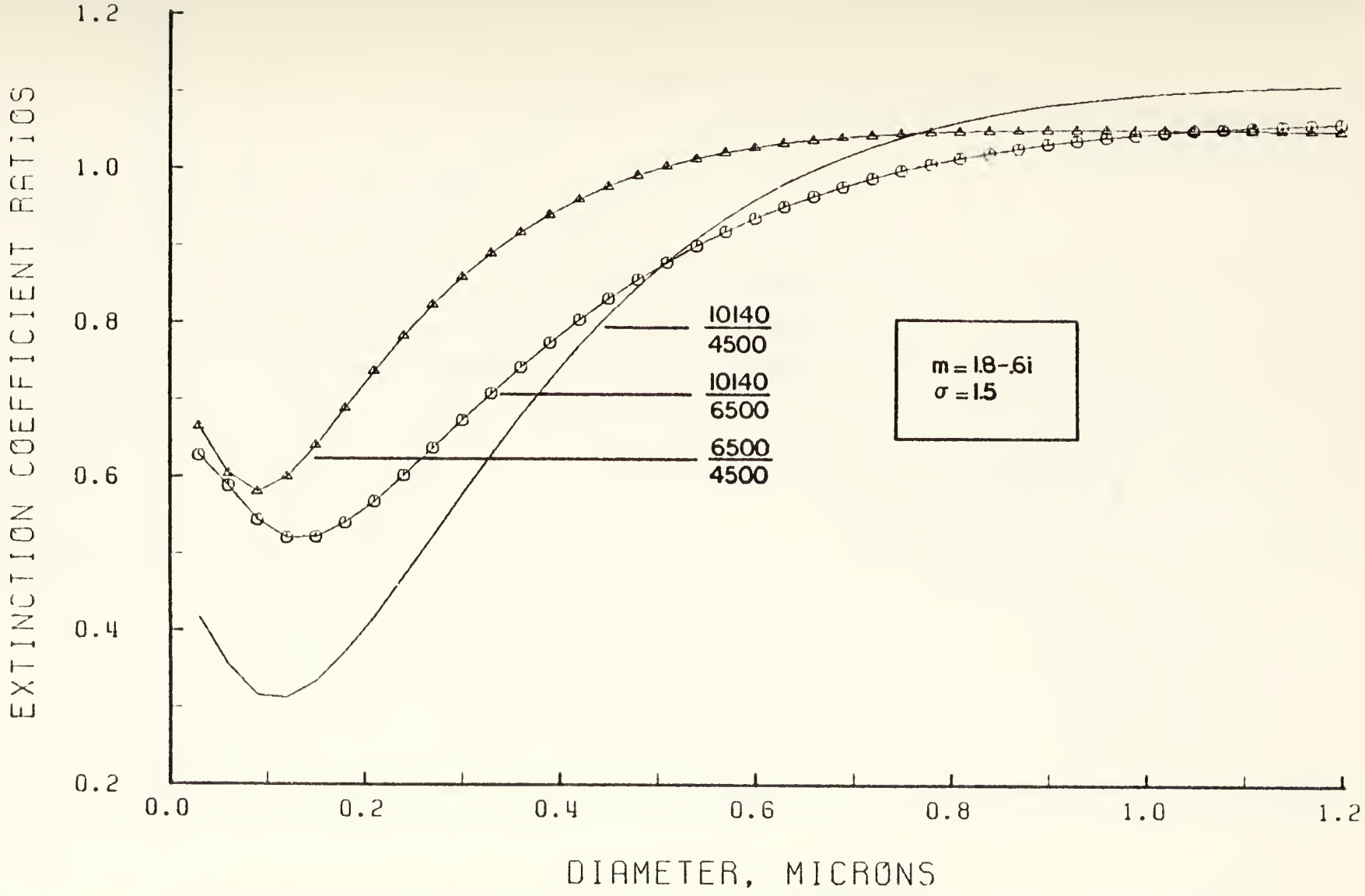

Figure 23. D_{32} vs. Extinction Coefficient Ratios (10140, 6500, 4500)
m = 1.8-.60i/1.5

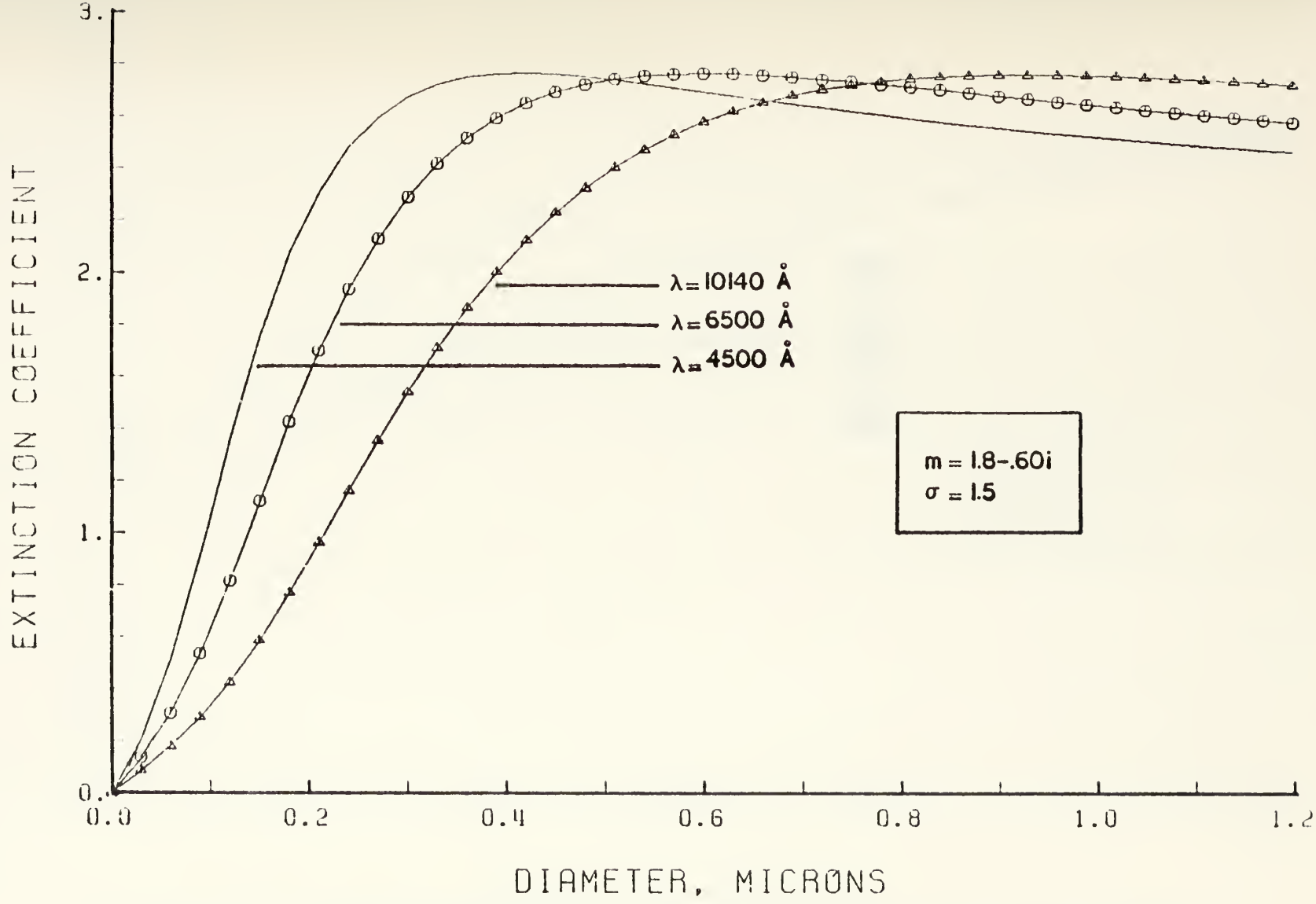

Figure 24. D_{32} vs. Extinction Coefficient (10140, 6500, 4500)
m = 1.80-.60i/1.5

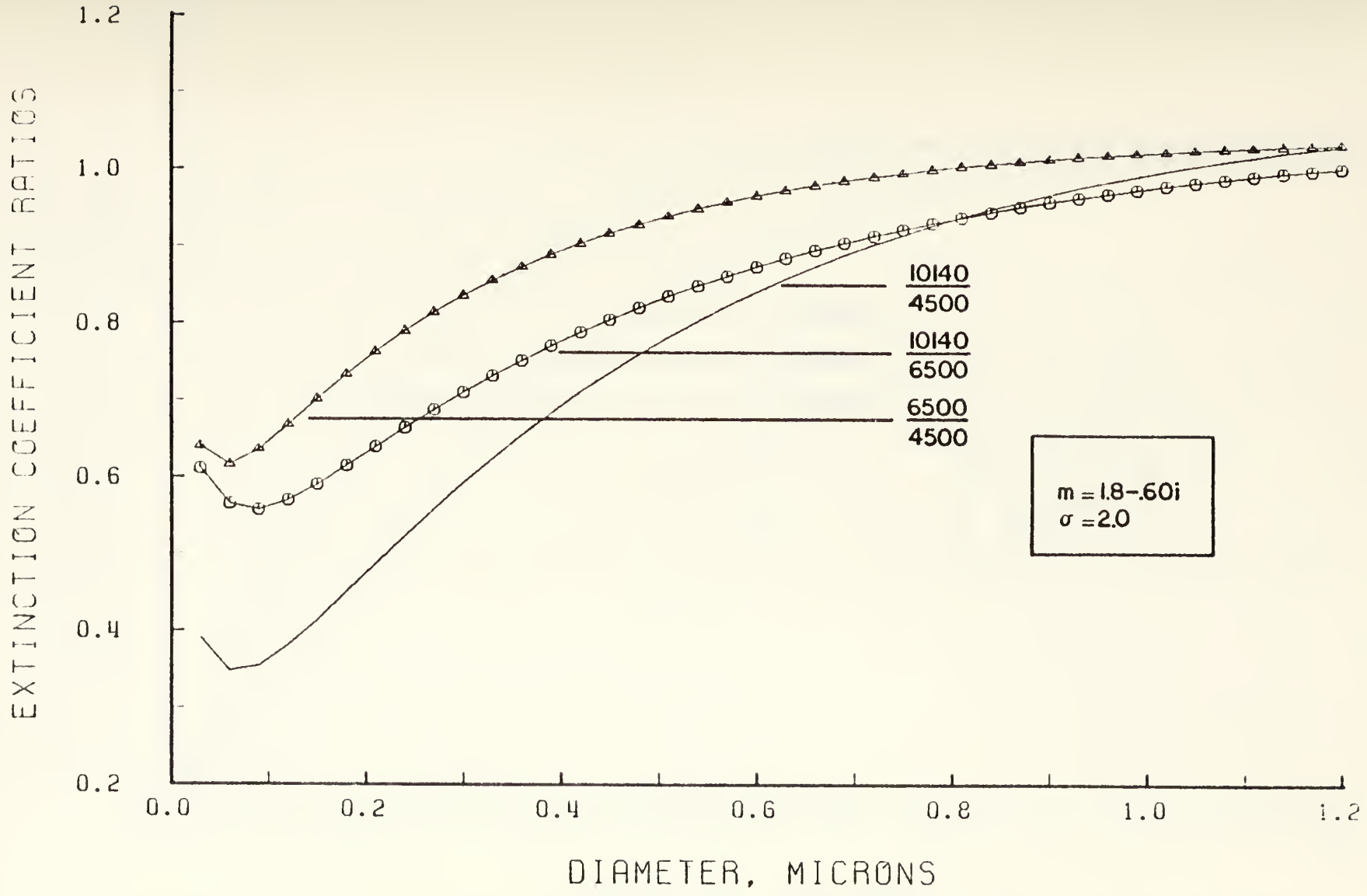

Figure 25. D_{32} vs. Extinction Coefficient Ratios (10140, 6500, 4500)
m = 1.80-.60i/2.0

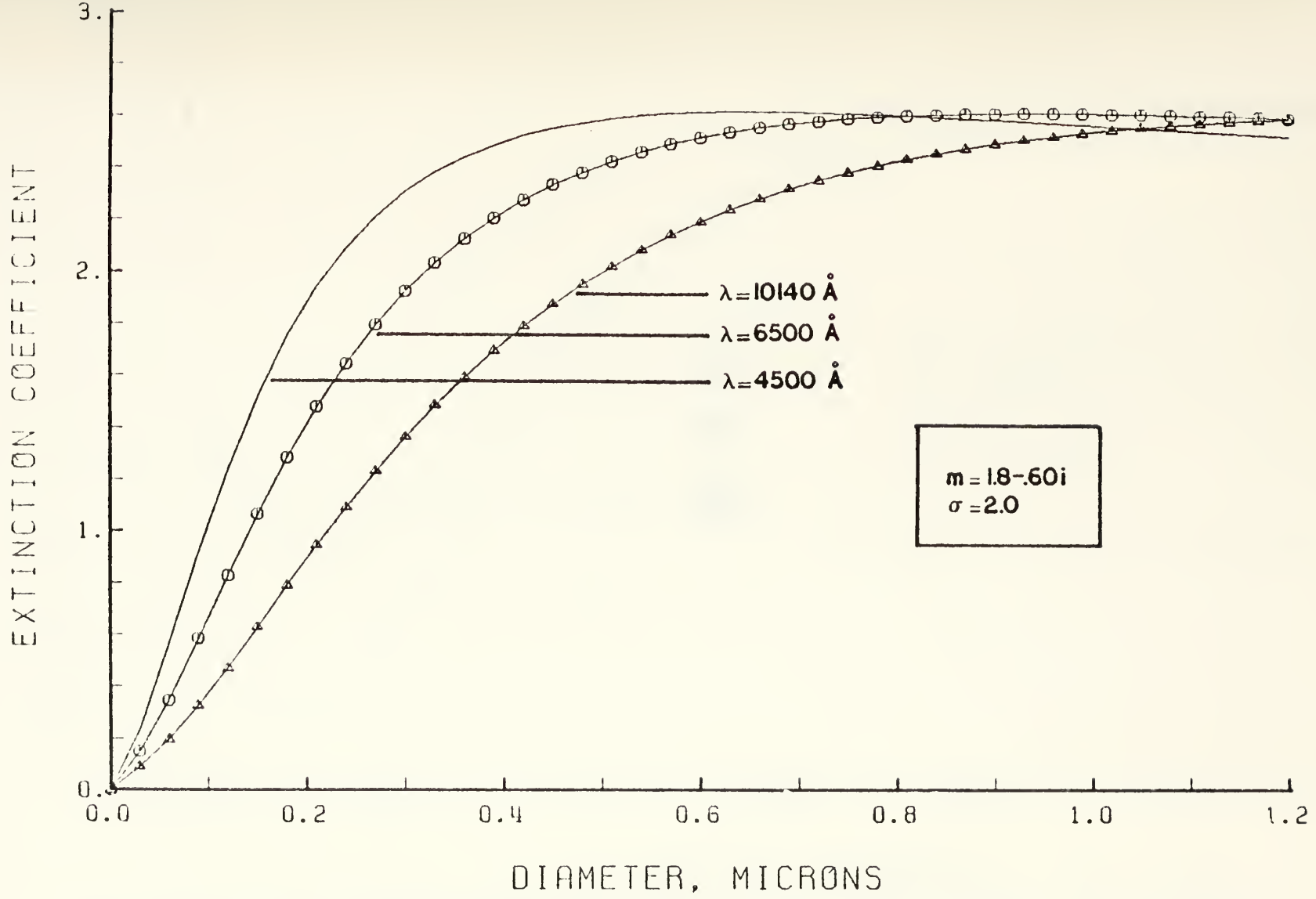

Figure 26. D_{32} vs. Extinction Coefficient (10140, 6500, 4500); m = 1.8-.6i/2.0

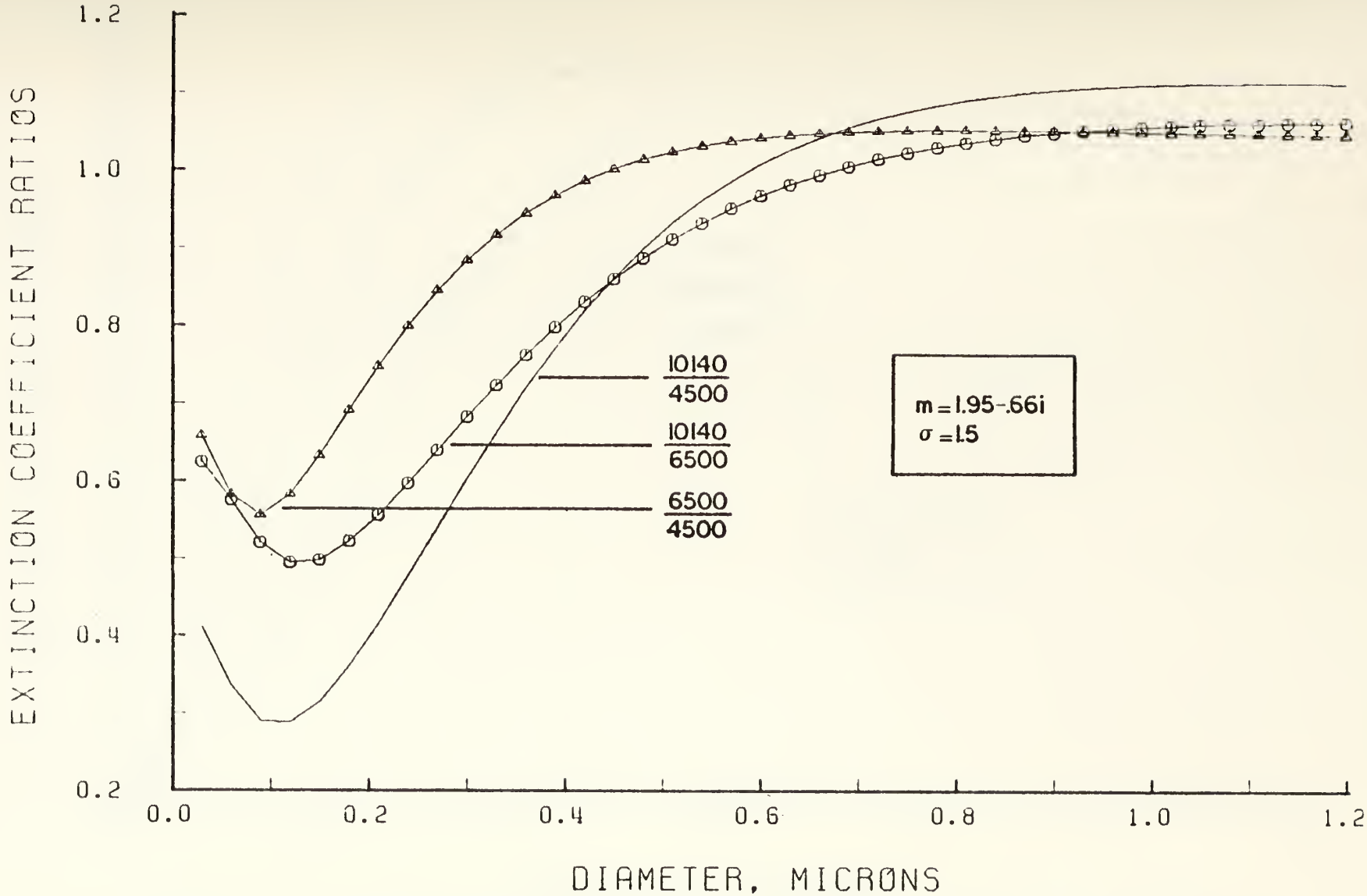

Figure 27. D_{32} vs. Extinction Coefficient Ratios (10140, 6500, 4500) m = 1.95-.66i/1.5

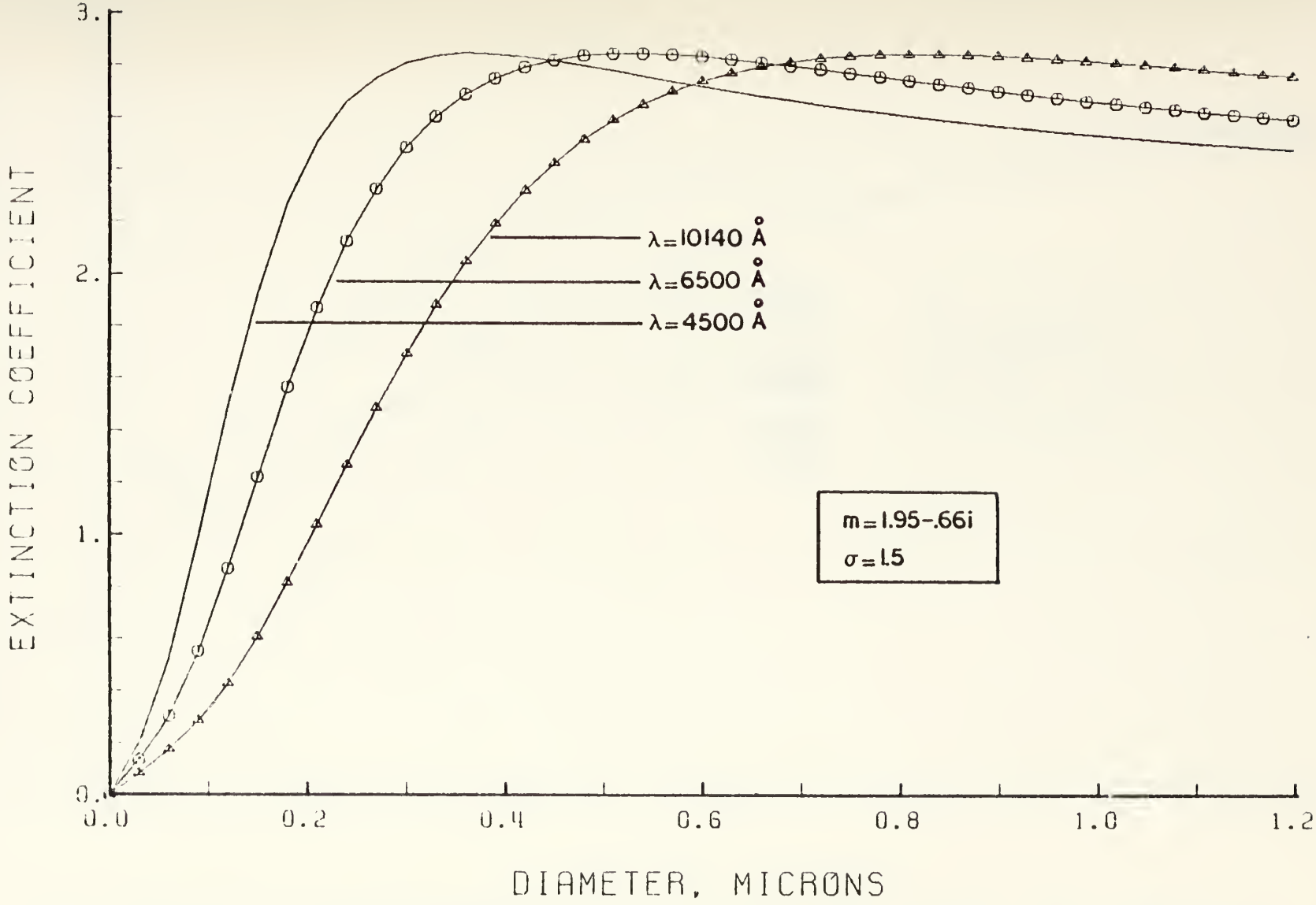

Figure 28. D_{32} vs. Extinction Coefficient (10140, 6500, 4500); m = 1.95-.66i/1.5

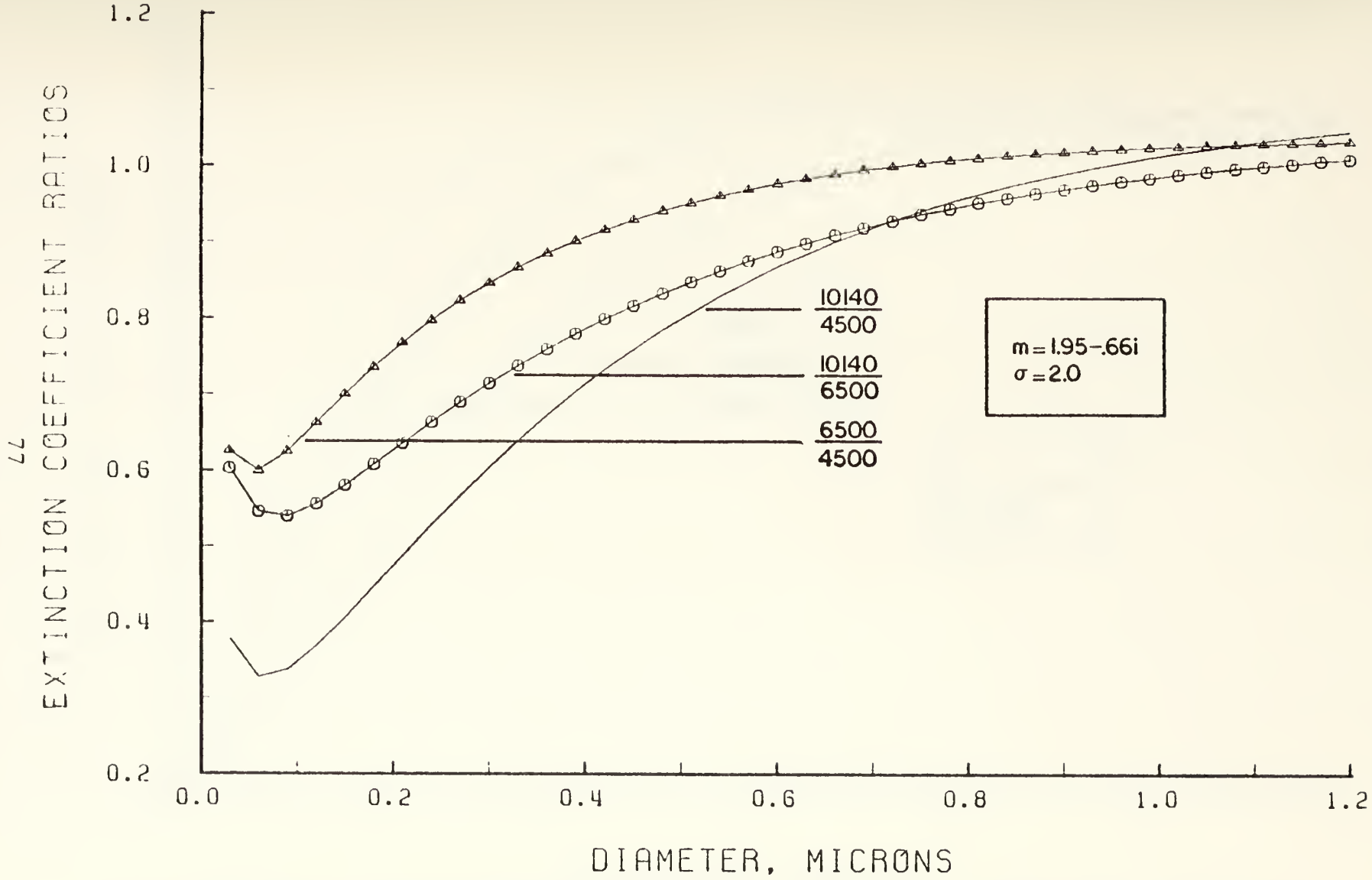

Figure 29. D_{32} vs. Extinction Coefficient Ratios (10140, 6500, 4500)
m = 1.95-.66i/2.0

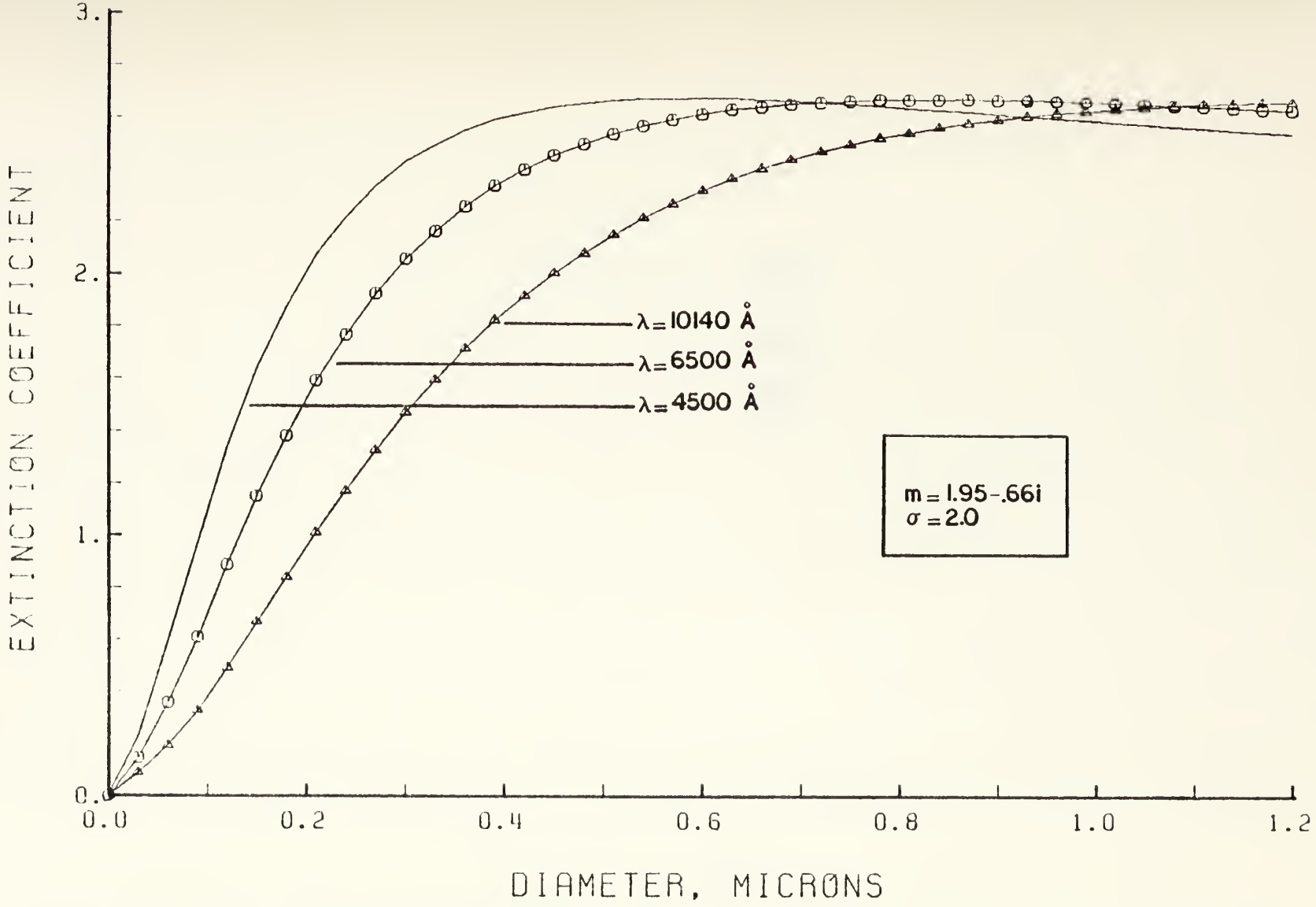

Figure 30. D_{32} vs. Extinction Coefficient (10140, 6500, 4500); m = 1.95-.66i/2.0

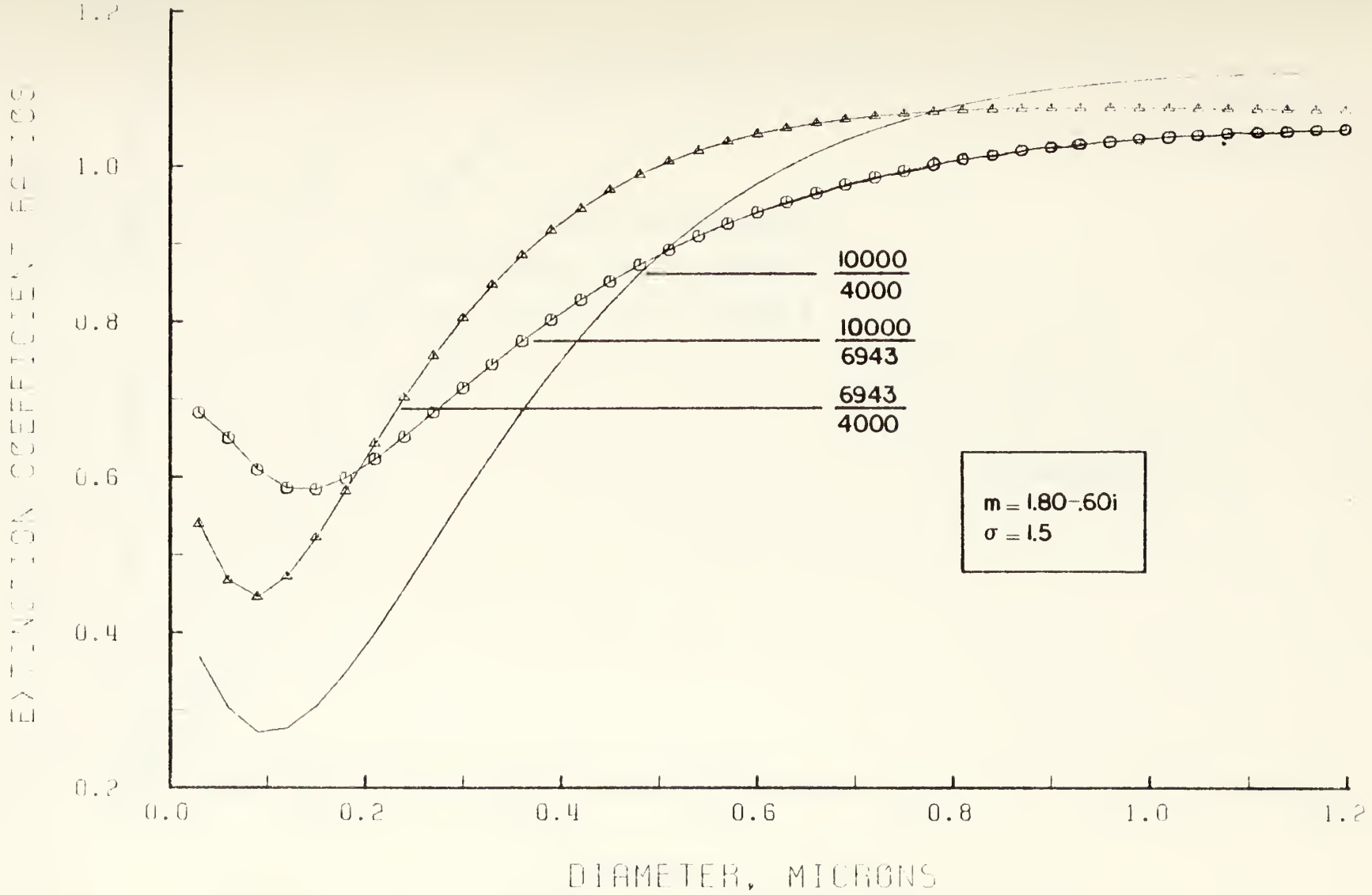

Figure 31. D_{32} vs. Extinction Coefficient Ratios (10000, 6943, 4000) m = 1.80-.60i/1.5

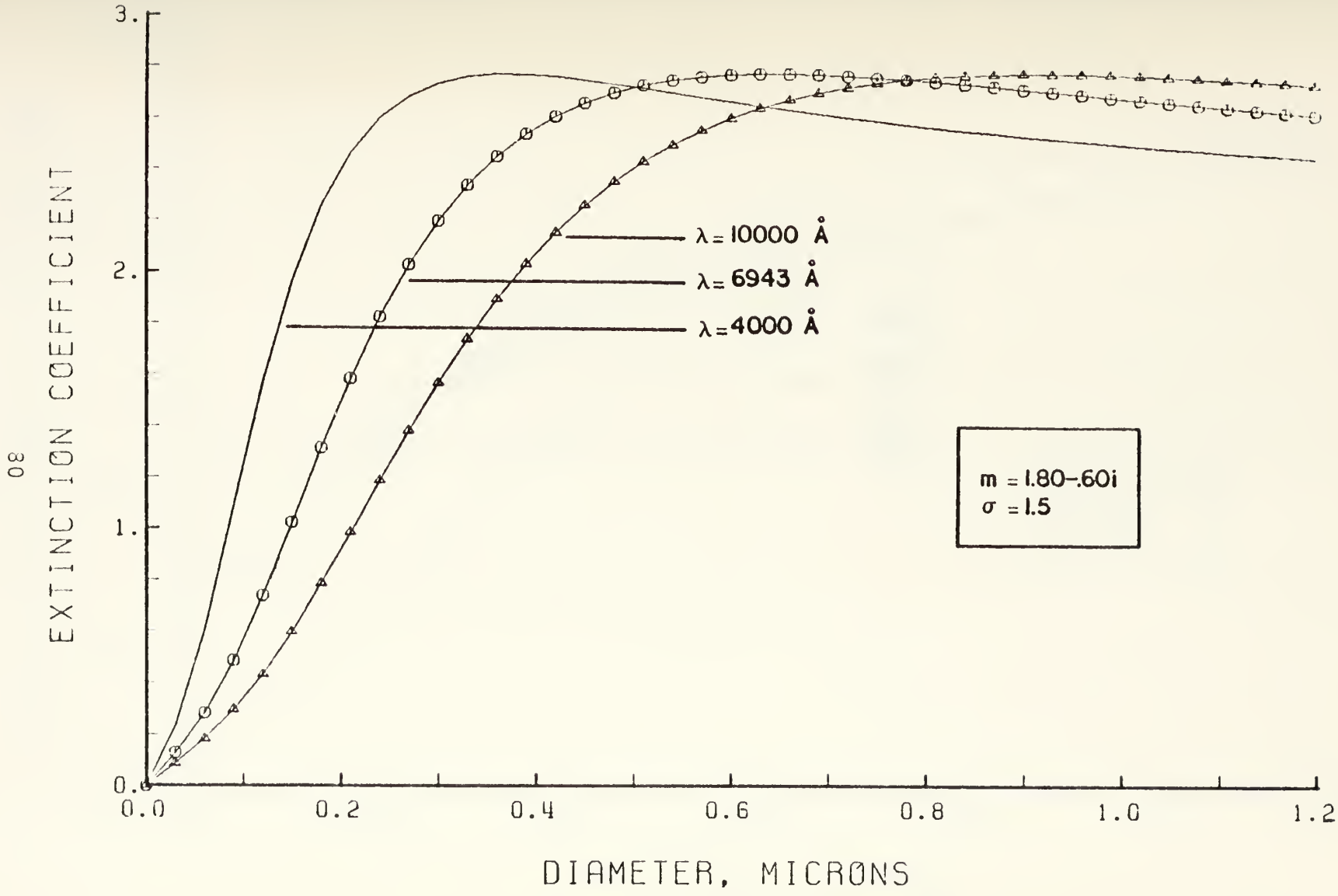

Figure 32. D_{32} vs. Extinction Coefficient (10000, 6943, 4000); m = 1.8-.60i/1.5

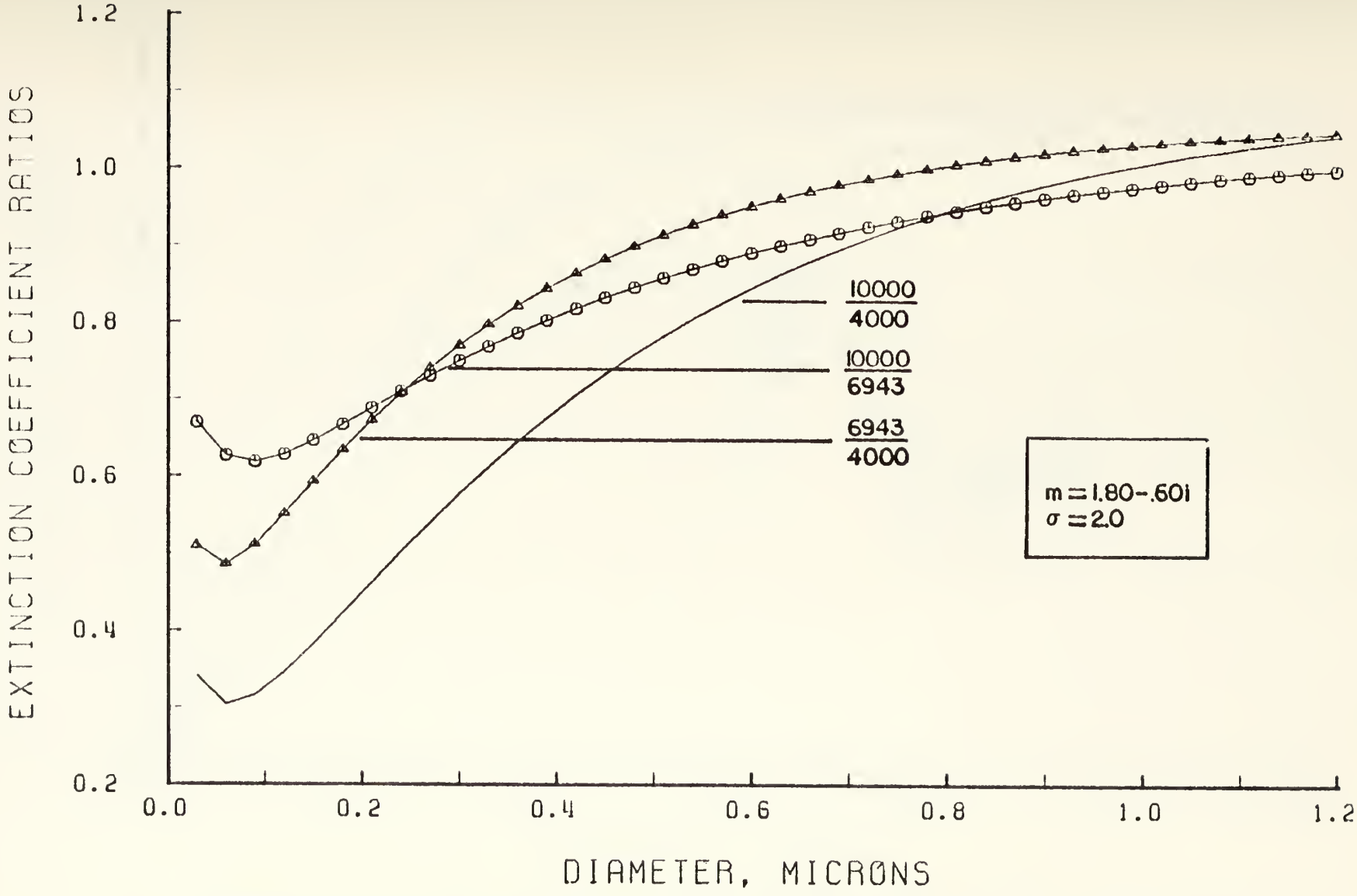

Figure 33. D_{32} vs. Extinction Coefficient Ratios (10000, 6943, 4000)
m = 1.80-.60i/2.0

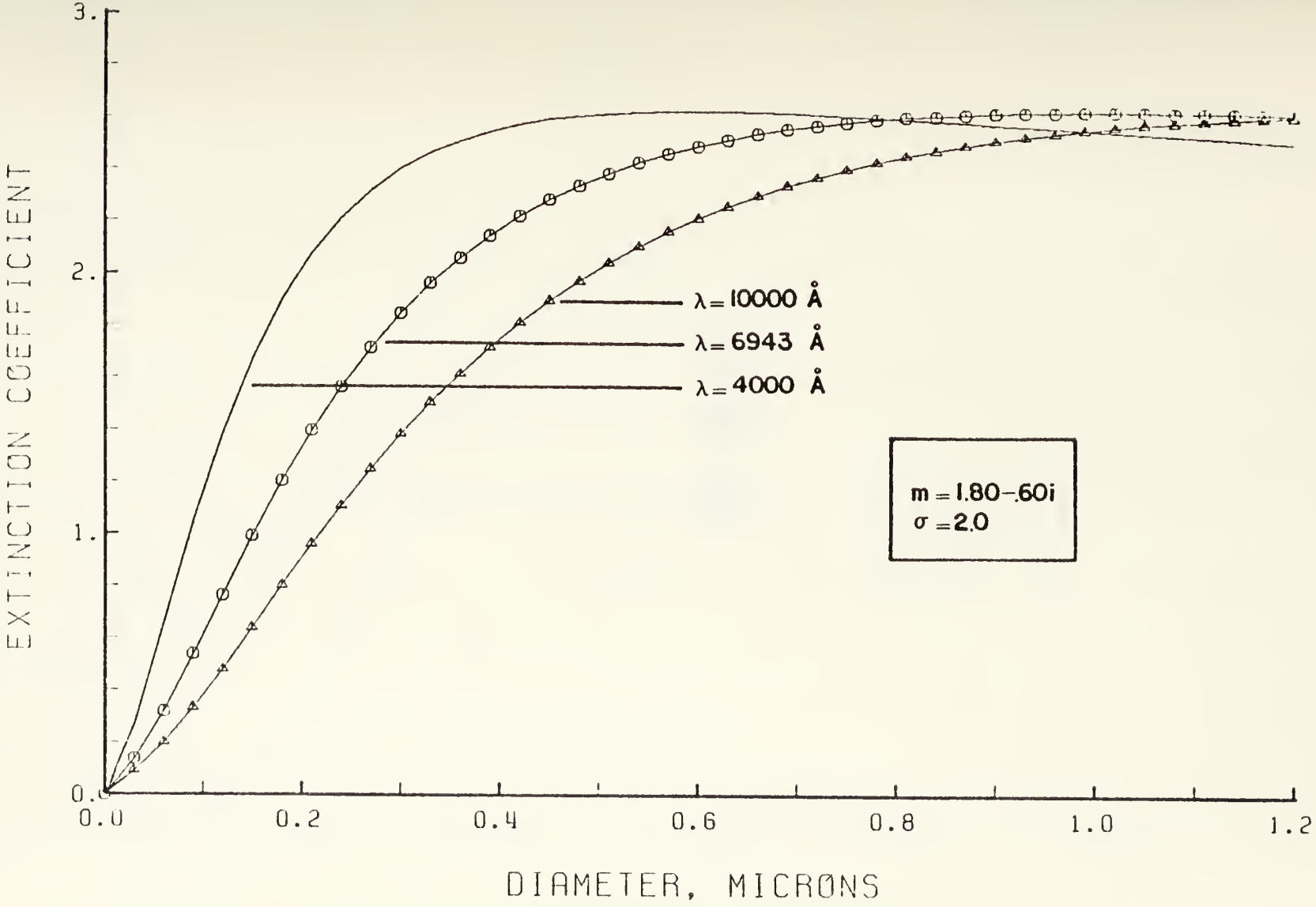

Figure 34. D_{32} vs. Extinction Coefficient (10000, 6943, 4000); m = 1.80-.60i/2.0

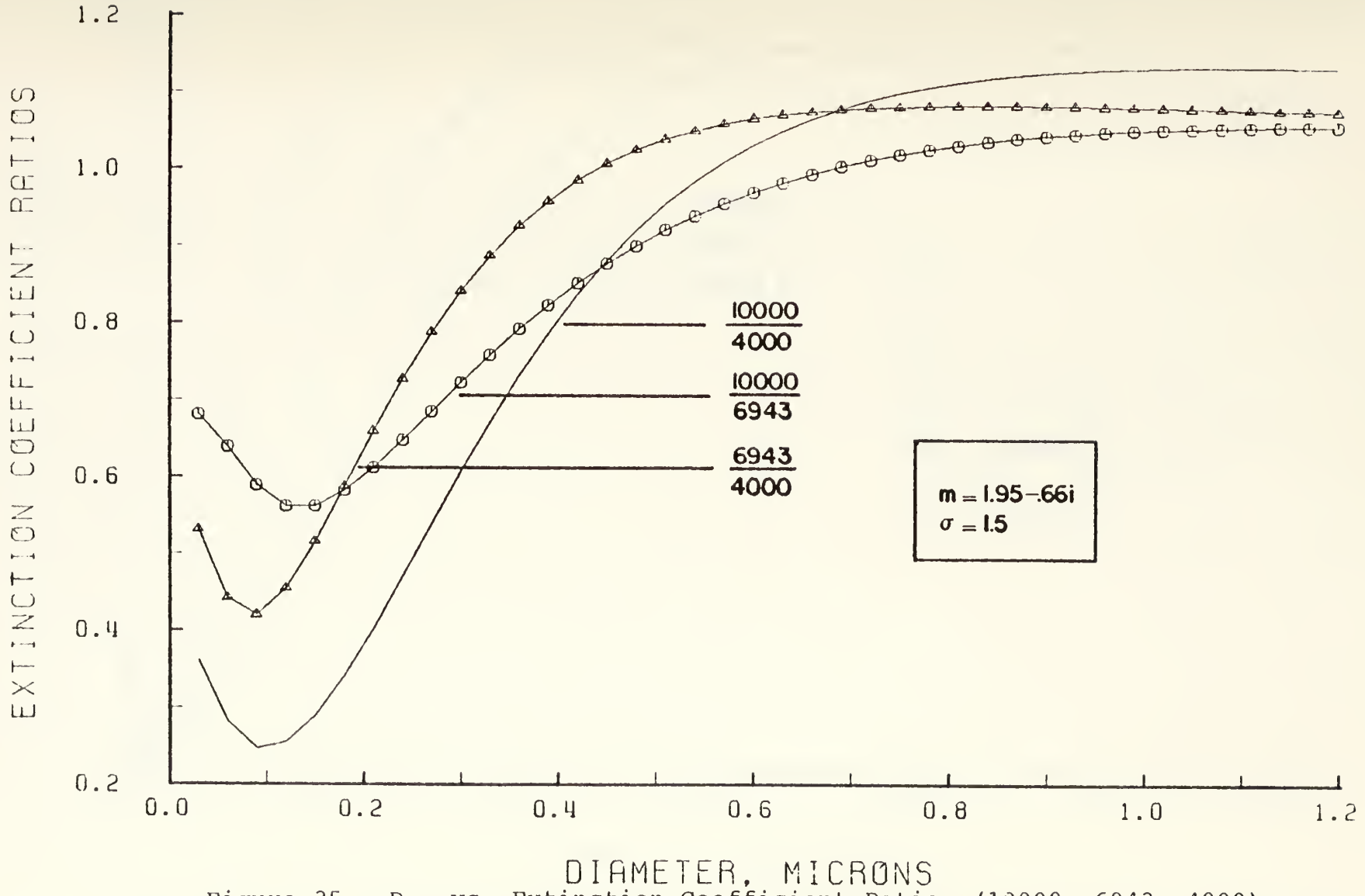

Figure 35. D_{32} vs. Extinction Coefficient Ratios (10000, 6943, 4000)
m = 1.95-.66i/1.5

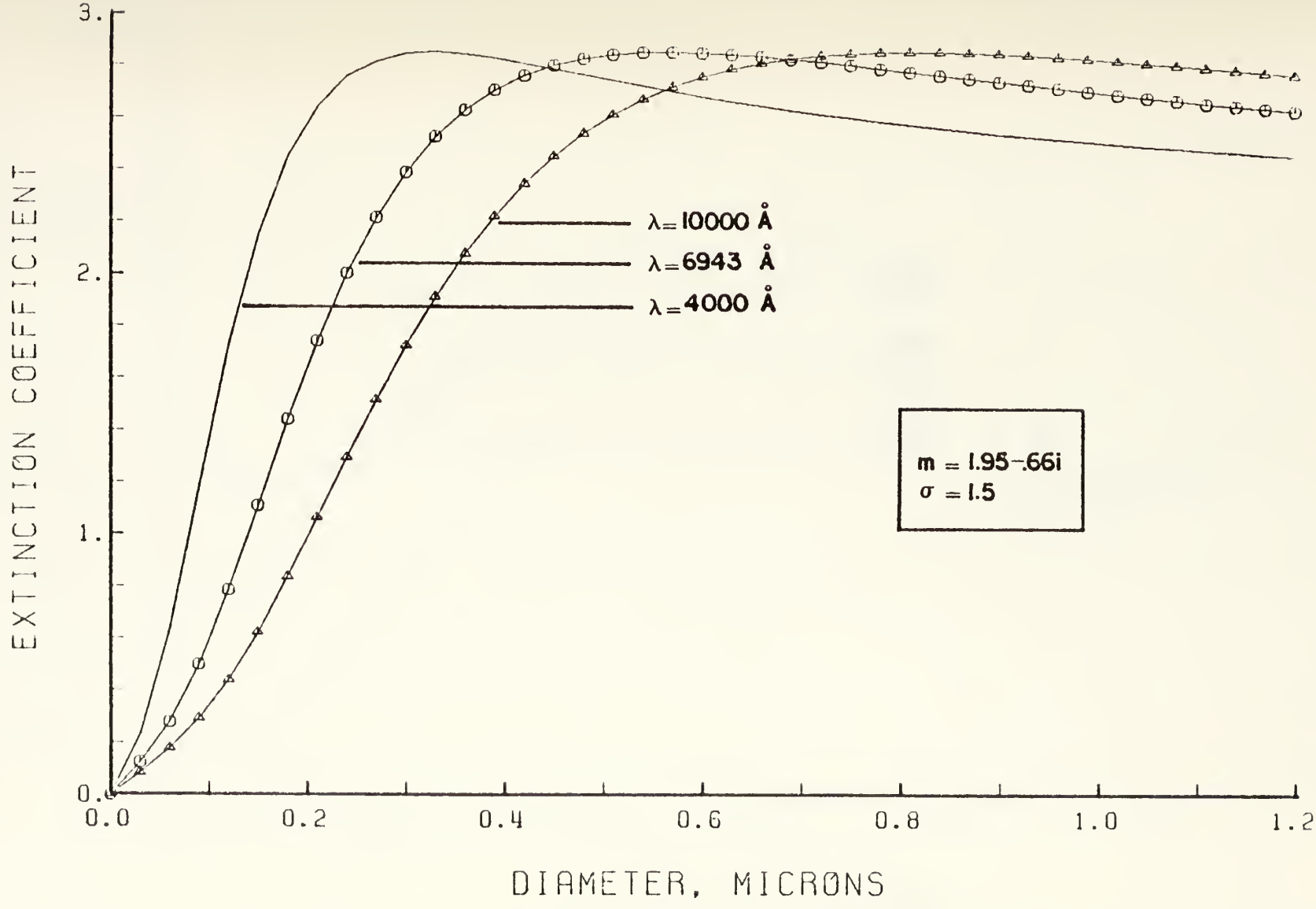

Figure 36. D_{32} vs. Extinction Coefficient (10000, 6943, 4000); m = 1.95-.66i/1.5

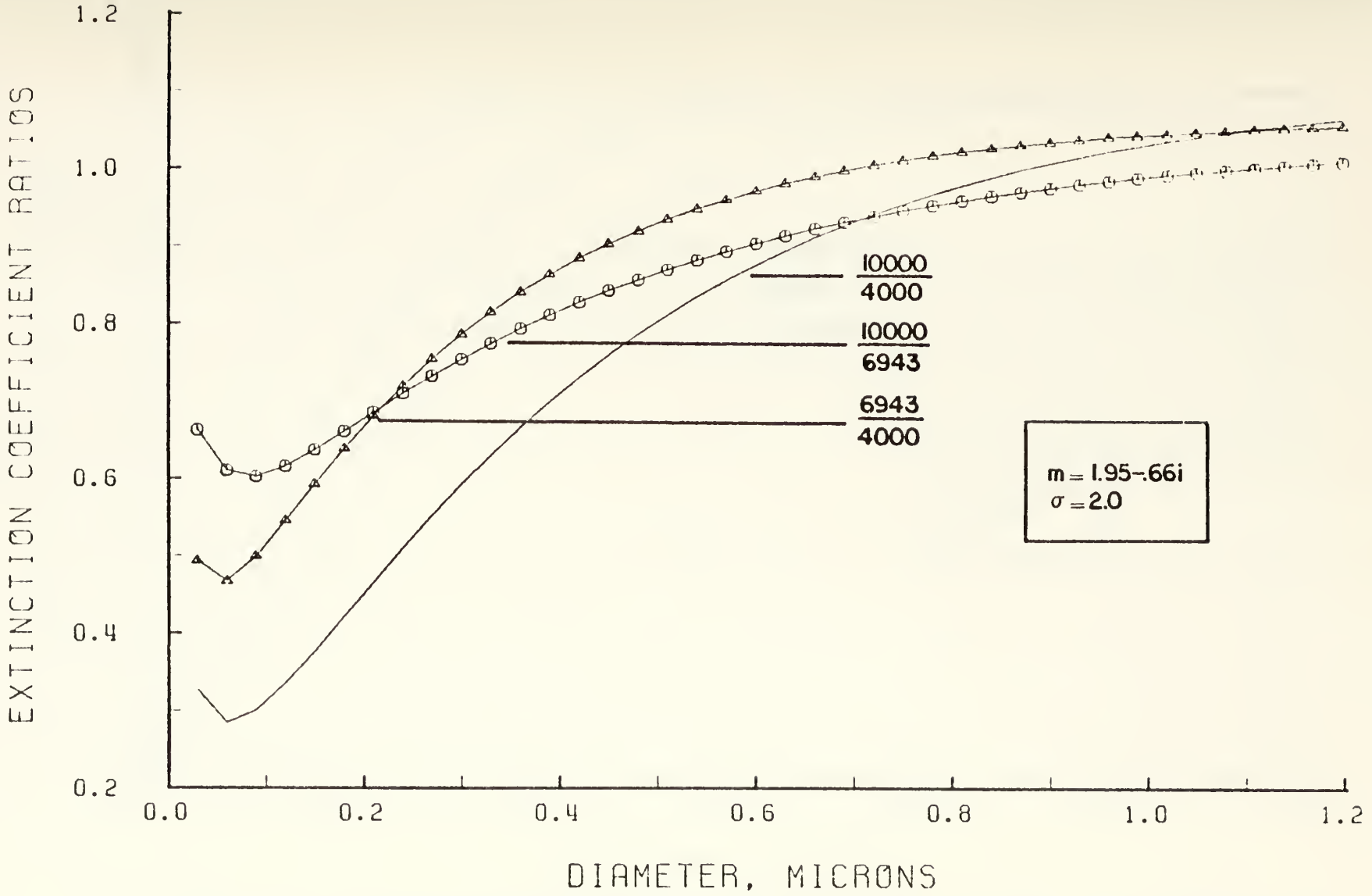

Figure 37. D_{32} vs. Extinction Coefficient Ratios (10000, 6943, 4000)
m = 1.95-.66i/2.0

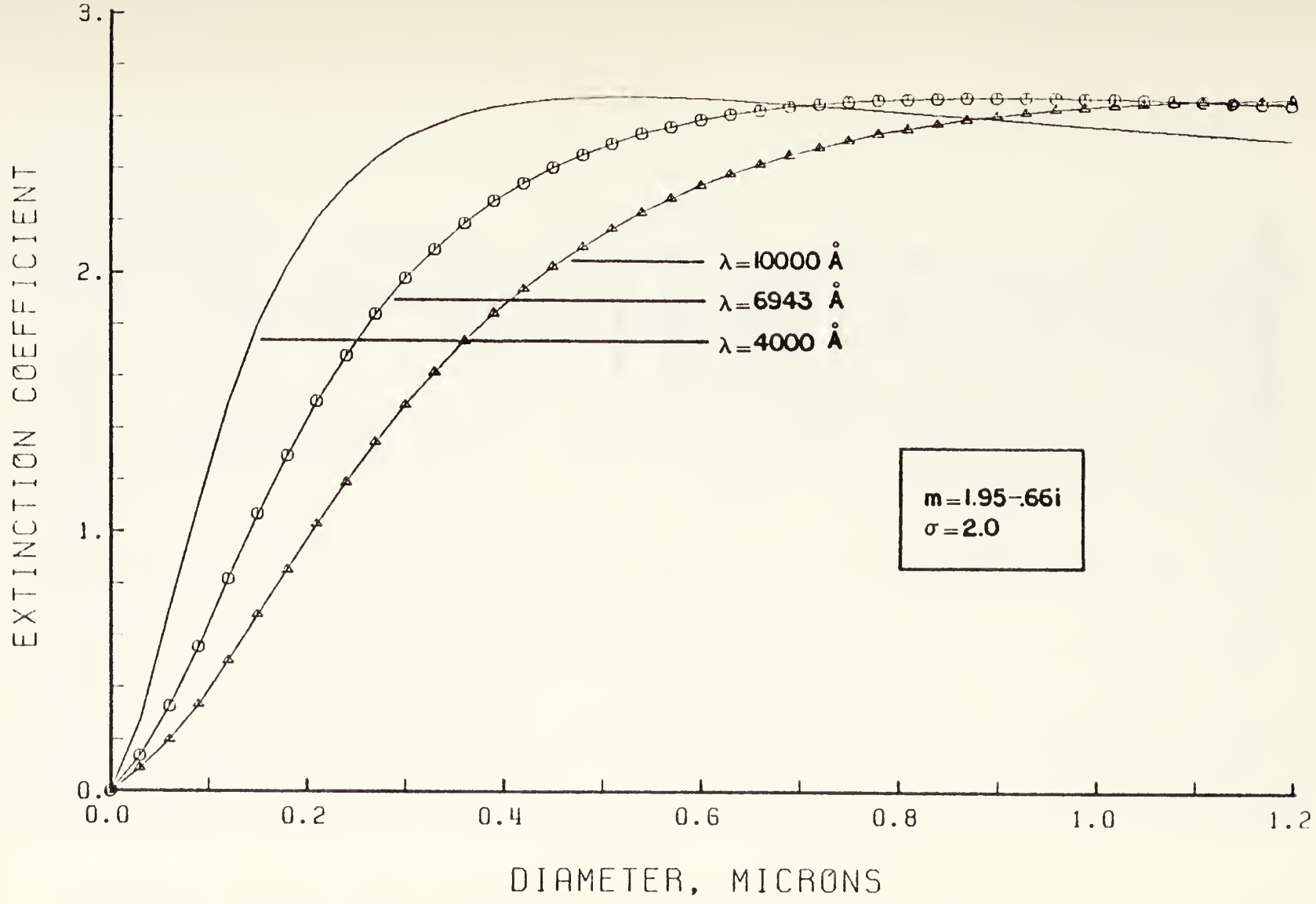

Figure 38. D_{32} vs. Extinction Coefficient (10000, 6943, 4000); m = 1.95-.66i/2.0

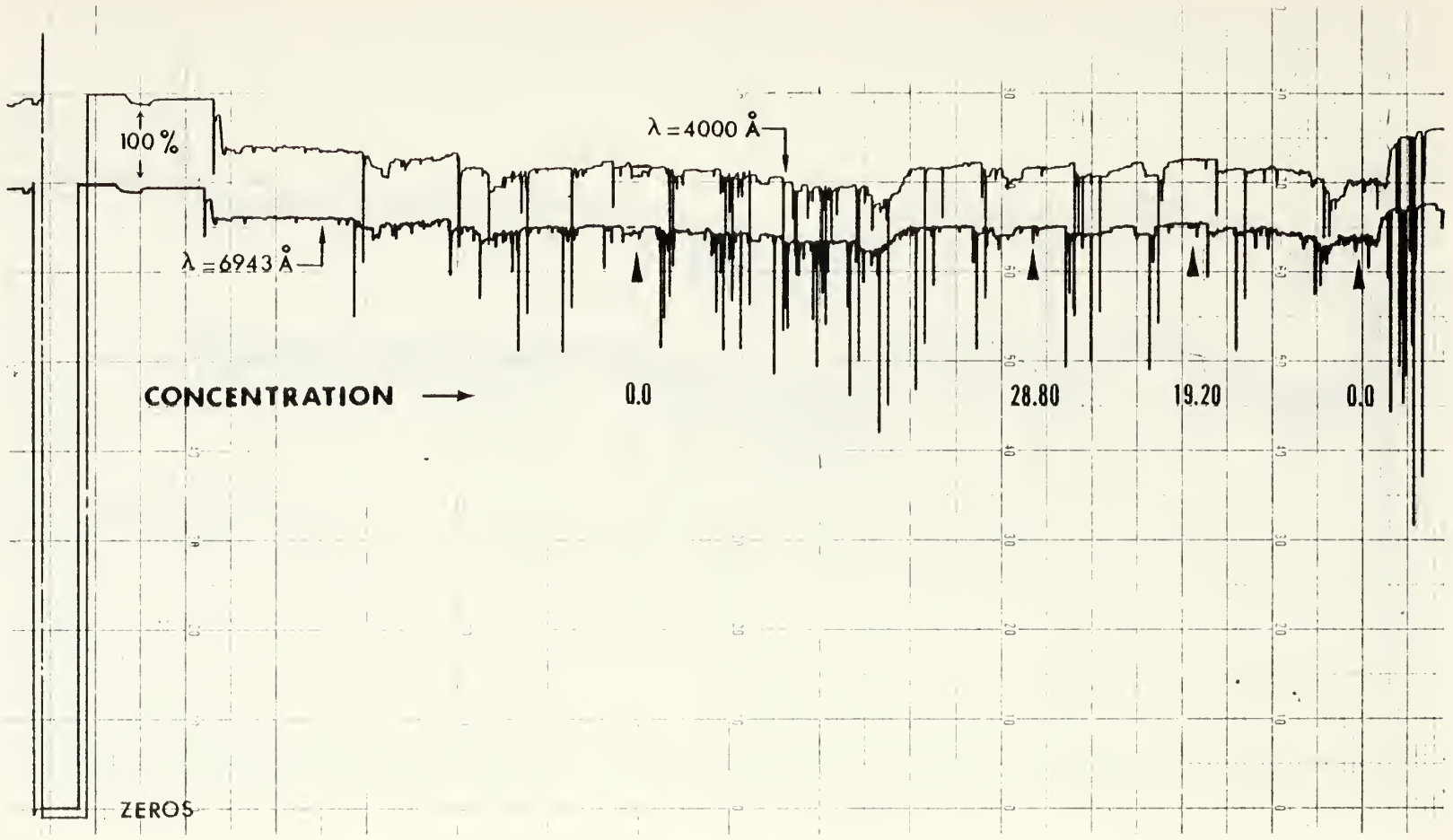

Figure 39. Strip Chart Recording of Ferrocene Test Conducted on 19 November 1981 (λ = 4000 Å; λ = 6943 Å)

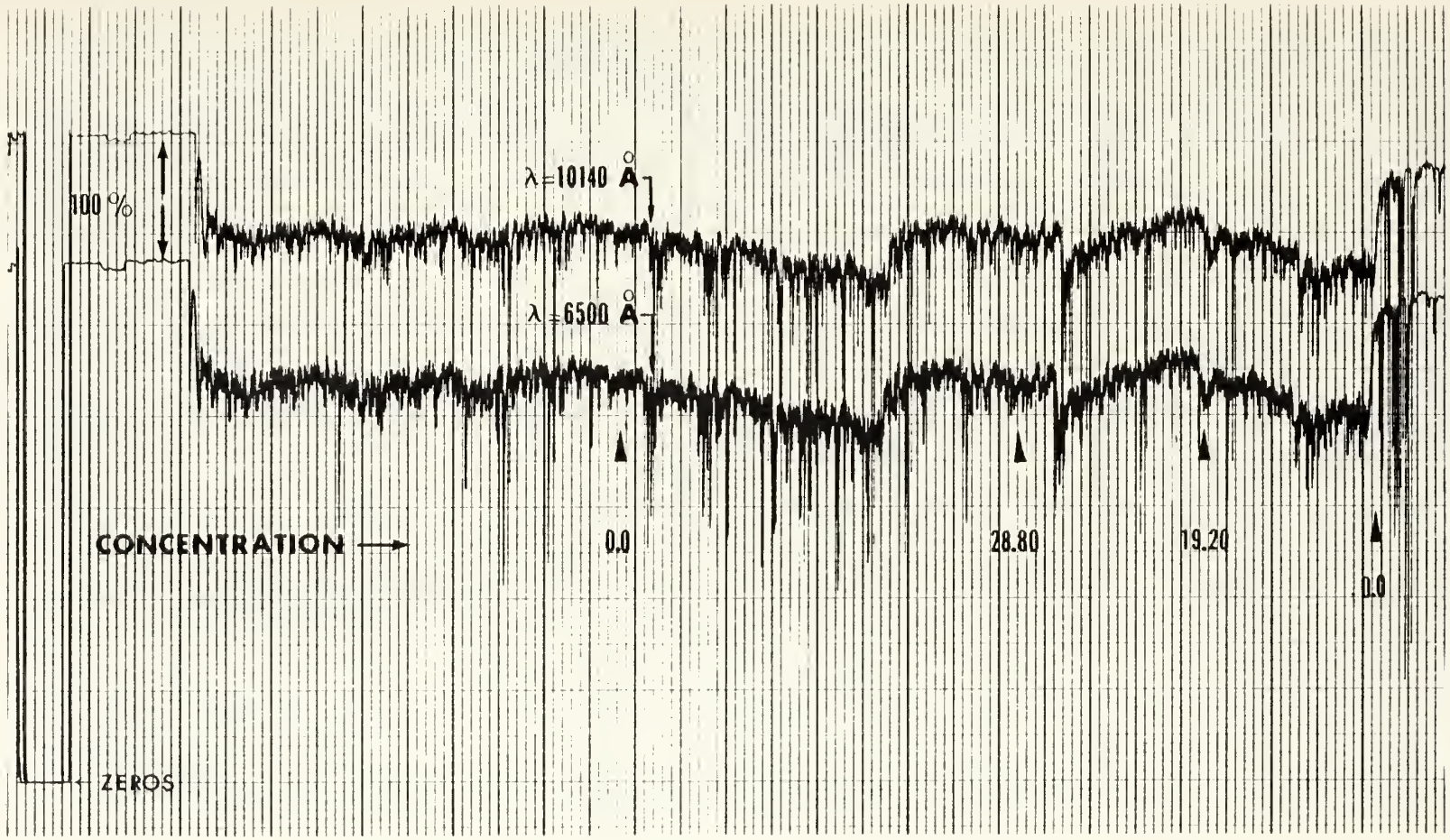

Figure 40. Strip Chart Recording of Ferrocene Test Conducted on 19 November 1981 (λ = 6500 Å; λ = 10140 Å)

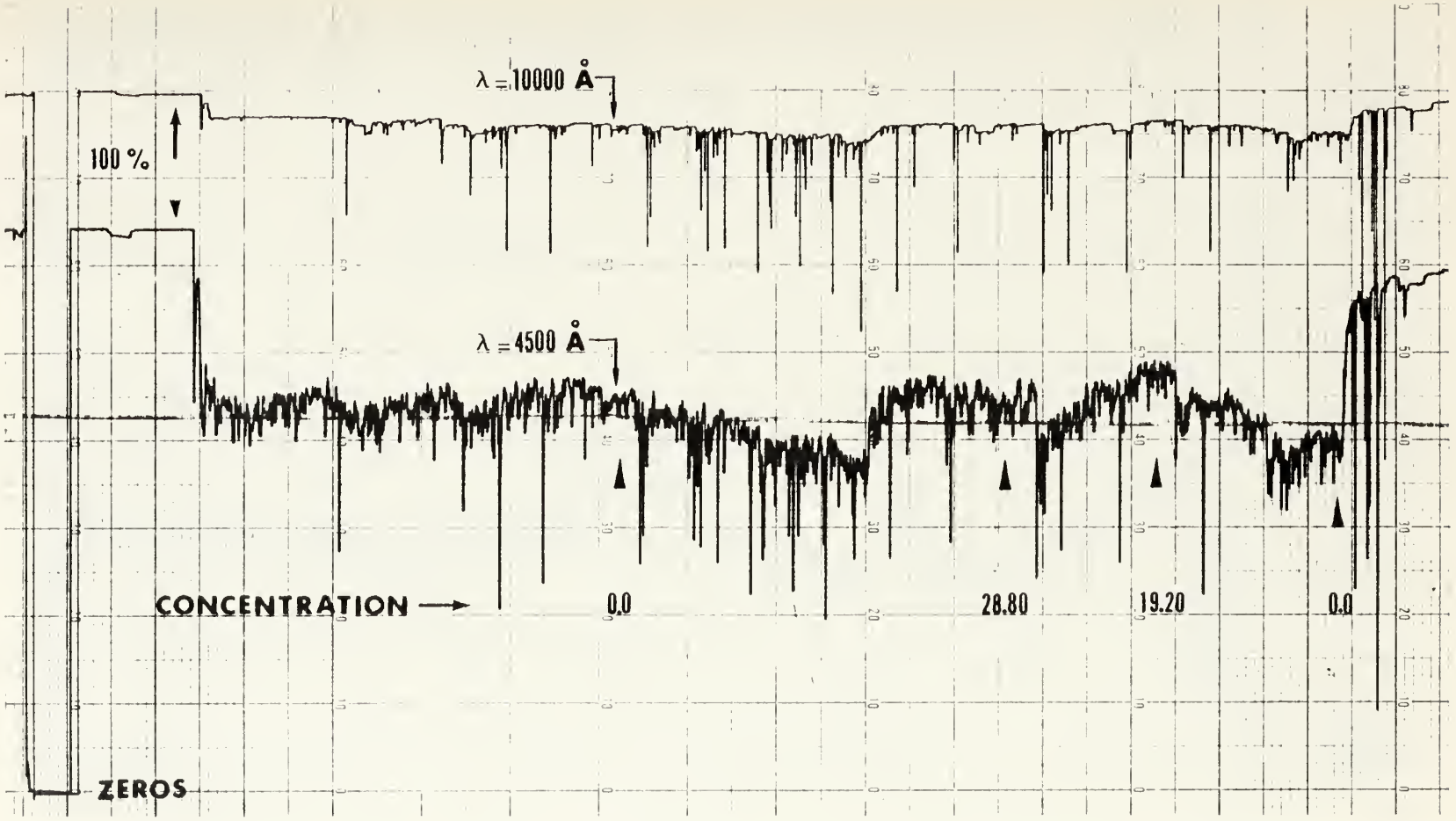

Figure 41. Strip Chart Recording of Ferrocene Test Conducted on 19 November 1981 (λ = 4500 Å; λ = 10000 Å)

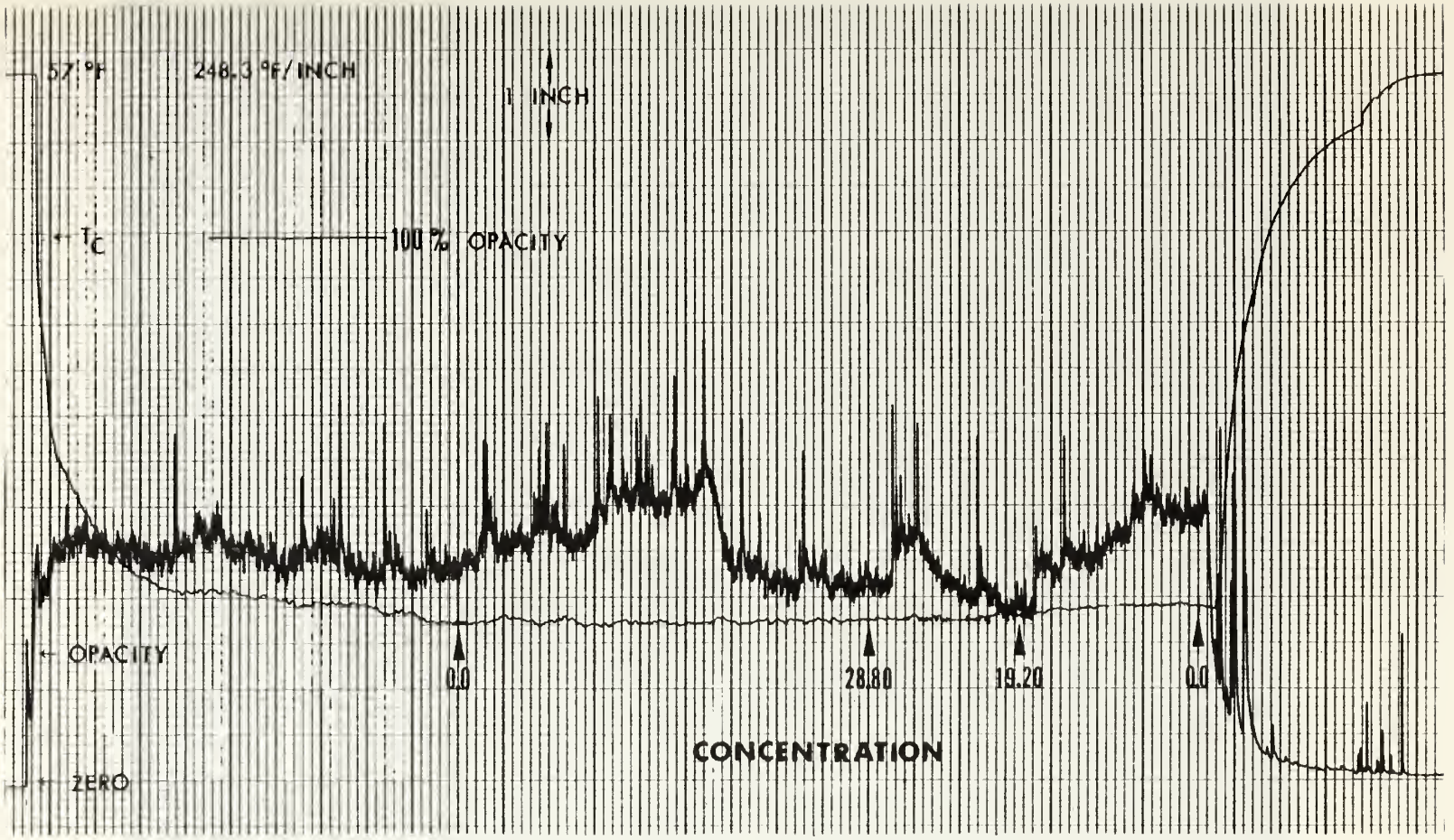

Figure 42. Strip Chart Recording of Ferrocene Test Conducted on 19 November 1981 (Combustor Exhaust Temperature (T_c) and Exhaust Gas Opacity)

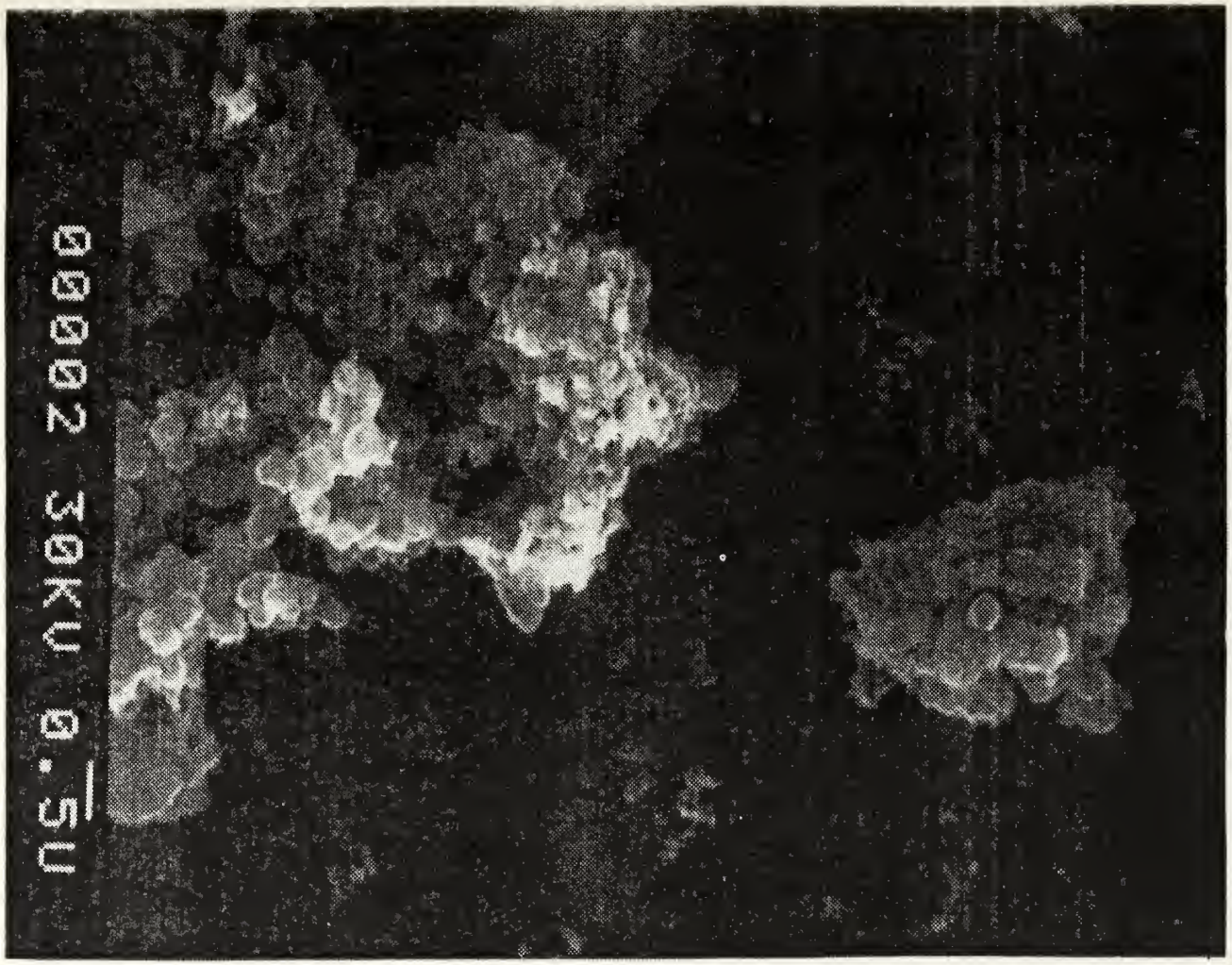

Figure 43. SEM Photograph of Engine Exhaust Particulate Sample Collected During Tests with JP-4 only on 10 November 1981 (10Kx Magnification)

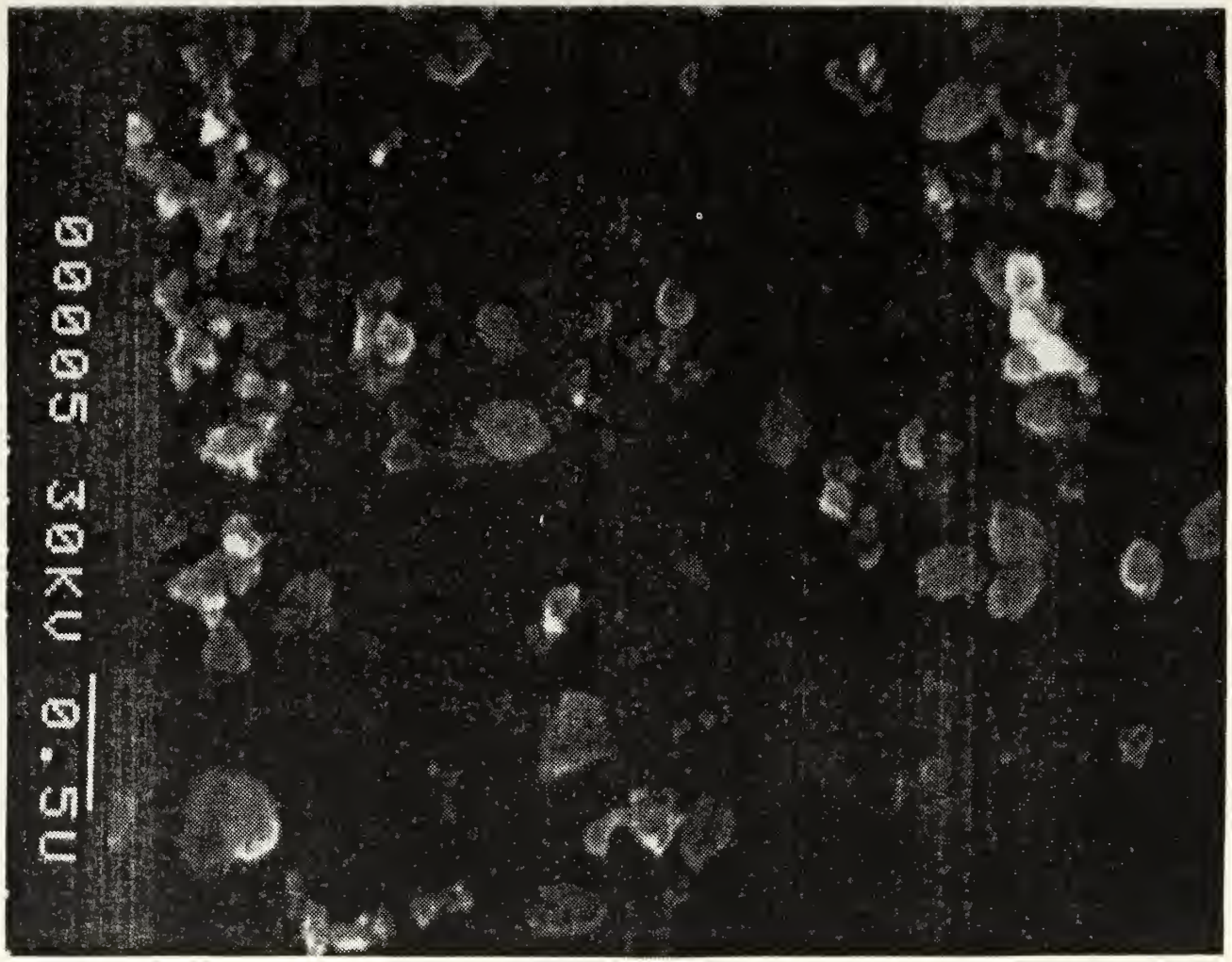

Figure 44. SEM Photograph of Engine Exhaust Particulate Sample Collected During Tests with JP-4 only on 10 November 1981 (25Kx Magnification)

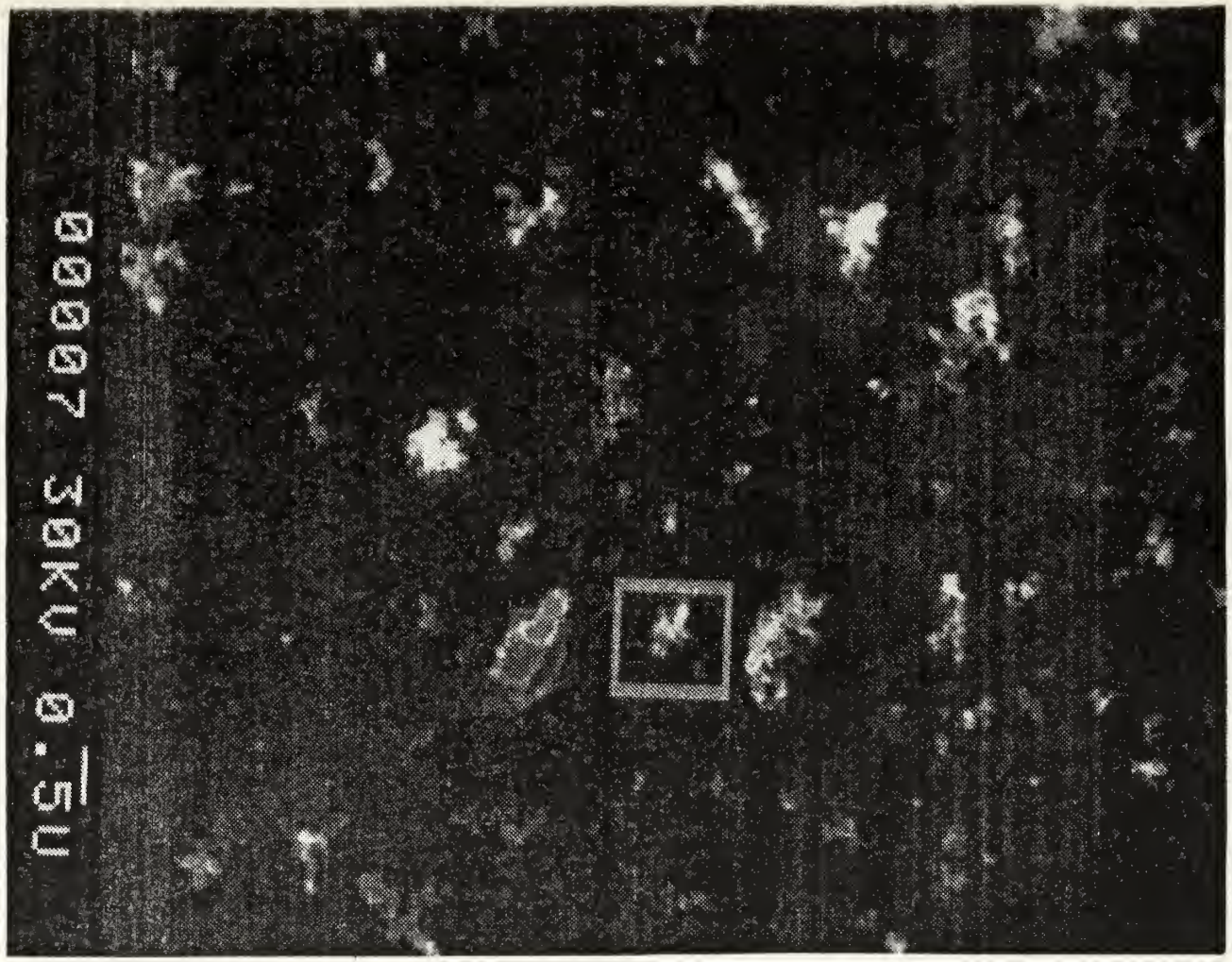

Figure 45. SEM Photograph of Engine Exhaust Particulate Sample Collected on 10 November 1981 During Tests with Ferrocene Concentrations of 32.30 ml. additive/gal. JP-4 (10Kx Magnification)

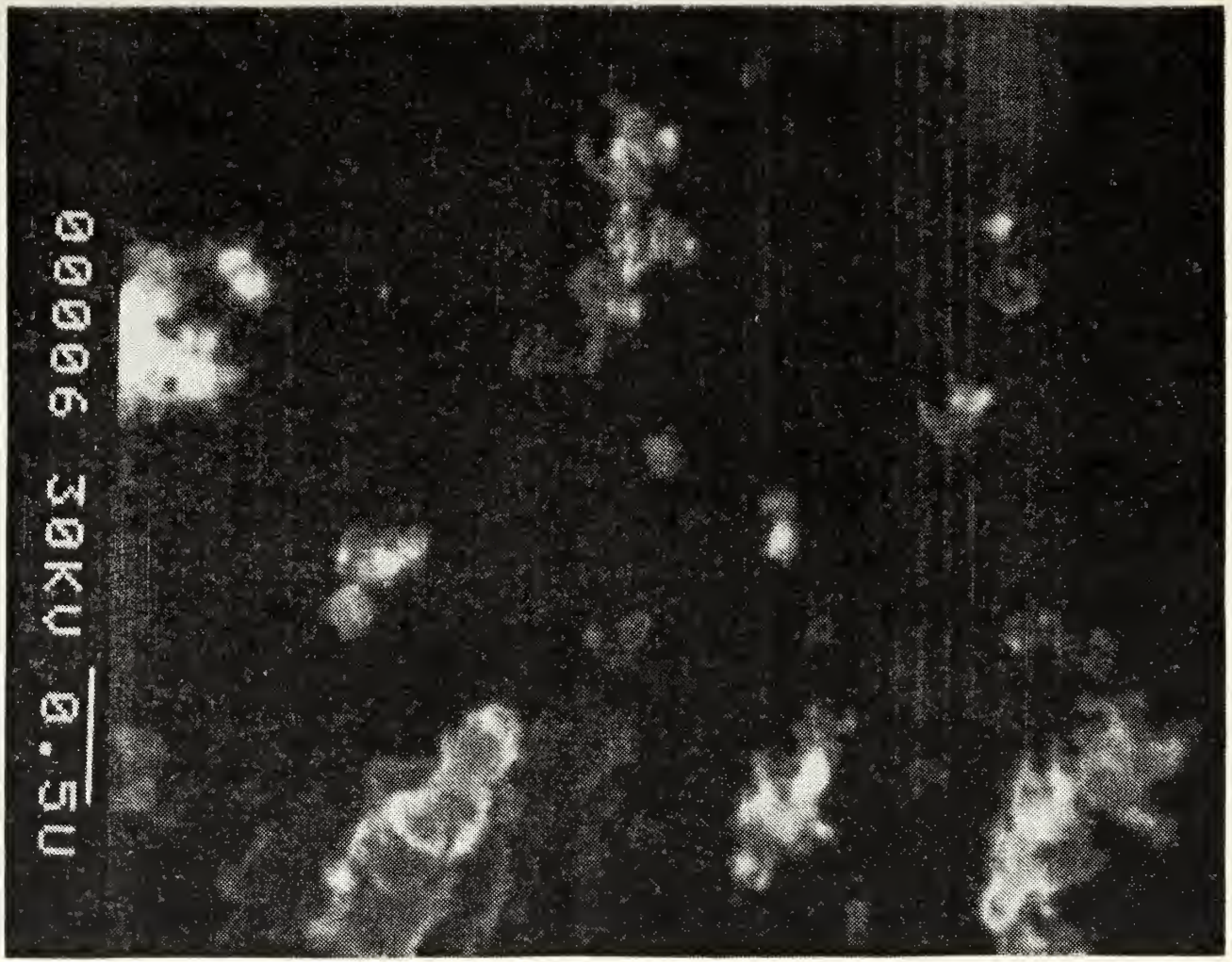

Figure 46. SEM Photograph of Engine Exhaust Particulate Sample Collected on 10 November 1981 During Tests with Ferrocene Concentrations of 32.30 ml. additive/gal. JP-4 (25Kx Magnification)

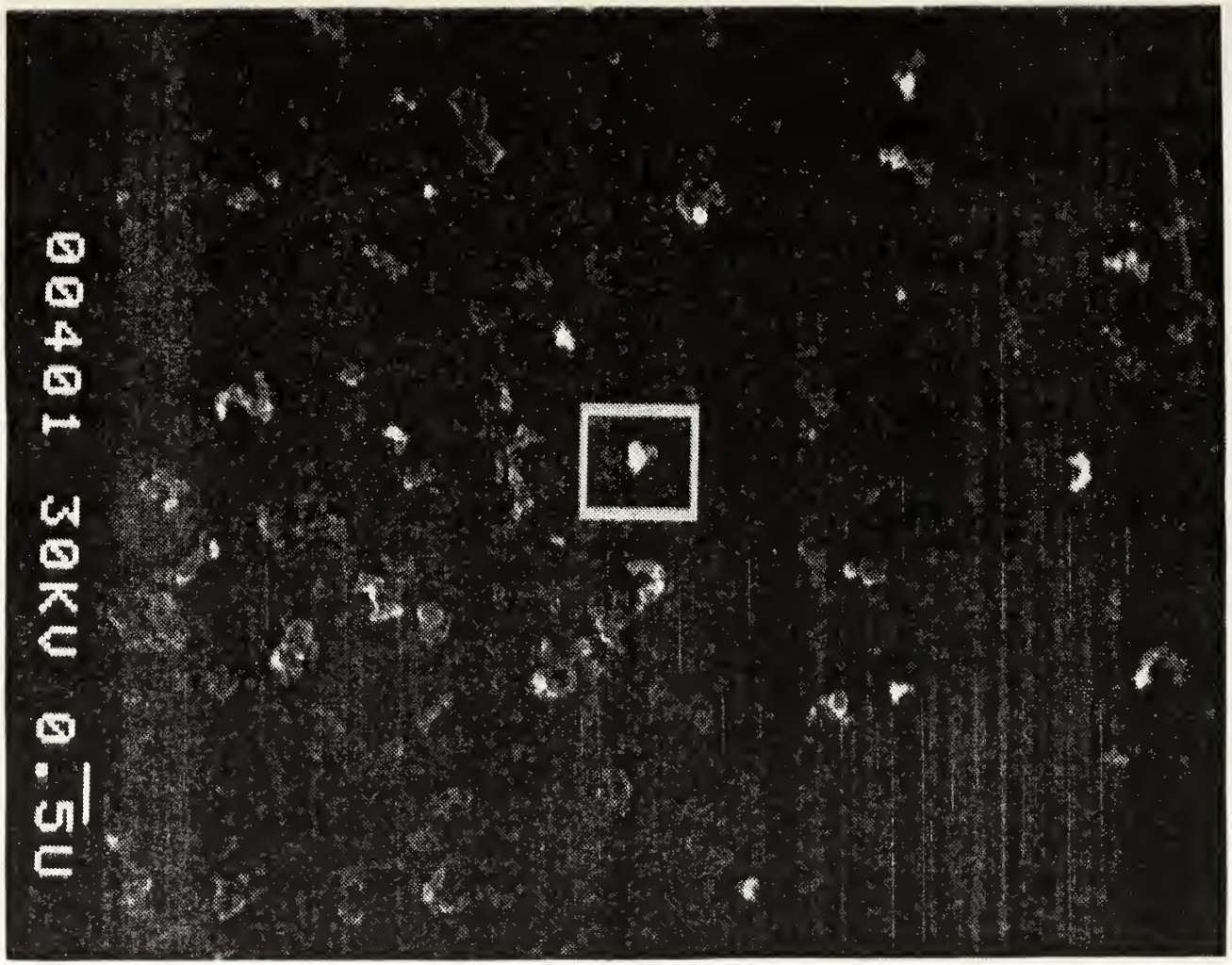

Figure 47. SEM Photograph of Engine Exhaust Particulate Sample Collected on 19 November 1981 During Tests with Ferrocene Concentrations of 19.20 ml. additive/gal. JP-4 (10Kx Magnification)

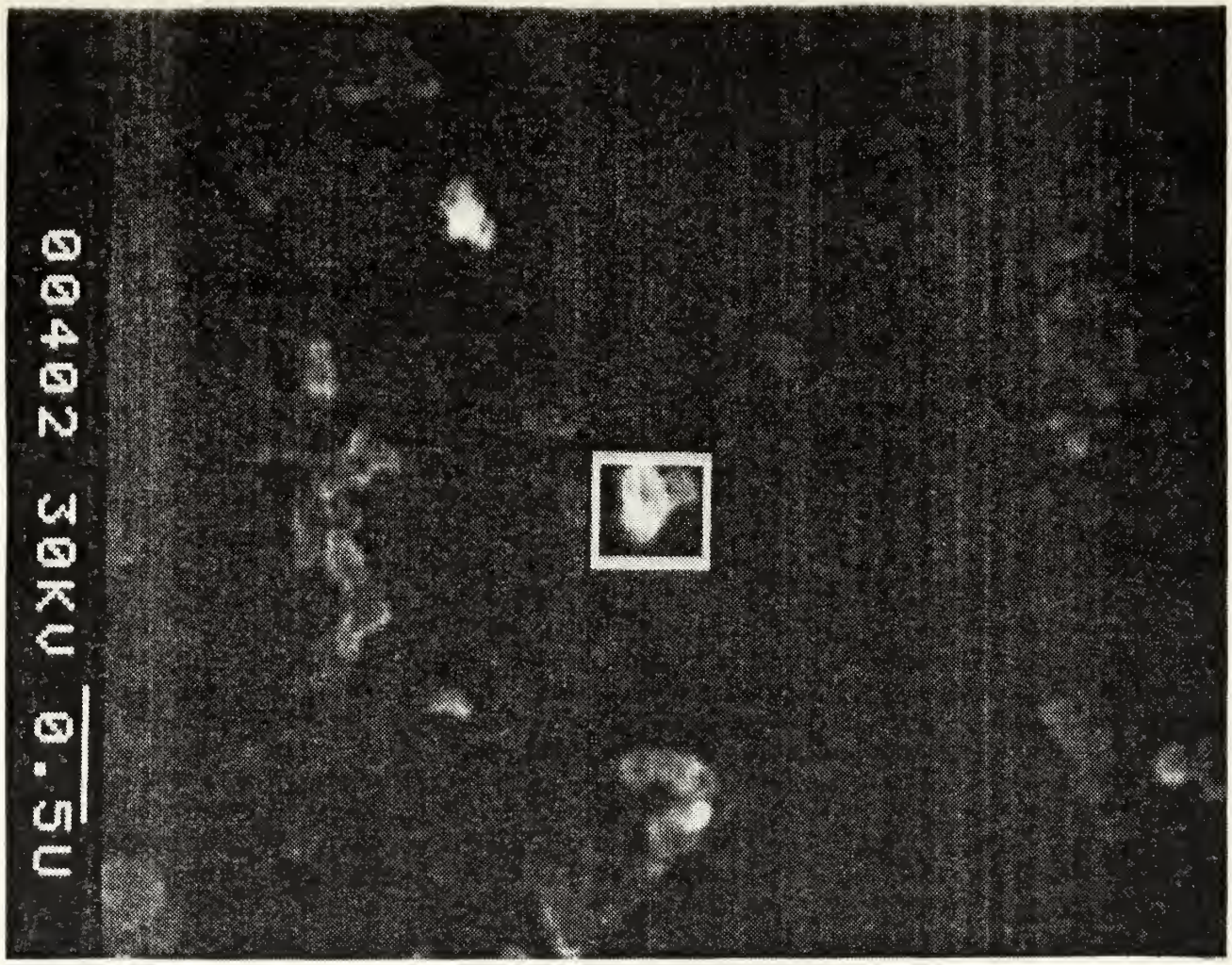

Figure 48. SEM Photograph of Engine Exhaust Particulate Sample Collected on 19 November 1981 During Tests with Ferrocene Concentrations of 19.20 ml. additive/gal. JP-4 (25Kx Magnification)

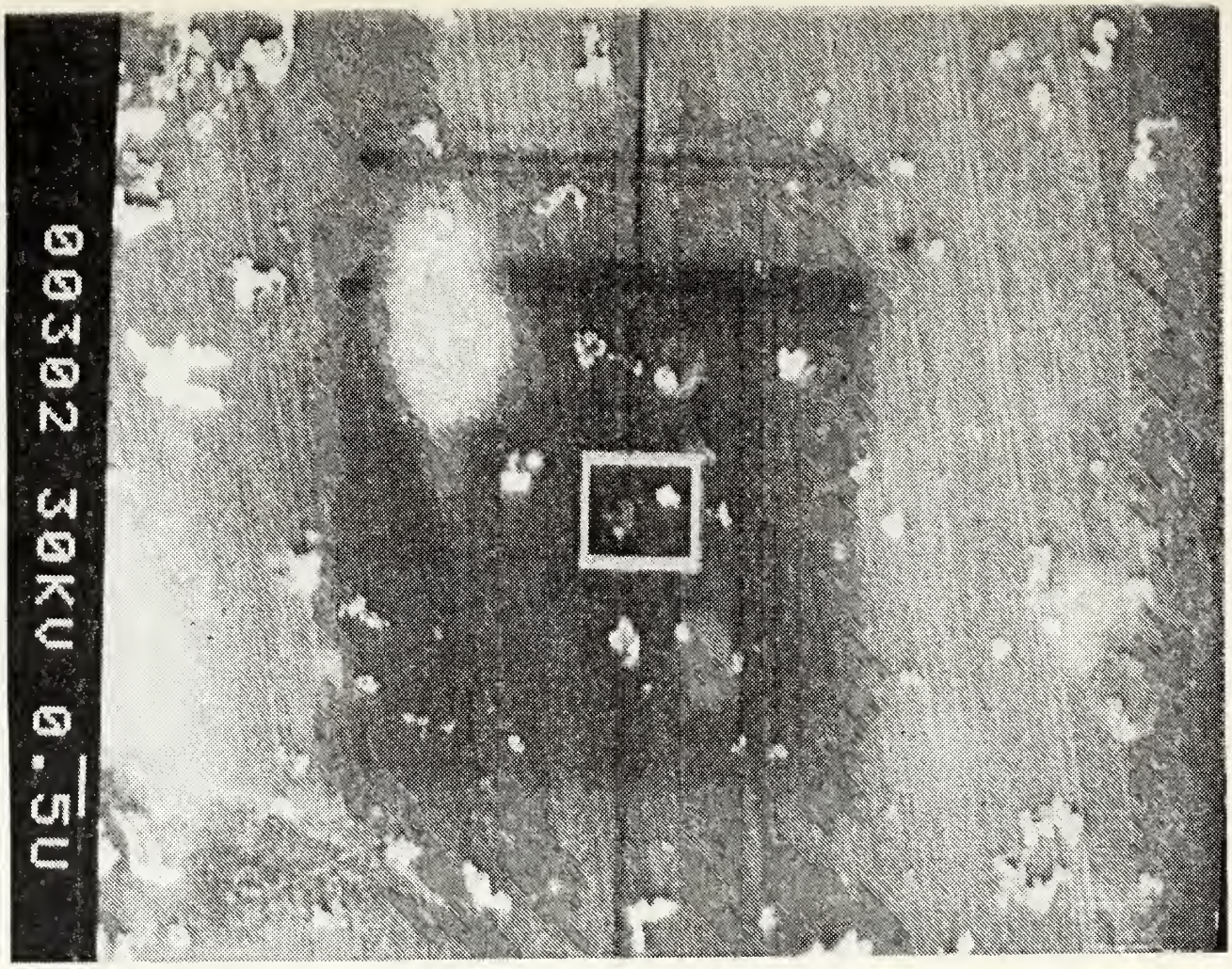

Figure 49. SEM Photograph of Engine Exhaust Particulate Sample Collected on 19 November 1981 During Tests with Ferrocene Concentrations of 28.80 ml. additive/gal. JP-4 (10Kx Magnification)

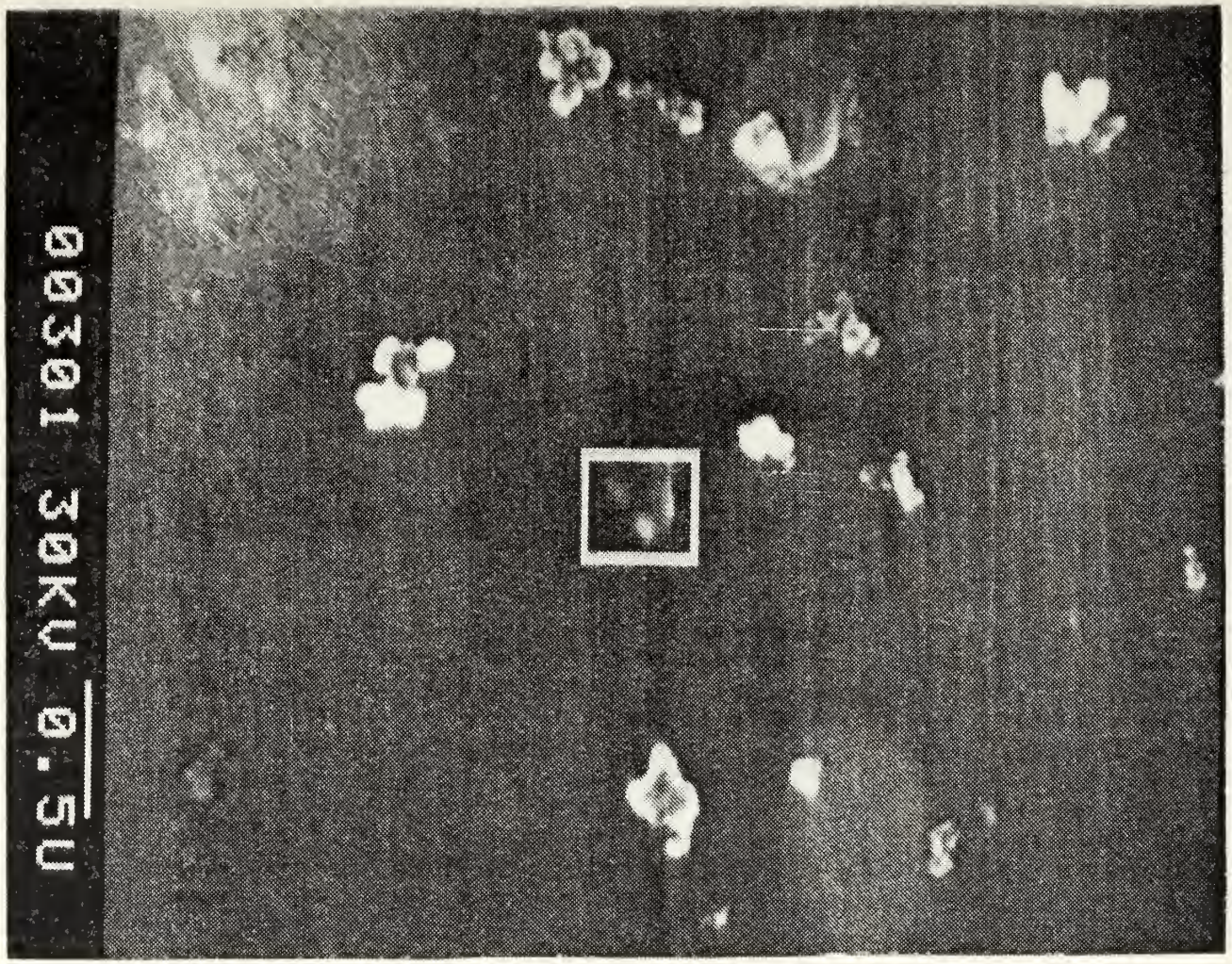

Figure 50. SEM Photograph of Engine Exhaust Particulate Sample Collected on 19 November 1981 During Tests with Ferrocene Concentrations of 28.80 ml. additive/gal. JP-4 (25Kx Magnification)

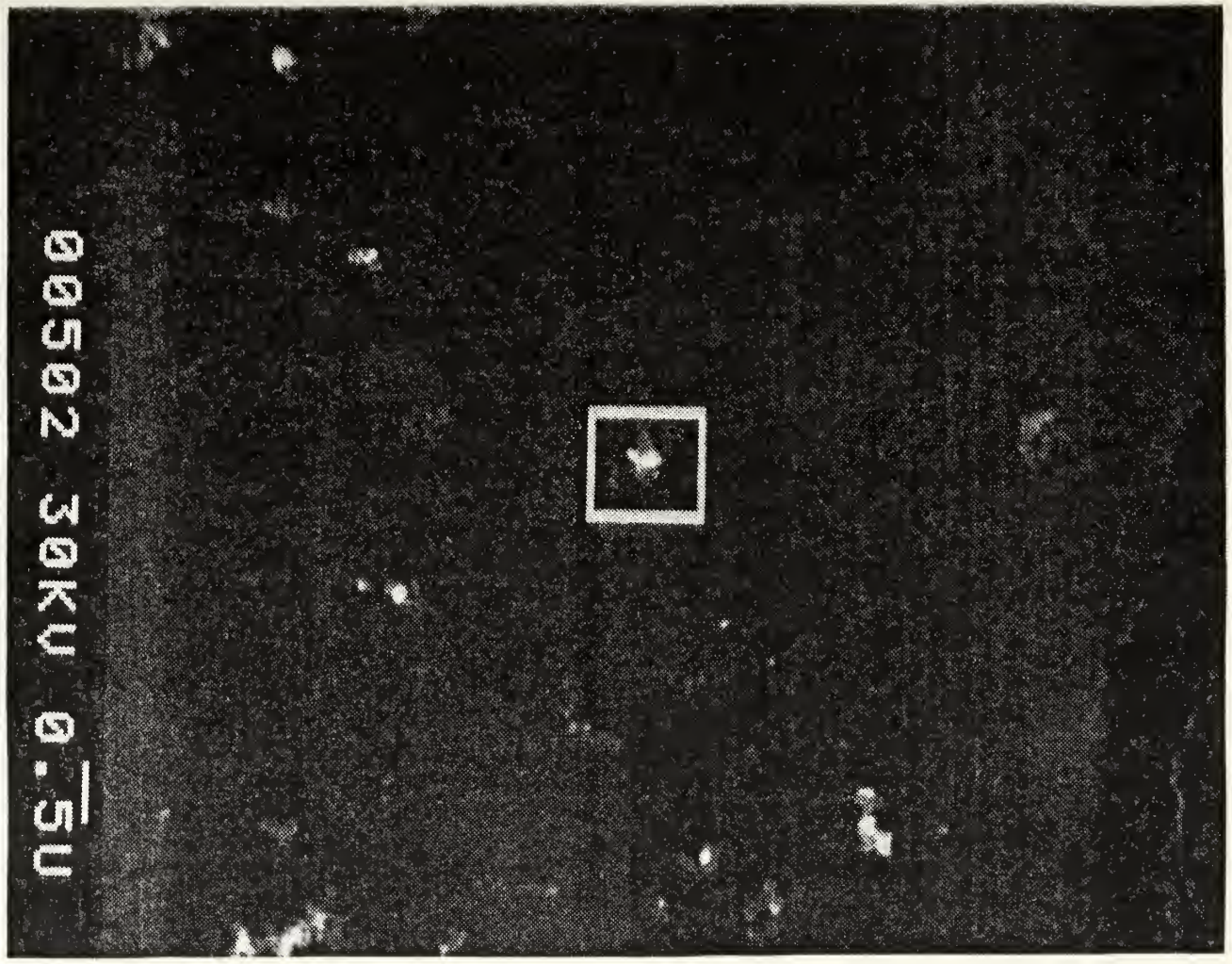

Figure 51. SEM Photograph of Engine Exhaust Particulate Sample Collected on 19 November 1981 During Tests with 12% Cerium Hex-Chem Concentrations of 19.10 ml. additive/gal. JP-4 (10Kx Magnification)

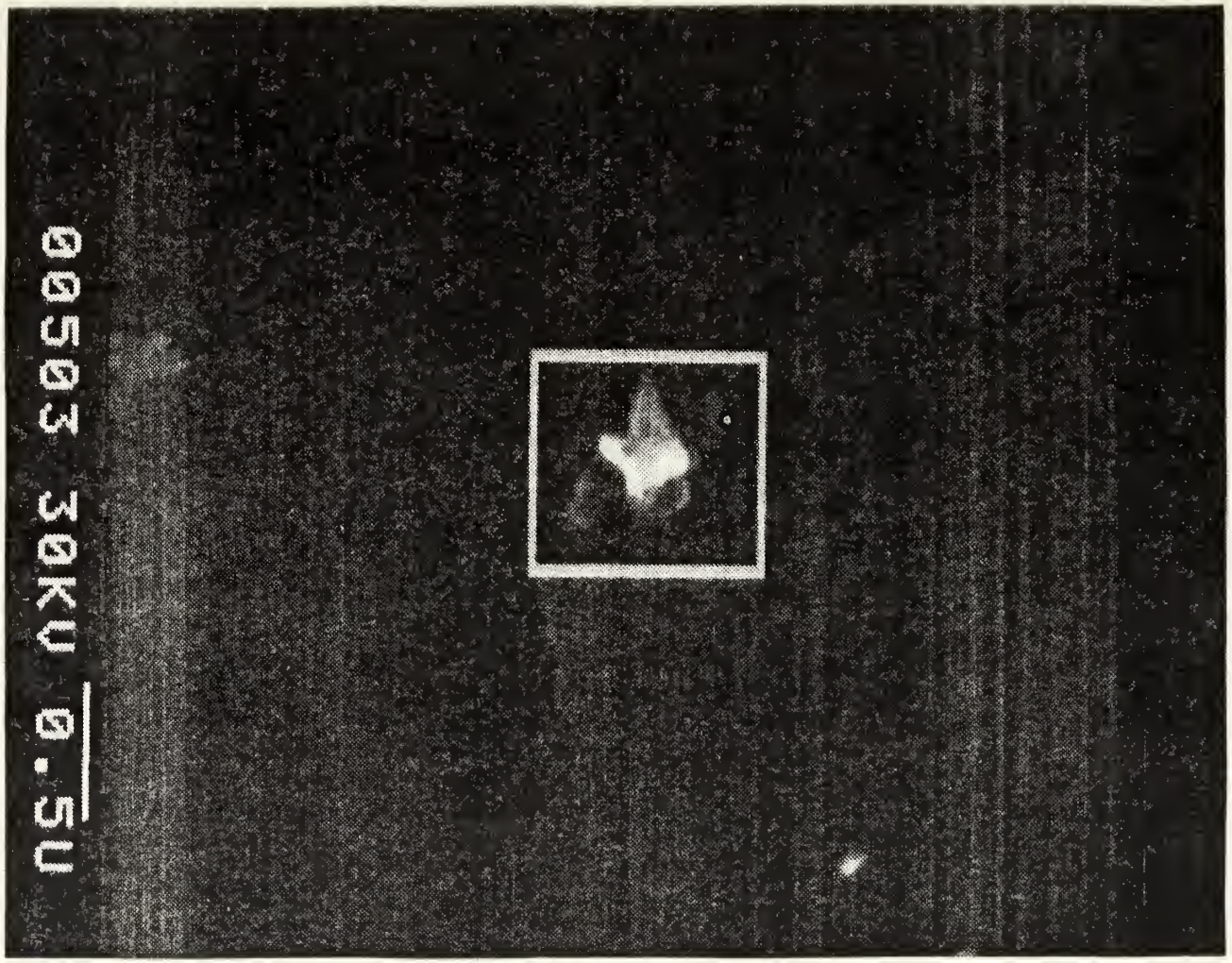

Figure 52. SEM Photograph of Engine Exhaust Particulate Sample Collected on 19 November 1981 During Tests with 12% Cerium Hex-Chem Concentrations of 19.10 ml. additive/gal. JP-4 (25Kx Magnification)

LIST OF REFERENCES

1. People of the State of California versus Department of the Navy, Civil Case No. C-76-0045 WHO, United States District Court for the Northern District of California of January 1976.

2. Darnell, T. R., Effects of Fuel Additives on Plume Opacity of a Sub-Scale Turbojet Test Cell with a Ramjet Type Dump-Combustor, M.S.A.E. Thesis, Naval Postgraduate School, Monterey, California, December 1979.

3. Naval Postgraduate School Report 67NT-77-091, A Sub-Scale Turbojet Test Cell for Evaluation and Analytical Model Validation, by Hewlett, H. W., Hickey, P. J., and Netzer, D. W., September 1977.

4. Hewlett, H. W., Design, Construction and Testing of a Sub-Scale Turbojet Test Cell, M.S.A.E. Thesis, Naval Postgraduate School, Monterey, California, 1977.

5. Charest, J. R., Combustor Design and Operation for a Sub-Scale Turbojet Test Cell, M.S.A.E. Thesis, Naval Post-graduate School, Monterey, California, 1978.

6. The American Society of Mechanical Engineers (ASME) PTC 19.5; 4, FLOW Measurement, Instruments and Apparatus, United Engineering Center, 345 East 47th, New York, 1959.

7. Cashdollar, K. L., Lee, C. K., and Singer, J. M., "Three Wavelength Light Transmission Technique to Measure Smoke Particle Size and Concentration," Applied Optics, Vol. 18, No. 11, June 1979, pp. 1763-1769.

8. Dobbins, R. A. and Jizmagian, G. S., "Optical Scattering Cross Sections for Polydispersions of Dielectric Spheres," Journal of the Optical Society of America, Vol. 56, No. 10, October 1966, pp. 1345-1354.

9. Kleiser, T. D., Design of a Particulate Matter Collection Train, AE-3815 Lab, Naval Postgraduate School, Monterey, California, June 1981.

10. Monitor Labs, Incorporated, Document 8440E, Instruction Manual Nitrogen Oxides Analyzer Model 8440E, 4202 Sorrento Valley Boulevard, San Diego, California, August 9, 1977.

INITIAL DISTRIBUTION LIST

		No. Copies
1.	Defense Technical Information Center Cameron Station Alexandria, Virginia 22314	2
2.	Library, Code 0142 Naval Postgraduate School Monterey, California 93940	2
3.	Department Chairman, Code 67 Department of Aeronautics Naval Postgraduate School Monterey, California 93940	1
4.	Professor D. W. Netzer, Code 67Nt Department of Aeronautics Naval Postgraduate School Monterey, California 93940	2
5.	LT D. W. Thornburg, USN 2611 Covington Pike Memphis, Tennessee 38128	2

Thesis
T4567
c.1

19551.5

Thornburg
An investigation of engine and test cell operating conditions on the effectiveness of smoke suppressant fuel additives.